

**USING PRIMARY AFFERENT NEURAL
ACTIVITY FOR PREDICTING LIMB
KINEMATICS IN CAT**

by

J. B. M. Wagenaar

M.S. in Electrical Engineering

University of Twente, 2005

Submitted to the Graduate Faculty of
the Swanson School of Engineering in partial fulfillment
of the requirements for the degree of

Doctor of Philosophy

University of Pittsburgh

2011

UNIVERSITY OF PITTSBURGH
SWANSON SCHOOL OF ENGINEERING

This dissertation was presented

by

J. B. M. Wagenaar

It was defended on

March 25th 2011

and approved by

D.J. Weber, Ph.D., Professor, Bioengineering Department

V. Ventura, Ph.D., Professor, Statistics Department, Carnegie Mellon University

A.B. Schwartz, Ph.D., Professor, Neurobiology Department

B.J. Yates, Ph.D., Professor, Neuroscience Department

C.G. Atkeson, Ph.D., Professor, Robotics Department, Carnegie Mellon University

Dissertation Director: D.J. Weber, Ph.D., Professor, Bioengineering Department

Copyright © by J. B. M. Wagenaar
2011

USING PRIMARY AFFERENT NEURAL ACTIVITY FOR PREDICTING LIMB KINEMATICS IN CAT

J. B. M. Wagenaar, PhD

University of Pittsburgh, 2011

Kinematic state feedback is important for neuroprostheses to generate stable and adaptive movements of an extremity. State information, represented in the firing rates of populations of primary afferent neurons, can be recorded at the level of the dorsal root ganglia (DRG). Previous work in cats showed the feasibility of using DRG recordings to predict the kinematic state of the hind limb using reverse regression. Although accurate decoding results were attained, these methods did not make efficient use of the information embedded in the firing rates of the neural population.

This dissertation proposes new methods for decoding limb kinematics from primary afferent firing rates. We present decoding results based on state-space modeling, and show that it is a more principled and more efficient method for decoding the firing rates in an ensemble of primary afferent neurons. In particular, we show that we can extract confounded information from neurons that respond to multiple kinematic parameters, and that including velocity components in the firing rate models significantly increases the accuracy of the decoded trajectory.

This thesis further explores the feasibility of decoding primary afferent firing rates in the presence of stimulation artifact generated during functional electrical stimulation. We show that kinematic information extracted from the firing rates of primary afferent neurons can be used in a real-time application as a feedback for control of FES in a neuroprostheses. It provides methods for decoding primary afferent neurons and sets a foundation for further development of closed loop FES control of paralyzed extremities.

Although a complete closed loop neuroprosthesis for natural behavior seems far away, the premise of this work argues that an interface at the dorsal root ganglia should be considered as a viable option.

Keywords: bioengineering, muscle spindle, primary afferent, nervous system, closed loop control, state-space modeling, neuroprostheses, FES .

TABLE OF CONTENTS

1.0 INTRODUCTION	1
1.1 SENSORIMOTOR PHYSIOLOGY	1
1.1.1 Advances towards understanding the sensory nervous system.	1
1.1.2 Firing rate properties of primary afferent neurons	3
1.1.2.1 The muscle spindle	3
1.1.2.2 Other afferent neurons	7
1.1.3 Proprioceptive coordinate frame	8
1.1.4 Role of somatosensory afferents in regulating motor output	12
1.1.5 The impact of spinal cord injury to primary afferent response	13
1.2 USING AFFERENT INFORMATION FOR NEURAL PROSTHESES	14
1.2.1 Using primary afferent or external sensors?	14
1.2.2 Sensorimotor control as a closed loop control system	15
1.2.3 Neural interfaces	17
1.2.4 Inferring limb state from afferent activity	18
1.2.5 Closed-loop control of FES using natural sensors	20
1.3 SPECIFIC AIMS	21
1.3.1 Direct decoding of primary afferent neuron firing rates	21
1.3.2 State-space decoding of primary afferent neuron firing rates	22
1.3.3 Improved decoding techniques for realtime applications.	22
1.3.4 Closed loop FES using primary afferent response as feedback	23
2.0 IMPROVED DECODING OF LIMB-STATE FEEDBACK FROM NATURAL SENSORS	24

2.1	INTRODUCTION	24
2.2	METHODS AND DATA	25
2.2.1	The experiment	25
2.2.2	Reverse regression	27
2.2.3	Direct regression methods	27
2.2.4	Contrasting methods	29
2.3	RESULTS	29
2.4	DISCUSSION	33
3.0	STATE-SPACE DECODING OF PRIMARY AFFERENT FIRING RATES	36
3.1	INTRODUCTION	36
3.2	METHODS AND DATA	38
3.2.1	Surgical procedures	38
3.2.2	The experiment	38
3.2.3	Current decoding paradigm: reverse regression	41
3.2.4	Firing rate models and likelihood decoding	43
3.2.4.1	Firing rate models in joint angle frame	44
3.2.4.2	Firing rate models in limb end point frame	45
3.2.5	State-space models	45
3.2.5.1	Kinematic models	48
3.2.6	Decoding efficiency	50
3.2.7	State space algorithm for decoding limb state	51
3.2.8	Details for solving eq. 3.6	54
3.3	RESULTS	54
3.3.1	Encoding models	55
3.3.2	Decoding joint angles	57
3.3.3	Decoding endpoint coordinates	62
3.4	DISCUSSION	64
3.4.1	State-space decoding methods of primary afferent activity	64
3.4.2	Natural feedback for FES control	67
3.5	CONCLUSIONS	68

4.0 ALTERNATIVE DECODING TECHNIQUES FOR PREDICTING LIMB STATE	70
4.1 DYNAMIC FUZZY NEURAL NETWORKS	70
4.1.1 Alternative implementation of the GD-FNN	73
4.2 SPLINE REVERSE REGRESSION	79
5.0 CLOSED LOOP CONTROL OF FUNCTIONAL ELECTRICAL STIMULATION	82
5.1 INTRODUCTION	82
5.2 METHODS	84
5.2.1 Surgical procedures	84
5.2.2 Experiment setup	85
5.2.3 Realtime encoding of firing rate models	87
5.2.4 Removing stimulation artifact	88
5.3 RESULTS	91
5.3.1 Realtime decoding of primary afferents	91
5.3.2 Decoding during stimulation	94
5.3.3 Closed loop control of FES	96
5.4 DISCUSSION	98
6.0 GENERAL DISCUSSION	102
6.1 SUMMARY	102
6.2 SIGNIFICANCE AND FUTURE WORK	104
6.3 FINAL THOUGHTS	108
BIBLIOGRAPHY	109

LIST OF TABLES

1	Summary of firing rate models	46
---	---	----

LIST OF FIGURES

1	Example firing rates of primary afferents during passive movement	4
2	Example of muscle spindle response to succinylcholine	6
3	Regression models in different coordinate frames	10
4	Comparison of coordinate frames	11
5	Schematic representation of motor control	16
6	Setup of the experiment	26
7	Example of decoded trajectories.	30
8	Afferent responses to variations in kinematic variables	32
9	Summary of results.	34
10	Experiment setup 1	39
11	Observed kinematics and neural response	49
12	Random walk demonstration	50
13	Example firing rate response	56
14	Summary of results	58
15	Example decoded trajectory	60
16	Summary of results	61
17	Summary of endpoint decoding results	63
18	Modeling non-linear functions using fuzzy logic.	71
19	Simple example of fuzzy logic neural network.	77
20	Decoding center-out movement using fuzzy neural network	78
21	Decoding center-out movement using spline reverse regression	80
22	Experiment setup for closed loop FES	86

23	Effects of blanking input	89
24	Schematic for removing stimulation artifacts.	90
25	Realtime encoding and decoding of the firing rates of primary afferents	92
26	Progression of regression coefficients during model encoding	93
27	Primary afferent firing rates during FES 1	95
28	Decoding ground reaction forces during functional electrical stimulation	95
29	Primary afferent firing rates during FES 2	97
30	Closed loop FES traces and stick-figure of hind limb	99

1.0 INTRODUCTION

This chapter introduces the research topics discussed in document. Biomedical engineering and in particular the neural engineering fields heavily rely upon both physiology of the nervous system and the engineering aspects in science. Both aspects will be discussed in this chapter followed by a section outlining the specific aims addressed in this work.

1.1 SENSORIMOTOR PHYSIOLOGY

Scientific discoveries unraveling the purpose and properties of primary afferent firing rates will be discussed, followed by a section describing the current technology available for using primary afferent neurons as an integrated part of a neural prosthesis.

1.1.1 Advances towards understanding the sensory nervous system.

Around the year 100 AD, Marinus described the 10th cranial nerve based on anatomic findings in human. It took approximately 1900 years (1889) before Cajal initiated a series of discoveries that lead to our current understanding of the nervous system as a complex network of individual neurons. Only 120 years after Cajal, the first interface with the vagus nerve was approved by the FDA as a treatment for people with Epilepsy. This shows a clear picture of the incredible advances have been made in neuroscience during the last century and might show a glimmer of the possibilities in the future.

Between 1889 and now, incremental scientific discoveries exposed the importance and complexity of the sensory nervous system. Quickly after Cajal's discovery, Camillo Golgi

described the Golgi tendon organ in 1896, followed by the discovery of the ruffini endings by Ruffini in 1898. Although the muscle spindle structure was described by Hassal in 1851, Kerschner was the first to suggest that it was a sensory receptor in 1888. This was later confirmed in 1894 when Sherrington described how muscle spindles remain intact in muscles from which all motor fibers have been removed by degeneration after cutting the ventral roots. He could therefore conclude that muscle spindles are innervated by fibers connecting to the dorsal roots of the spinal cord and are therefore related the sensory nervous system [101].

Electric fields resulting from muscle activity and stretch had been described since the second half of the eighteen-hundreds. However, nobody had recorded the response from single afferent fibers until 1926 [57]. That year, Adrian and Zotterman recorded from frog's sciatic nerve and showed that by sectioning part of the muscle, they could isolate a single afferent neuron [1]. They concluded that: 1) the afferent firing rate was a function of the muscle load, 2) There is an all or nothing response by the neuron and 3) There is adaption of the neuron's excitability which they attributed to a change in the refractory period [2]. Adrian and Sherrington would receive the Nobel Prize for their work on the function of neurons in 1932.

The term proprioception was first coined by Sherrington in 1906 to indicate the awareness of movement from afferent information [102]. It originates from the integration of afferent inputs in the central nervous system (CNS), provides vital information about the state of the limb during movement and serves as feedback during motor control to create stable and accurate movements. Although the exact pathways leading to movement perception are not fully understood, science is continuously trying to understand the underlying sensory system.

During the 1950's, the mechanisms responsible for the discrete responses from the sensory neurons were unraveled when intracellular recordings enabled Hodgkin and Huxley to perform their famous work on the giant axon of squid [49, 48]. Their discoveries have since been the foundation of a plurality of modeling the nervous system at a cellular level [74].

Research by Adrian and others laid the foundation for more detailed analysis of the function of the sensory nervous system in later years. Leading into the second half of the century, technological improvements lead to increasingly accurate data on afferent behavior,

the ability to record from multiple neurons simultaneously and the realization that targeted stimulation of neurons could evoke sensory perceptions [104]. Continuing today, research is being conducted to understand the role of the sensory nervous system in our everyday life and how we can utilize the information that the sensory nervous system provides in devices aimed at restoring extremity functionality in physically impaired people.

1.1.2 Firing rate properties of primary afferent neurons

This section will discuss some of the firing rate properties of primary afferent neurons. Insight in the firing rate response of primary afferent to kinematic perturbations will be used in later chapters as a basis for algorithms to estimate limb kinematics.

1.1.2.1 The muscle spindle In contrary to earlier beliefs that the muscle spindles are the only sensory receptor involved in proprioception, the current thought includes other afferent types as contributors to proprioception. However, the muscle spindle is still thought to be the main contributor [35]. An example of muscle spindle response to passive kinematic movement is shown in figure 1. Here, the limb was manipulated through a series of ramp and hold patterns in different directions. The cartesian coordinates of the metatarsophalangeal joint and the instantaneous firing rate of six muscle spindle afferents are plotted over time.

Various models with increasing complexity have been proposed for the muscle spindle firing rate [68, 51, 80, 82, 66, 72]. These models are able to provide accurate predictions of spindle firing rates as a function of muscle length and presumed gamma drive inputs. A thorough classification of the muscle spindle and the afferents innervating the sensory receptor was described as early as 1963 by Matthews. He identified two groups of afferents originating from the muscle spindle; group 1 afferents (primary endings) and group 2 afferents (secondary endings). In addition, he described two efferent fibers innervating the spindle; γ_1 motor neurons and γ_2 motor neurons [68].

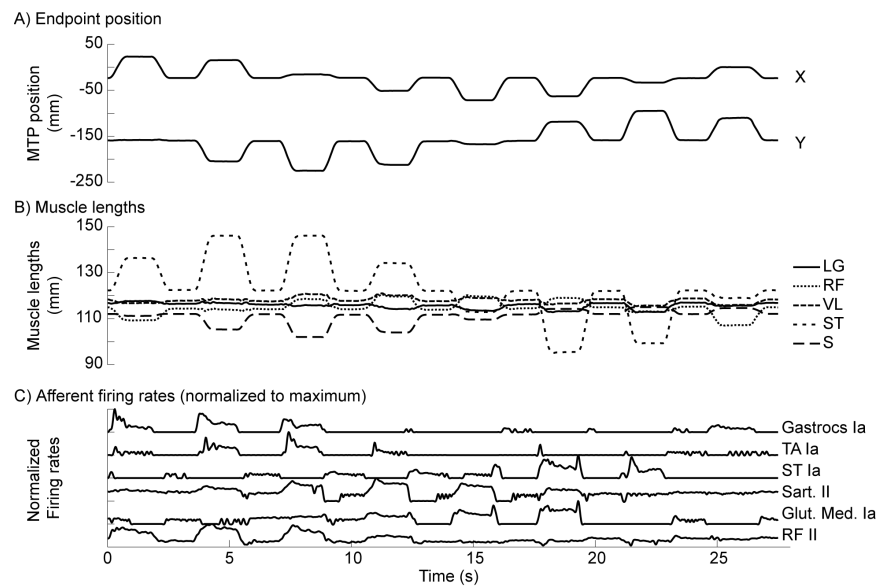


Figure 1: Example firing rates of primary afferents during passive movement. A) Cartesian coordinates of the metatarsophalangeal joint B) Muscle length estimates using the Goslow model [40] C) Instantaneous firing rates of 6 primary afferent neurons

In 1969, Matthews and Stein discussed the muscle spindle firing rate in terms of its response to sinusoidal muscle stretch and concluded that muscle spindle response is definitely non-linear in contrast to beliefs at the time [69]. In addition, there experiments showed that muscle spindle output could significantly be increased when they stimulated the γ - motor neuron innervating the spindle [69].

More recent work investigating the properties of the muscle spindle suggests that the classification between two types of γ - motor neurons might be too simple and more work is needed to understand the system [113, 72]. Mileusnic et al. presented the most complex muscle spindle model in 2007. Their model consists of 22 model parameters and is a clear demonstration that muscle spindle modeling is still a daunting task [72].

Alneas et al. found that background fusimotor activity in spinalized cat marked an increase in the dynamic frequency of the firing rate of the primary muscle spindle neurons but only slightly increased their response to static extensions [3]. The neural basis for gamma motor drive has been topic for discussion for many years and various hypotheses have been put forward. Prochazka et al. compared muscle spindle response in freely moving cats with those recorded under anesthesia and found that gamma drive is likely set by the CNS to different levels depending on the performed task [83]. A similar conclusion was reached by Taylor et al. in 2000 when looking at decerebrate preparations [113].

A muscle spindle neuron can easily be detected from a neural pool of afferent responses by its combined dynamic and static components of the firing rate response during a ramp and hold flexion and extension of the muscle. In addition, an intravenous injection of succinylcholine will temporarily paralyze the muscles while increasing the muscle spindle response [87, 114]. Figure 2 shows an example of a muscle spindle response during flexion/extension of the muscle during a succinylcholine injection. At the beginning of the trial, the succinylcholine is administered intravenously and the instantaneous firing rate of the muscle spindle is plotted for the following 10 minutes. It can be seen clearly that the instantaneous firing rate of the neuron increases after administration of the drug and that the effect diminishes over time. In addition, we can see the difference between the dynamic and static contributions of the instantaneous firing rate increases (dynamic index) which is a well described phenomenon [87].

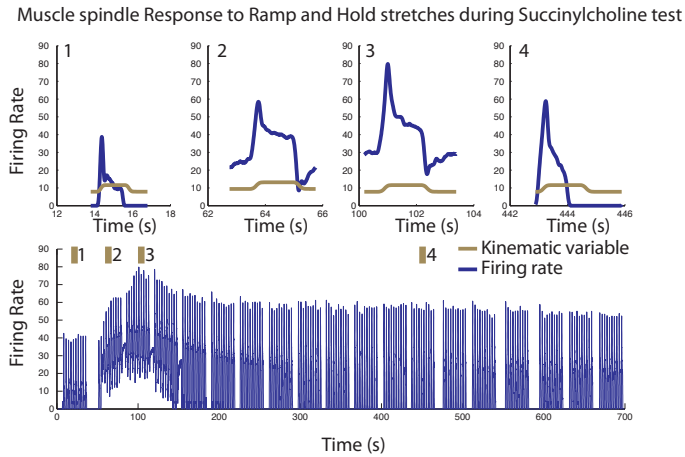


Figure 2: The response of a muscle spindle to succinylcholine during ramp and hold flexion and extension of the left hindlimb in cat. The muscle spindle response was recorded by the author in the L7 dorsal root ganglion under Isoflurane anesthesia. The first row of figures are expanded sections of the data in the bottom figure. The numbers correspond with the associated sections in the lower figure. In each figure, the ramp and hold trajectory is displayed as well as the instantaneous firing rate of the primary afferent. The bottom figure shows the instantaneous firing rate of the neuron over the duration of the trial.

1.1.2.2 Other afferent neurons Although most focus has been on the behavior of muscle spindles, it has been shown that other afferents, and in particular cutaneous afferents, contribute to the sense of proprioception [33]. For example, Collins and Prochazka showed that electrical stimulation as well as skin stretch of the back of the hand can induce illusions of movement [25]. The importance of cutaneous afferents on motor control during walking was confirmed in rat [116] and cat [14, 15] as the animals showed altered walking behavior in its absence.

There are a number of different cutaneous receptor types which all have much simpler characteristics than the muscle spindle as they are not innervated by any γ -motor neurons. Although these sensors directly convey information about pressure and skin displacements, they will indirectly signal information on global limb state due to the mechanics of the extremity. For example, Haugland et. al. used compound afferent cutaneous information to determine gait phase using a nerve cuff placed on the Sural nerve [45]. In addition, given the premise that some cutaneous receptors modulate their response in a consistent way with skin stretch, it is feasible that when the extremity is moved through its range of motion, the firing rate of these neurons correlates with the global kinematic variables.

The Golgi tendon organ (GTO) is another sensory receptor of interest to proprioception. As the GTO is located between the insertion point and the muscle belly, its firing rate response is primarily correlated with muscle strain and lacks the dynamic response characteristic for the muscle spindle [73]. In addition, as muscle spindles are located in series with the muscle, they only respond when under sufficient strain. During passive movement of the extremity, these afferents are therefore most active at the extreme extension/flexion of the joints as there is little muscle tone [34, 4].

It can be argued that specific knowledge about the origin and class of the recorded neurons is useful for decoding purposes. Indeed, if we knew exactly what was encoded by the neuron and we knew exactly where the neuron was recorded, we could include this knowledge in the decoding strategy. However, DRG recordings are often very noisy recordings and many channels can only be classified as multi-unit activity. Therefore, a more general approach is utilized in this thesis which infers the properties of the recorded neurons from a training data set and models its behavior accordingly.

As we are interested in kinematic trajectories which are defined by position and velocity of the limb segments, we aimed to extract these variables from the neural afferent firing rates. This does not imply that the primary afferents only encode for these variables, but we are only interested in these variables for the aims specified in section 1.3.

1.1.3 Proprioceptive coordinate frame

There are different opinions about the reference frame the CNS uses for proprioception [13, 12, 11]. In order to use afferent information as part of a neuroprosthetic controller, one needs to identify the kinematic reference frame in which interesting information is encoded. Previous efforts have focussed mainly on endpoint kinematics and joint angle reference frames.

At the DRG level of the afferent pathways, sensory integration is non-existing as the recorded signals are the direct response of the sensory units. However, as the global kinematic variables are linked to the sensory afferent intrinsic response characteristics, we can infer information about global kinematic variables when we look at populations of these primary afferent neurons.

Although coordinate frames are interesting from a decoding point of view, it is far more difficult to determine the proprioceptive strategy of the CNS based on the primary afferent responses. For instance, it is possible that the CNS processes afferent information in a non-orthogonal, non-linear and highly redundant manner [98]. Scott et al. also found that the distribution of muscle spindles in human extremities do not favor any particular coordinate frame [98].

Because of the intrinsic properties of the extremity, all suggested coordinate frames are correlated. To investigate this relationship and the effects on the accuracy of linear regression, we compared the musculo-skeletal model proposed by Goslow et al. [40] (see figure 1), endpoint and joint angle coordinate frames using regression methods proposed in [106, 122].

Figure 3 shows the R^2 - values of the fitted models $Y = a_0 \sum_{i=1}^k a_i F_i$ with Y being the kinematic variable (position or velocity) and F_i being the instantaneous firing rate of the

i -th afferent neuron (results are based on data from a single animal). See section 2.2.2 for a detailed description of the method. During a random movement trial (see 3.2.2), kinematics and neural data were recorded. For each kinematic variable, the neuron with the highest correlation was selected and the R^2 -value was found (black bars in figure). Subsequently, neurons were added to the model as long as each consecutive neuron added $> 1\%$ to the R^2 value. The number on top of each bar indicates the number of neurons included and the total length of the bar is the resulting R^2 -value of the model.

We can see that the same population of neurons can represent kinematic variables in various coordinate frames and that position tends to be better represented than velocity. This seems to agree with results presented by Weber in 2007 although these results were observed during awake behaving animals [123]. Note that we are only looking at linear models and that we cannot make any conclusions about how the CNS interprets these signals.

Innervating of the muscle spindles by γ -motor neurons have raised various theories about the coordinate frame that is represented by the firing rates of these neurons. It is widely accepted that the muscle spindle firing rate is directly correlated by the muscle fiber stretch and stretch velocity when gamma-motor activation is held constant (see section 1.1.2.1). However, modulation of the gamma-drive during active movement of the extremity could potentially result in a reference frame change. Muscle spindle behavior in freely moving cats have shown large changes in the responsiveness to limb kinematics depending on the type of movement. This suggests that the fusimotor action can be independently set by the CNS depending on the motor control task at hand [83]. Therefore, we can deduct that γ activity is not used to statically transform coordinate systems. This is confirmed by human microneurography studies that showed that γ -motor neuron activity is modulated by attention [88, 50]. Ribot-Ciscar et.al. found that when the subject was asked to focus on the final position in a reach task, the muscle spindle activity increased sensitivity to position and decreased sensitivity to velocity components [88].

In absence of significant γ fluctuations during motor task, muscle spindles are known to responds to stretch and stretch-velocity components of muscle. A simulation study was performed to quantify the ability to infer global kinematic variables from muscle length information. Thereto, we modeled the muscle lengths as a linear function of global variables

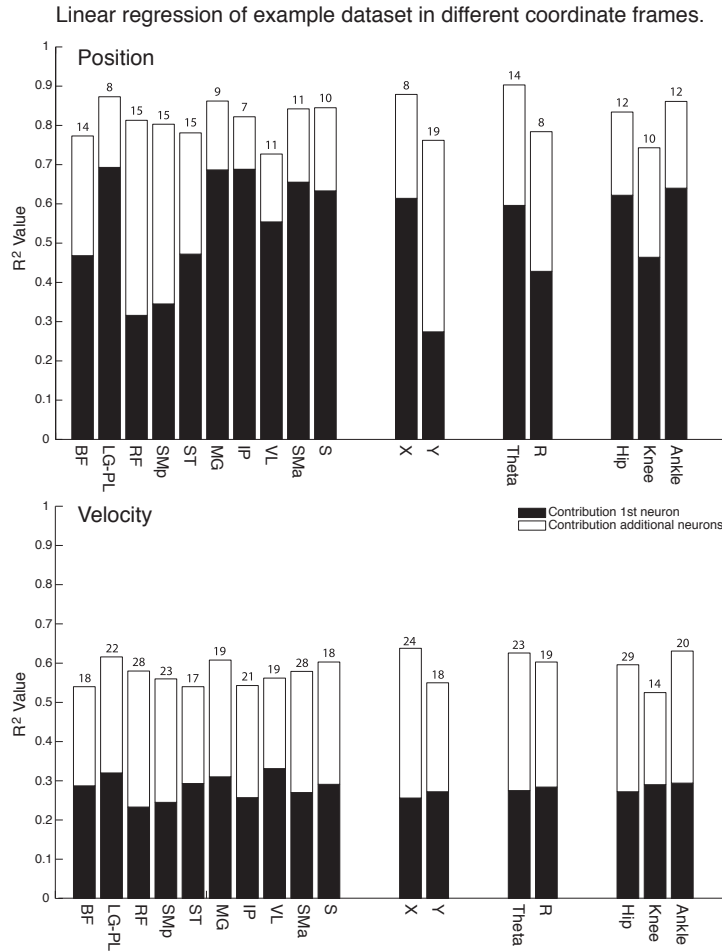


Figure 3: R^2 -values indicating the amount of variability explained by the neural data. The black bars indicate the efficiency of the best neuron, the white bars indicate the efficiency using multiple neurons. The best n neurons were selected per kinematic variable based on their added value to the decoded variable.

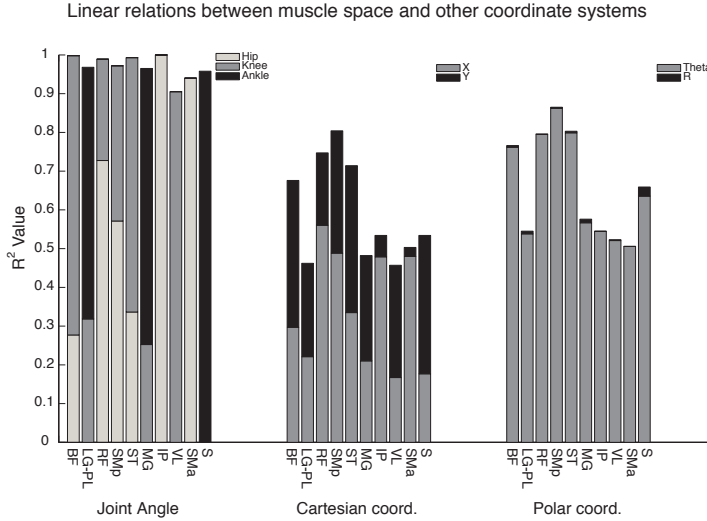


Figure 4: The goslow muscle model [40] compared to other coordinate frames. A simulation modeled various global kinematic variables onto the muscle lengths provided by the goslow model. The R^2 value is based on the fitted data of the model.

(joint coordinates, cartesian endpoint coordinates and polar endpoint coordinates). Goslow’s musculo-skeletal model was used to generate simulated kinematics throughout the range of motion of the hindlimb of cat [40]. Figure 4 shows the resulting R^2 values after fitting each muscle length as a linear function of the global variables. It is clear that joint angles are more linearly related to muscle length than endpoint kinematics.

This figure shows that the joint angles are closest related to the muscle length coordinate frame. If we assume that muscle spindles are primarily responsible for generating proprioception, it is likely that the firing rate of muscle spindles are best modeled with joint angles as the global kinematic variables. Similar results were shown in Stein et al. 2004 [106].

In summary, suggestions about the implementation of coordinate frames for proprioception in the CNS has been a topic of discussion over the past 20+ years. It has been shown that activity in higher areas of the CNS related to motor planning can be describe in terms of polar coordinates of the endpoint [75, 94, 38]. Although the direct response characteristics of primary afferents are well documented and thoroughly described (see section 1.1.2), the in-

herent kinematic correlations of the extremity result in the ability to infer global kinematics at the level of the primary afferents. Sensory integration of these signals can further result in a global representation of limb kinematics in higher regions of the CNS [105, 98, 12, 11].

1.1.4 Role of somatosensory afferents in regulating motor output

As previously mentioned, the exact role of somatosensory afferents in motor control remains unsolved. However, ever since the discovery of the ‘simple reflex’ by Sherrington in the early 1900’s, it has been clear the somatosensory afferents have a direct impact on motor control.

The increased firing rate of muscle spindles during stimulation of the γ - motor neurons has resulted in different ideas on the role of sensory integration in motor control [69]. Several suggestions were proposed to explain the purpose of the γ drive including the ‘follow-up length servo’ and the direct servo mechanism. Although these claims have since been disputed, no concluding understanding exists about the strategies underlying the fusimotor system and γ -motor drive [83, 113].

A relatively recent review on the effects of afferent input in locomotion revealed that cutaneous afferents as well as muscle afferents influence the locomotion pattern generated at the spinal cord level [90]. Removing cutaneous inputs from the hindlimb in cat will not prevent the animal from walking on a treadmill. However, when walking on a horizontal ladder, the animals were not able to place their feet on the rungs during the first 3-7 weeks following de-afferenting the extremity. Although the animal regained the ability to perform this task, the walking behavior never went back to normal [15, 14]. In addition, when spinalized, the regained walking behavior disappeared and the animals were no longer capable of correctly placing their paws on the rungs in contrast to spinalized animals with intact cutaneous afferents. The role of cutaneous afferent input thus appears to be crucial for the expression of locomotion and recovery of locomotion after spinal cord injury [90].

Proprioceptive control of movement is thought to depend on the co-operation of sensory neurons from multiple modalities such as muscle spindles, joint and cutaneous afferents [37]. Gandevia et. al. also found evidence that motor commands contribute to proprioception. In experiments where the subjects were asked to match wrist angle in the absence of vision,

they found that the subject perceived movement of the wrist even in the case where the joint-muscles were paralyzed and anesthetized [36]. It is therefore clear that proprioception and motor control are tightly interwoven which is reinforced by the knowledge that there are many connections between motor- and sensory cortex.

1.1.5 The impact of spinal cord injury to primary afferent response

The short and long term effects of spinal cord injury on primary afferent firing rate response is not well documented although multiple hypotheses have been brought forward over the years. Muscle spindles are modulated by static and dynamic γ -motor neurons during intact behavior. Studies in acute decerebrate and spinal cats showed that static and dynamic gamma drive is still present in the preparations and could be measured independently during pharmaceutically induced walking. In both preparations, muscle spindle activity was increased after onset of the locomotion with a decrease in stretch reflex sensitivity [7]. This suggests an increase in static gamma drive during walking. There have not been any studies that have looked at the long term property changes of muscle spindles after spinal cord injury.

Arutyunyan described muscle spindle response to chronic de-efferentation in 1981 [6]. He found that the sensitivity of the muscle spindles increase over time and attributes this to atrophy of the de-efferented muscles. These findings do not necessarily compare to those in spinal cats. In 1965, Alnaes found that the dynamic fusimotor system is largely driven by spinal mechanisms initiated by afferent inputs and that the static gamma drive is mediated by descending tracks from higher brain regions based on dorsal root recordings in spinalized and decerebrated cats [3].

Spasticity with associated hyper-reflexia is a common complication after spinal cord injury where hyper-reflexia is defined as an increased excitability of the velocity-dependent stretch reflex. Although it was previously believed that a decreased inhibition of fusimotor drive was inherent to the increase in reflexivity, nowadays, it is thought that different mechanics, such as recurrent inhibition of motoneurons and/or a reduced presynaptic inhibition of Ia afferents, are involved in this behavior [76]. Qualitative results of upper extremity

spindle responses in unilateral cerebral stroke patients with spasticity seem to confirm these beliefs. They show no difference in muscle spindle behavior with respect to healthy control subjects suggesting that the fusimotor system does not contribute significantly to the hyper-excitability of the stretch reflex [125].

1.2 USING AFFERENT INFORMATION FOR NEURAL PROSTHESES

Neural prostheses relying on neural signals for control require a stable interface with the nervous system. The type and location of the interface determines the types of signals that can be processed. This section will discuss some of the uses for afferent neural interfaces and give a brief summary on currently used electrodes used to interface with the nervous system.

1.2.1 Using primary afferent or external sensors?

For FES-based neural prostheses, one can question whether using afferent information to infer limb kinematics has sufficient advantages over externally placed sensors that it justifies the associated invasive surgical procedures. Depending on the application and complexity of the neural prostheses, the answer might differ. For example, compensating foot-drop during gait using FES can well be addressed by using a simple foot-switch [22]. However, when we increase the number of variables we are interested in, using external sensors likely results in problems with usability and reliability.

Using primary afferent information to decode the limb state can also potentially be favorable as the DRG can be used as a centralized access point for recording sensory information throughout the extremity. The alternative of multiple external sensors is practically difficult to achieve. It is my opinion that extracting information from primary afferent neural activity for the use in neural prostheses will provide a better alternative than external sensors for complex FES-applications.

1.2.2 Sensorimotor control as a closed loop control system

Control of extremities in the intact person can roughly be seen as a closed loop controller. An intention is transformed into a set of instruction that activate synergies of muscles which in turn produce the necessary torques on the skeletal structure to produce movement. Sensory receptors in the musculo/skeletal plant as well as other sensory inputs relay information about the actual state of the limb back to the CNS. This information is used to adapt the instruction set to correct for errors and to provide perception to the person (figure 5).

When part of this control system is damaged, intention can no longer control movement without external aid of a neural prosthesis. Figure 5 distinguishes between two categories of damage; 1) The person has a spinal cord injury and is paralyzed in the extremity but has intact sensation 2) The person is amputated at the extremity. In both scenarios, a brain computer interface (BCI) is needed to translate intention into a command for the neural prosthesis, however the difference between the scenarios lays within the handling of the feedback loop.

Paralyzed muscles can be activated using functional electrical stimulation (FES). Feedback to the FES controller can be realized by intercepting the afferent pathways that carry the intrinsic feedback information to the CNS. This has the advantage over externally placed sensors in the sense that it requires less external hardware and has the potential to be accurate and reliable.

In amputees, the neural prosthesis includes the electrical/mechanical plant and feedback to the controller is therefore not an issue. The feedback that needs to be restored in this scenario is sensory information from the neural prosthesis to the CNS. One way of achieving this is to stimulate afferent pathways in order to mimic the natural response. In either case, it is necessary to understand the manner in which these afferents code proprioceptive information and, in case of paralysis, how that changes the way that this information is generated.

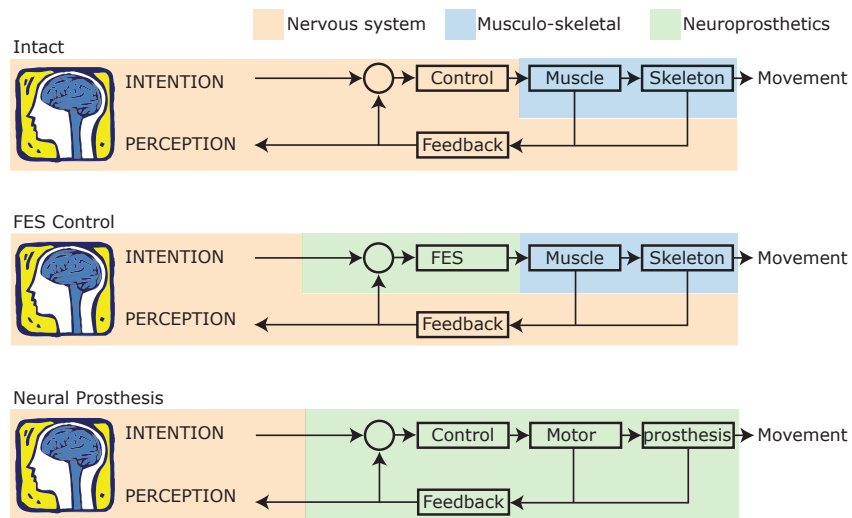


Figure 5: Schematic representation of motor control in three different scenarios. 1) Intact system 2) FES control for paralysis 3) bidirectional BCI for Amputees. Arrows that cross boundaries between domains indicate a translation of a signal between neural, mechanical and electric domain.

1.2.3 Neural interfaces

Electric discharges from muscle tissue and neurons have been recorded since the eighteenth century [57]. However, not until recently were we able to record from large populations of neurons simultaneously due to electrode fabrication and signal processing demands. These developments have enabled neuroscientists to analyze population responses in the nervous system and advanced the idea of a neuroprosthesis [121, 95]. In this section, the most commonly used electrode interfaces for neural interfaces are discussed. Because this field is rapidly expanding and progress is made continuously, I do not pretend, nor strive to include all actively used electrodes.

In 1992, Jones et al. published a method for manufacturing a glass/silicon composite intracortical electrode array (Utah-array, Blackrock Microsystems, Utah) which has since been the standard for microelectrode arrays (MEAs) [55]. Although the array was originally designed for intracortical recordings, it has been used in numerous studies in different levels of the nervous system in animal [77, 16, 115, 106] and human [47, 58] subjects. Some of the current developments using this type of array include new wafer fabrication technologies [8] and the development of a wireless version of the array [24].

NeuroNexus (Neuronexus technologies, Ann Harbor) has been a very successful spinoff company from the University of Michigan. They fabricate electrodes based on thin film MEMS processes which are much cheaper to fabricate than the previously mentioned Utah array [46, 59]. They typically contain 16-64 electrodes per probe and are better suited for recording activity at different layers in the brain as the recording sites are located along the insertion direction. Continuous advances in electrode design are aimed at reducing tissue encapsulation [100], drug delivery [99], and improvements in biocompatibility using specialized coatings [27].

Microwire arrays, fabricated by TDT (Tucker Davis Technologies, Alachua, USA) and MicroProbes (MicroProbes for Life Science, Gaithersburg, USA), are the third type of MEAs currently available and have been used for recording and stimulation studies in both acute and chronic experiments [99, 124]. Penetrating multi electrode arrays are currently the most viable and reliable solution for neural prostheses that require high specificity on multiple channels and are currently used by the Braingate and BrainGate2 projects to interface cortical areas in human [31, 96].

Intrafascicular electrodes can be used to do multiunit recordings of motor or afferent information in the peripheral nervous system.[70, 39, 61] In 1996, Yoshida et al. demonstrated that LIFE electrodes could be used in a closed loop FES system to control ankle flexion/extension. Here, LIFE electrodes were inserted in the common peroneal nerve and the tibial nerve to record afferent activity related to the ankle angle while a third LIFE electrode was placed in a fascicle of the tibial nerve innervating the medial gastrocnemius muscle for stimulation [132].

Non-penetrating interfaces include EEG, MEG, Nerve cuffs and ECoG arrays. Nerve cuffs have been used for recording and stimulation of peripheral nerves. Haugland used a nerve cuff to detect the start of the stance phase from the activity of the Sural nerve as a control for a foot-drop orthosis [45]. Other groups have proposed similar usage of nerve cuffs for gait detection which are well documented in the 2002 review on portable FES-Based Neural orthoses by Lyons et al. [65]. As the other interfaces are incapable of being used in the peripheral nervous system, they will not be discussed in this section.

1.2.4 Inferring limb state from afferent activity

Decoding information from neural populations has been investigated for a long time with, perhaps, its most appealing example being control of a robotic prosthesis using population decoding in motor cortex [38]. The work presented in this thesis utilizes an interface with the nervous system at the level of the DRG. This has three main reasons; 1) All recorded neurons in the DRG are, by definition, primary afferents 2) There is no integration of neuronal signals at this level and therefore the spatial/temporal resolution is very high and 3) The DRG are

easily accessible. When recording in the DRG, the afferent cell type can easily be classified as either a muscle spindle, tendon organ or cutaneous. In the proposed project, this information will be used to increase the accuracy of the prediction of kinematics.

Although a variety of models predict muscle spindle firing rate from the kinematic variables, it is inherently more difficult to invert these models to predict kinematics. Primary reasons for this are 1) Non-linear behavior of the muscle spindle and 2) Ambiguity of position and velocity components of the firing rate. To date, decoding efforts have not attempted to invert the muscle spindle models but rather have based the decoding on computing a weighted average of a population of neurons [105, 122, 106]. In this technique, a kinematic variable (Y) such as extremity endpoint, joint angle or their velocities is modeled by a weighted average of afferent firing rates (F) ($\hat{Y} = a + \sum_i b_i F_i$). It was shown that a limited number of neurons could provide accurate predictions of the kinematic variable. When decoding velocities, position could be inferred by integrating the output. However, despite the good predictions, this model fails when it comes to generalizability. When a different kinematic data set is used to train the model, accuracy quickly diminishes. In addition, the model tends to overestimate the kinematic variable during higher velocities due to the fact that the model is trained on a single kinematic parameter. We refer to this approach as ‘reverse’ regression since the natural relationships between the dependent and explanatory variables are reversed. Chapter 2 and 3 will provide more details on the classification of ‘reverse’-regression as well as indicate some of the problems that occur as a result of this reversal relationship.

The next two chapters of this thesis propose new decoding methods to extract kinematic information from primary afferents. These methods consists of modeling the firing rates of the primary afferents as functions of the kinematic parameters, and inverting these models via a state-space procedure to decode simultaneously all limb kinematics. Preliminary results were presented in [119] and an extension of these methods was proposed in Wagenaar et al (2009). We compared the efficiencies of the resulting estimates with those predicted using reverse regression [106, 122] and discuss the feasibility of using natural feedback decoding in neuroprostheses. The results of these studies are described in later chapters of this thesis.

Finally, the coordinate frame in which limb kinematics are decoded has typically been based on polar coordinates of the endpoint of the limb or the individual joint angles [123, 12]. Scott et al. (1994), found no evidence for a particular coordinate frame based on modeling studies of muscle spindle distributions [98]. Stein et al. (2004), also found no significant difference in correlation coefficients when comparing PA firing rates to kinematic state in polar endpoint coordinates and joint angle space [123, 106]. We included both endpoint and polar coordinates in the analysis of this paper since both representations are relevant for implementation in neural prostheses. In 1998, Prochazka described the possibility to decode muscle lengths from primary afferent firing rates by inverting the firing rate models [82]. However, the manuscript does not elaborate on the methods which were used and if these were actually decoded trajectories from a single or multiple neural responses.

1.2.5 Closed-loop control of FES using natural sensors

In applications where functional electrical stimulation (FES) is used to restore limb functions such as gait, posture or foot drop, it is important to provide feedback information to the controller in order to be able to cope with perturbations, muscle fatigue and non-linear behavior of the effected muscles [67, 126, 123]. Accessing and decoding the activity in native afferent signaling pathways can be a natural way to determine the kinematic state (i.e. position and velocity) of the controlled extremity [44]. Feasibility of this approach has been demonstrated by controlling the ankle angle in a closed loop controller using the compound afferent input recorded from LIFE electrodes by Yoshida [131]. Micera et al. used nerve cuffs, implanted around the Peroneal and Tibial nerve ,to infer ankle angle estimates using neuro-fuzzy network decoding algorithms [71].

The methods used by Yoshida and Micera predicted a continuous representation of a single kinematic variable from the neural data. Although this might be sufficient for simple closed loop FES controllers, it is likely not specific enough for a complete neural prosthesis. For continuous predictions of multiple variable relating to the kinematic state of the extremity, one needs to record from a larger and more diverse population of primary afferents to attain a more complete estimate of limb state. One solution is to record at the dorsal

root ganglia where all proprioceptive information converges into the central nervous system. Recording at this site with multi-electrode arrays grants access to a wide variety of state information distributed across many individual neurons [106, 122, 123].

Instead of a continuous representation of limb kinematics, one could implement closed loop control using an event based classification system as suggested by Borisoff et al. [10]. Although this work was triggered by closed loop FES for bladder control [54], it could easily be extended to specific kinematics states of the extremity. Using classifiers instead of continuous estimates of limb state could provide a couple of advantages. In example, if stimulation parameters for FES should be changed depending on a certain threshold in the limb kinematics, classifiers might be better predictors of this threshold than continuous decoders. Section 6.2 of this thesis will elaborate a little further on the use of classifiers for closed loop FES systems. The rest of this thesis is focussed on continuous decoding of limb kinematics and the use of firing rate models to infer these variables.

In summary, it is widely recognized that a FES system would benefit tremendously from sensory feedback in terms of adaptability and functionality as long as the feedback system would be reliable [79, 67]. Using closed loop control of FES, it is possible to change the stimulation parameters dynamically depending on the feedback from the sensors. When accurate predictions of limb state are available to the FES controller, it will be able to compensate for muscle fatigue and external perturbations.

1.3 SPECIFIC AIMS

This section describes the specific aims addressed in this manuscript. Each specific aim is discussed in a separate chapter following this introduction.

1.3.1 Direct decoding of primary afferent neuron firing rates

In this aim, we propose a new method for decoding primary afferents by modeling the firing rate of each recorded neuron to infer limb state variables. We hypothesize that direct

regression will improve the decoded trajectories as it correctly models the observed firing rates and can take into account the multivariate response of an individual neuron.

- Hypothesis: Direct regression using non-linear firing rate models improves limb kinematic estimates over currently used reverse regression methods.

1.3.2 State-space decoding of primary afferent neuron firing rates

The previous aim confirmed the fact that it is possible to estimate limb position from afferent recordings using direct linear regression techniques. However, the dynamic muscle spindle response mediated by limb velocity is not incorporated in those linear models. The focus of this SA is to develop non-linear models to include both position and velocity information from muscle spindles to resolve the ambiguity of position and velocity contributions in the afferent firing rate models. In addition, contrary to currently used decoding algorithms, the decoding models will be able to predict multiple kinematic parameters, such as joint angles, simultaneously, thus finding the best prediction of the limb kinematics rather than treating each variable as independent.

- Hypothesis 1: State-space decoding will be able to take into account the kinematic constraints of the extremity and improve decoding accuracy using this information.
- Hypothesis 2: Including the derivatives of the kinematic variables to the firing rate models will result in more accurate predictions of limb kinematics.

1.3.3 Improved decoding techniques for realtime applications.

In order to utilize the decoding techniques in a realtime FES application, non-linear models will be implemented in a real-time setup which will enable the use of these decoding techniques in a neural prosthesis environment. Although the decoding methods described in the previous specific aims produce accurate results, the decoding speed is insufficient for any realtime application. In this specific aim, non linear methods are described that are capable of predicting limb kinematics in ‘real-time’.

- Hypothesis: Alternative methods using non-linear reverse regression methods can improve limb kinematic decoding accuracy while continue to be able to be implemented in a ‘real-time’ environment.

1.3.4 Closed loop FES using primary afferent response as feedback

Mechanical sensors have proven difficult to implement in prostheses due to their unreliability, fragility and other practical difficulties. Most FES systems use open-loop controllers as a result of these limitations. However, a closed-loop feedback controller will increase the adaptability and stability of the FES system. Specific Aim 4 will focus on developing a controller for FES-evoked closed-loop walking. This will be implemented using a finite state controller, alternating between states based on the estimated limb state as provided by the neural decoder. By closing the loop, we hypothesize that the controller will be able to generate reliable walking behavior under various conditions.

- Hypothesis 1: Primary afferent firing rates can be used to predict limb kinematics during functional electrical stimulation.
- Hypothesis 2: Estimates of limb state can be used to control functional electrical stimulation in a closed loop state feedback mechanism.

2.0 IMPROVED DECODING OF LIMB-STATE FEEDBACK FROM NATURAL SENSORS

The contents of this chapter are published as: “Improved decoding of limb-state feedback from natural sensors” which was published in Conf Proc IEEE Eng Med Biol Soc, 1:42069, 2009, ©[2009] IEEE [119]. It covers specific aim 1 of this thesis and describes an alternative to previously suggested methods for decoding limb kinematics from primary afferent firing rates.

2.1 INTRODUCTION

During movement, proprioceptors constantly assess and relay sensory information about the physical state of the peripheral musculature to the central nervous system (CNS). This feedback allows the CNS an indication of the actual state of the limb and consequently to adapt motor drive in order to realize stable and efficient movements. When functional electrical stimulation (FES) is used to restore action to paralyzed limbs, a similar feedback mechanism is required for executing complex movements and adapt for perturbations or fatigue of the muscles. Accessing and decoding the activity in native afferent signaling pathways would be a natural way to determine the kinematic state (i.e. position and velocity) of the controlled extremity [131]. Our initial goal is therefore to predict/decode the kinematic state of the leg using the ensemble activity of primary afferent neurons, recorded with arrays of penetrating micro-electrodes in the dorsal root ganglia (DRG).

Previously, reverse regression methods were used to estimate limb kinematics from ensembles of simultaneously recorded primary afferent neurons in the dorsal root ganglia of

anesthetized [106] and alert, locomoting cats [123]. However, direct regression methods are more efficient and flexible than reverse regression approaches. Direct regression methods include population vectors [38], optimal linear estimators [92], maximum likelihood [20], Bayesian [93] methods, and filtering/dynamic Bayesian methods [133]. See [19] for a review and references therein. Our goal for this paper is to determine if the simplest likelihood method can improve upon reverse regression to decode limb position from the spiking activity of a small ensemble of primary afferent neurons.

2.2 METHODS AND DATA

2.2.1 The experiment

Center-out patterns in a 2-dimensional plane were imposed on the hind limb of an anesthetized cat by a robotic arm (figure 6:b). These movements spanned a significant part of the range of motion for the limb. See Stein et al. [106] for complete details.

The ankle (A_1), knee (A_2), and hip (A_3) angles of the hind leg were recorded at 120 Hz with a high speed video capture system using markers placed at the Iliac Crest (IC), Hip, Knee, Ankle and Metatarsophalangeal (MTP) joints (figure 6:c). Figure 7 shows the recorded joint angles of knee and ankle as functions of experimental time during one trial of the experiment. The trials were repeated to create separate data sets for model fitting (i.e. encoding) and testing (i.e. decoding).

Primary afferent neurons were recorded using penetrating microelectrode arrays with 50 and 40 electrode sites (5x10 and 4x10, 400 μ m spacing). The arrays were inserted in the L7 and L6 dorsal root ganglion using a high velocity inserter. The neural signals were acquired with a sampling frequency of 30 kHz and bandpass filtered with cutoff frequencies of 100Hz - 3000Hz. Spikes were sorted offline via cluster analysis; figure 6:a shows the raster plot of the spike trains of 15 neurons. We then smoothed the spike trains using a one-sided normal distribution kernel with SD 0.15 sec. We denote by FR_i the resulting firing rate of neuron i .

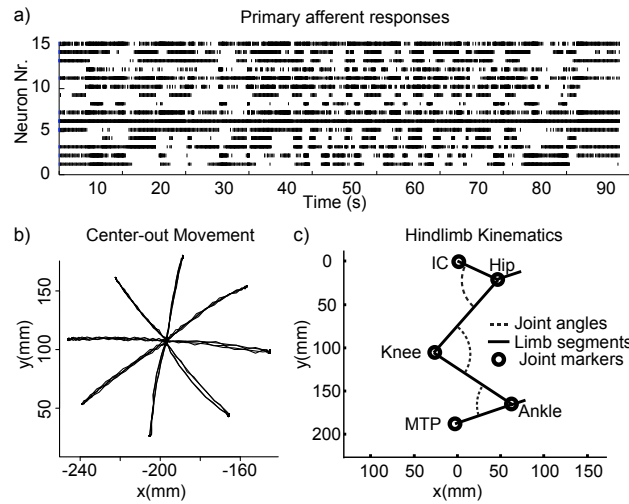


Figure 6: ©[2009] IEEE, a) Responses of different neurons to passive movement of the leg. Each vertical line represents an action potential. b) The endpoint kinematics of the hindlimb during passive center-out movement. This movement is imposed on the hindlimb using a robotic manipulator. c) Schematic of the hindlimb; joint angles are being decoded to represent the kinematic state of the limb.

2.2.2 Reverse regression

Reverse regression/correlation was used previously to estimate angular positions and velocities for the hip, knee, and ankle joints [122, 106]. The “reverse” describes the reversal of the natural roles played by the stimulus and spike-activity response. Although in reality, it is the neural activity that varies as a function of joint angular position, reverse regression treats the firing rates as if they were the inputs (the x ’s in regression notation), while the joint angles are considered the output (the Y variable). That is, the joint angles A_k , $k = 1, 2, 3$, are expressed as

$$A_k = \beta_{k0} + \sum_{i \in S_k} \beta_{ki} FR_i \quad (2.1)$$

where FR_i is the firing rate of neuron i , and S_k indexes the set of neurons whose firing rates correlate most strongly with A_k [106]. Then given a training set of angles and firing-rate combinations, one computes the usual least-squares estimates $\hat{\beta}$ of the β ’s; this step is usually referred to as encoding. In the decoding stage, given the firing rates FR_i^* of all neurons in a small window of time, the predictor of joint angle k is then

$$A_k^* = \hat{\beta}_{k0} + \sum_{i \in S_k} \hat{\beta}_{ki} FR_i^*$$

To allow for the possibility that the relationships between neurons’ firing rates and joint angles are not linear, we will consider in place of Eq.2.1 the more flexible non-parametric generalization

$$A = \beta_0 + \sum_{i=1}^N s_i(FR_i)$$

where the $s_i(\cdot)$ are taken to be moving lines with 4 non-parametric degrees of freedom (DOF).

2.2.3 Direct regression methods

Direct regression methods include population vectors, optimal linear decoding, as well as likelihood-based and dynamic decoding. Firing rates are considered random variables whose

distributions, often just the means, vary with joint angles. Assuming that firing rates are approximately normal with constant variances σ_i^2 , the simplest relationship one could consider for neuron i is

$$FR_i = \alpha_{0i} + \alpha_{1i}A_1 + \alpha_{2i}A_2 + \alpha_{3i}A_3 + \sigma_i^2\epsilon_i, \quad (2.2)$$

$i = 1, \dots, N$, where ϵ_i are standard normal random errors. Note that Eq. 2.2 specifies one relationship per neuron, whereas Eq. 2.1 specifies one relationship per angle. Then given a training set of angles and firing-rate combinations, encoding consists of computing the maximum likelihood/least-squares estimates of the α_{ji} and σ_i^2 . In the decoding stage, the observed firing rates FR_i^* of all neurons in a small window of time are each assumed to have distributions specified by Eq. 2.2, where the α_{ji} and σ_i^2 are now taken to be equal to their estimates from encoding. The predictor of joint angle is then the least square/maximum likelihood estimate of (A_1, A_2, A_3) obtained from the set of N models in Eq. 2.2, $i = 1, \dots, N$.

Eq. 2.2 is the simplest firing rate model we could consider. To allow for non-linear relationships between firing rates and angles, we will instead use $s_{ji}(A_j)$ in place of $\alpha_{ji}A_j$, $j = 1, 2, 3$, where $s_{ji}(\cdot)$ are splines with 4 non-param. DOF. Our model will also include interactions between pairs of joint angles, to allow for the possibility that relationships between firing rates and a particular angle vary with another angle. The data supports this possibility, as illustrated by Figure 8. We also considered hind limb biomechanics and physiology to guide our choice of physiologically plausible firing rate models: muscle afferents (i.e. primary and secondary muscle spindles, tendon organs) encode maximally two out of the three joint angles (bi-articulate muscles span either hip/knee or knee/ankle). Therefore, each neuron is modeled to encode either for one angle (hip, ankle or knee), or for two angles (hip and knee or ankle and knee). That is, for each neuron i , we considered the two families of firing rate models

$$FR_i = \alpha_{0i} + s_{ji}(A_j) + s_{ki}(A_k) + s_{ji}(A_j) : s_{ki}(A_k) + \sigma_i^2\epsilon_i, \quad (2.3)$$

for $j, k = 1, 2$ (ankle/knee) and $j, k = 2, 3$ (knee/hip), where $s_{ji}(A_j) : s_{ki}(A_k)$ denotes an interaction between angles j and k , and within these two families of models, we determined the statistical significance of each term using the Bayesian information criterion (BIC) and selected the best model based on this measure.

2.2.4 Contrasting methods

Direct regression offers several theoretical advantages over reverse regression. In direct regression, all angles are allowed to contribute to explaining the firing rates of each neuron, whereas in reverse correlation, angles are each decoded separately, using different groups of neurons. From a physiological view point, direct regression is more appropriate because Eq. 2.2 attempts to model how each neuron encodes joint angles, whereas there is no physiological basis for Eq.2.1.

From an efficiency view point, if all neurons encoded single joint-angles, both methods should predict approximately similar trajectories. As most muscles span multiple joints, responses from muscle afferents code for multiple angles simultaneously. Fig. 8 shows an example of a neuron whose firing rate depends not only on the hip angle but also on the knee angle. Reverse regression decodes each angle separately so it cannot properly extract the information in firing rates about several angles. In contrast, direct regression makes efficient use of this information provided the firing rate model in Eq. 2.3 is accurate. For example, if one of the joint angles is consistently better represented in the afferent data set, the weaker contributor will be poorly estimated by a reverse regression method. On the other hand, direct regression combines the information of strongly and weakly encoded angles to improve the prediction of both.

2.3 RESULTS

We first selected the best 25 neurons, encoded using the first center-out movement sequence of the experiment, and decoded with the second center-out movement trial. Fig. 7 shows true knee and ankle trajectories, along with the decoded trajectories using reverse and direct regression. Ankle and hip angles gave similar results so we do not show the latter. The two decoding methods produce visually comparable results.

The integrated squared error (ISE) provides a more quantitative assessment of efficiency. For a particular data set, the ISE is the squared difference between the decoded and actual

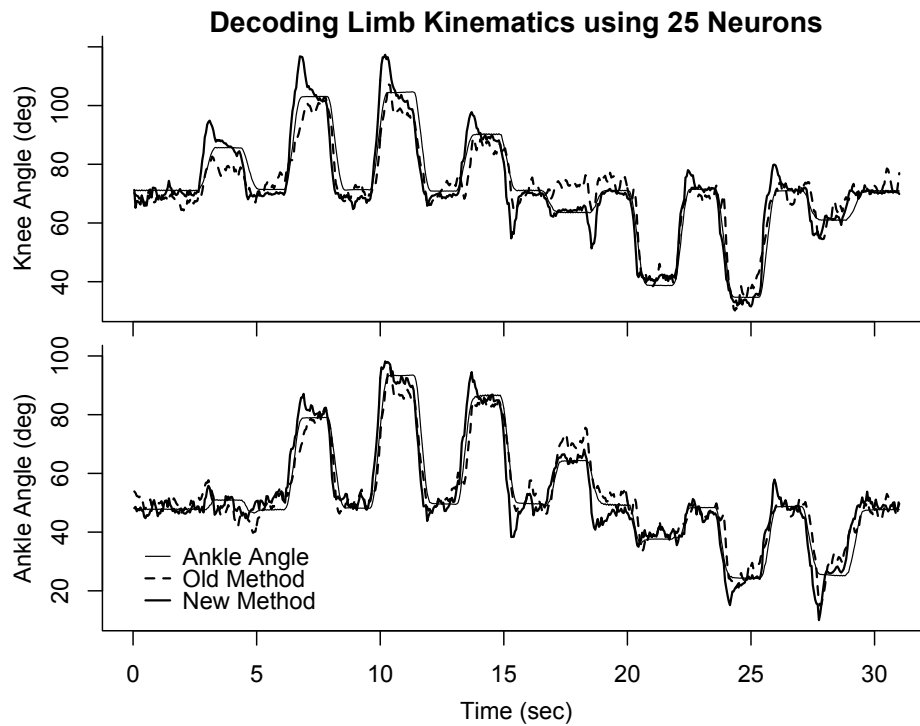


Figure 7: ©[2009] IEEE, True knee and ankle trajectories (solid thin curves), along with decoded trajectories using reverse regression (dashed) and direct regression (solid). Decoded trajectories are based on the best 25 neurons.

trajectories, integrated over all time bins. For this particular experiment, the time bins corresponding to the rest position account for over half of all bins. We therefore downweighted these bins so that their contribution would be comparable to the contribution of each of the 8 angle configurations. The ISE is a useful efficiency measure because it typically decreases proportionally to the inverse of the number of neurons. Therefore, based on this measure, the accuracy of a method based on N_1 neurons will be comparable to the accuracy of another method based on N_2 neurons when $N_2 = N_1 \times R$, where $R = ISE_1/ISE_2$ is the ratio of the ISEs of the two methods.

The ISE ratios for knee and ankle in Fig. 7 are 1.12 and 0.97 respectively which indicates both methods are approximately equally efficient. This is somewhat surprising because most neurons actually encode more than one joint angle. Indeed, when we consider Figure 8, which shows the firing rate of a typical neuron versus hip angle: the relationship is not random, which suggests that this neuron encodes for hip angle. Note also that the + and o plotting symbols correspond to small and large knee angles respectively: the two sets of symbols hardly overlap, which suggest that the neuron also encode information about knee angle. Moreover, the relationship between firing rate and hip angle varies with knee angle, which suggests an interaction between hip and knee angles. These characteristics are common to most afferent neurons we examined.

Because direct regression models how each neuron encodes information about joint angles, it makes better use of the information about angles in the neurons' firing rates. The comparatively good efficiency of reverse regression might be due to robustness against model misspecifications: while reverse regression uses one model per angle, direct regression specifies a different model for each neuron, so that even minor model misspecifications can add up across neurons. It also might be attributed to the number of neurons used and the careful selection of the neurons used to predict limb kinematics. The results in Fig. 7 used 25 neurons from 2 recording sites. We are unlikely to have that many well defined neurons in practice, so we are interested in the performance of the two methods given neuron populations of different sizes.

Fig 9 shows the result of the following analysis. We first selected a pool of neurons encoding “well” for knee and ankle angles: we regressed the firing rates of all neurons on a

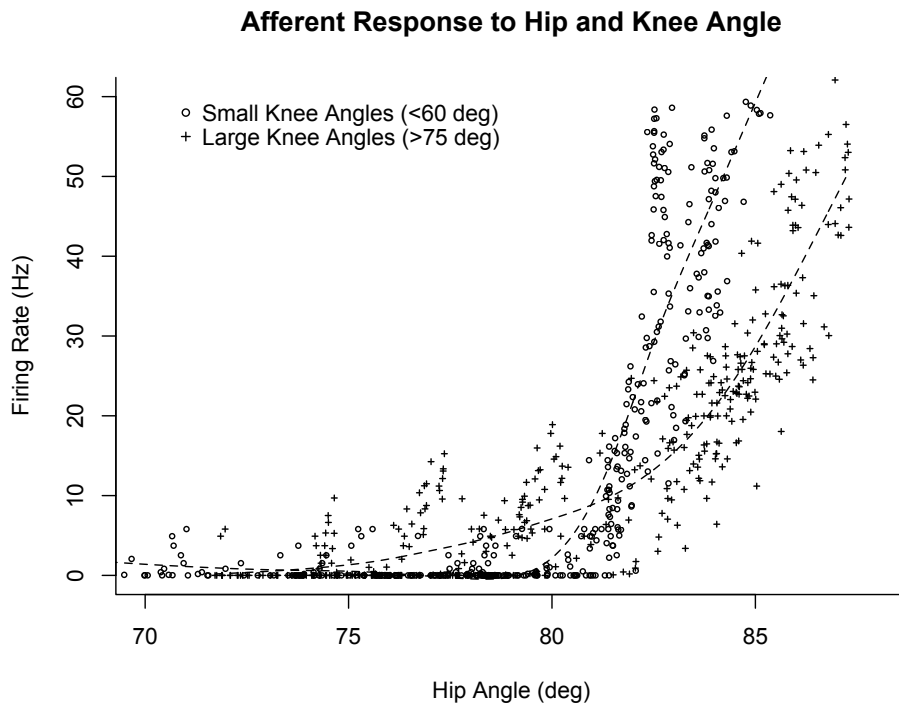


Figure 8: ©[2009] IEEE, Firing rate of a typical neuron varies with hip angle, in response to passive movement of the leg. The + and o plotting symbols correspond to large and small knee angles resp. A spline was fitted through each of the two subsets and is plotted as a dashed line. The clear separation between the lines indicate that the neuron encodes for knee angle as well as hip angle.

smooth function of knee and ankle angles, and retained only the neurons for which the two angles explained more than 40% of firing rate variations. We thus retained 64 of the 153 total neurons. We then selected m neurons at random out of this pool of 64 neurons, decoded knee and ankle trajectories using these m neurons using reverse and direct regression, and calculated the ISE ratio of the two methods. We repeated this 99 more times to obtain 100 ISE values, which we plotted versus m as a violin in Fig. 9. We repeated this simulation for several values of m .

Direct regression has clear advantages over the inverse regression methods for all number of included neurons for the knee and up to 20 neurons for the ankle. This agrees with the fact that most neurons primarily encode ankle angle and that only direct regression can extract knee information from those neurons. However, when using higher neuron counts, the sensitivity of the direct regression approach to inaccuracies in the individual firing rate models becomes problematic, giving reverse regression methods an advantage.

2.4 DISCUSSION

The results show that direct regression methods are more efficient in using all information from afferent firing rates which is predominantly due to the ability to include multiple joint angles in a single model. Being more efficient, this method requires fewer neurons to predict limb kinematics accurately. Although the CNS might not be sensitive to confounding information due to the large redundancy in the primary afferent population, the implications are more severe for neuroprosthetics which have access to a limited subset of the neural population. For practical reasons, it is desirable to use a decoding method that extracts the information as efficiently as possible.

Reverse regression treats each kinematic parameter as an independent decoding problem and will therefore suffer due to confounded information. The ability of direct regression to use this information results in a better effective use of the afferents predominantly in the kinematic variables that are poorly represented in the neural population (i.e. A_2).

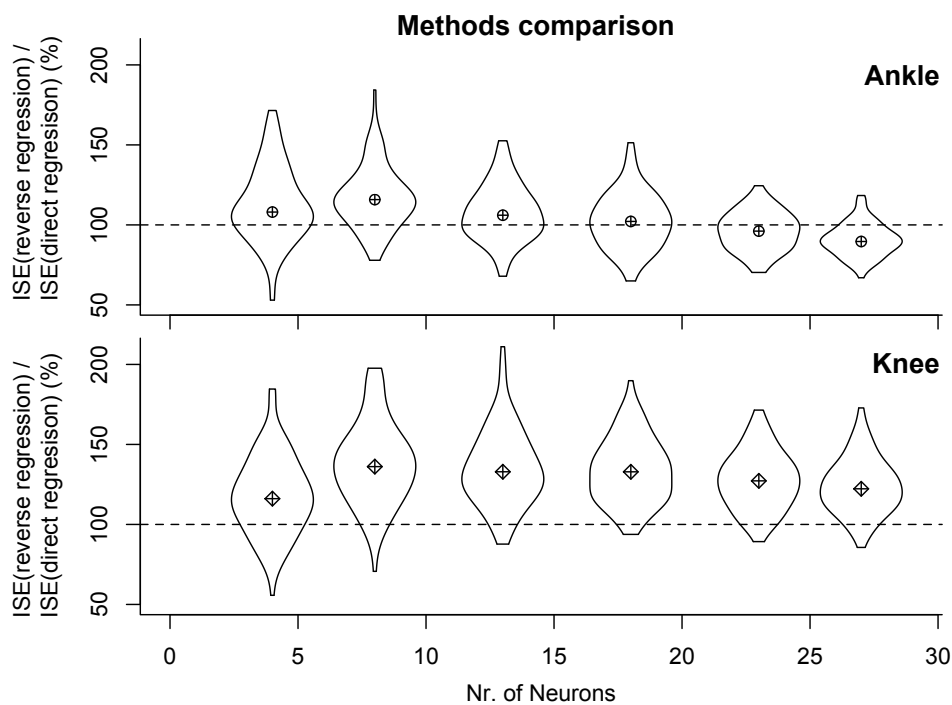


Figure 9: ©[2009] IEEE, Violin plots of 100 ISE ratios for several neuron population size m . The mark at the center is at the median. Violin plots are similar to boxplots but they provide more information: they show the full smooth histogram of the data (here the 100 ISEs) whereas boxplots would only show quartiles and outliers. Independent of the available neural population, reverse regression would need approx 25% more neurons to be as efficient as direct regression to decode knee angle.

The direct regression method also truly models the stimulus-response encoding properties of each neuron. In contrast to reverse regression, where model coefficients are arbitrary, direct regression coefficients convey information to what is encoded by each individual neuron. Insight into what the neurons encode is therefore apparent from the fitted models. Classification of the origin of a particular neuron can theoretically be extracted from the model parameters. Although, as noted in the results section, model selection should include more complex and afferent modality specific models to predict neural type accurately.

Because of its flexibility, it is possible to improve the estimate accuracy by improving the firing rate models. Although a basic model was chosen to demonstrate the possibilities in this paper, there are several more sophisticated models of muscle spindles suggested in the literature. [82, 73, 72] Any of those models can theoretically be implemented using direct regression methods and will contribute to the prediction accuracy. Fig. 7 shows large overshoots during the reaching movements. It is believed that the dynamic component of primary muscle spindles is one of the leading causes for this behavior. Including a velocity component is only possible when decoding using direct regression methods and will likely improve the accuracy of the estimated kinematic limb state.

3.0 STATE-SPACE DECODING OF PRIMARY AFFERENT FIRING RATES

As a natural extension of the paper discussed in the previous chapter, the following paper was published in the Journal of Neural Engineering with the title: “State-space decoding of primary afferent neuron firing rates” and is included integrally in this chapter with the permission of IOPScience [120]. It reflects the goals outlined in specific aim 2. Correlations between the kinematic variables were addressed using a state-space model of the system and derivatives of the kinematic variables were included in the neural firing rate models to improve decoding accuracy.

3.1 INTRODUCTION

Proprioception, or the sensation of movement and position, results from the integration of afferent inputs in the central nervous system (CNS). It provides vital information about the state of the limb during movement and serves as feedback during motor control to create stable and accurate movements. In applications where functional electrical stimulation (FES) is used to restore limb functions such as gait, posture or foot drop, it is important to be able to include feedback information to be able to cope with perturbations, muscle fatigue and non-linear behavior of the effected muscles [67, 126, 123]. Accessing and decoding the activity in native afferent signaling pathways would be a natural way to determine the kinematic state (i.e. position and velocity) of the controlled extremity [44]. Feasibility of this approach has been demonstrated by controlling the ankle angle in a closed loop controller

using the compound afferent input recorded from LIFE electrodes by Yoshida [131]. However, a larger and more diverse population of primary afferent recordings is needed to attain a more complete estimate of limb state. One solution is to record at the dorsal root ganglia where all proprioceptive information converges into the central nervous system. Recording at this site with multi-electrode arrays grants access to a wide variety of state information distributed across many individual neurons [106, 122, 123].

Although it is generally accepted that proprioception is evoked by a variety of primary afferent (PA) inputs, including muscle, cutaneous, and joint receptors, the muscle spindle afferents are believed to be the main contributor [35]. Various models with increasing complexity have been proposed for the muscle spindle firing rate [68, 80, 82, 72]. These models are able to provide accurate predictions of spindle firing rates as a function of muscle length and presumed gamma drive inputs. While it might be desirable to invert these models to decode muscle length or limb-state from the firing rates of muscle spindles, such an inversion is not trivial because the models are non-linear, and position and velocity components of the firing rate are confounded. Similar limitations are applicable for including cutaneous afferents as they are often related to limb kinematics in a non-linear fashion.

To date, decoding efforts have avoided these difficulties by directly modeling each of several kinematic variables as independent functions of the afferent firing rates [106, 122]. These studies used separate regression models to estimate the kinematic state of the hind limb as a weighted sum of the firing rates in a population of PA neurons recorded in the dorsal root ganglia (DRG) of cats during passive and active movements. In this paper, we refer to this approach as reverse regression since the natural relationships between the dependent and explanatory variables are reversed. We will discuss the limitations of that approach and propose an alternative decoding approach that does not have these limitations. This method consists of modeling the firing rates of the primary afferents as functions of the kinematic parameters, and inverting these models via a state-space procedure to decode simultaneously all limb kinematics. Preliminary results were presented in [119]. In this paper, we extend the methods proposed in Wagenaar et al (2009) to include time-derivatives of the kinematic variables (velocities) and allow for decoding multiple correlated kinematic

variables. We compare the efficiencies of the resulting estimates with those predicted using reverse regression [106, 122] and discuss the feasibility of using natural feedback decoding in neuroprostheses.

Finally, the coordinate frame in which limb kinematics are decoded has typically been based on polar coordinates of the endpoint of the limb or the individual joint angles [123, 12]. Scott et al. (1994), found no evidence for a particular coordinate frame based on modeling studies of muscle spindle distributions [98]. Stein et al. (2004), also found no significant difference in correlation coefficients when comparing PA firing rates to kinematic state in polar endpoint coordinates and joint angle space [123, 106]. We included both endpoint and polar coordinates in the analysis of this paper since both representations are relevant for implementation in neural prostheses.

3.2 METHODS AND DATA

3.2.1 Surgical procedures

All procedures were approved by the Institutional Animal Care and Use Committee of the University of Pittsburgh. Two animals were used in these procedures. Both were anesthetized with isoflurane (1-2%) throughout the experiment. Temperature, end tidal CO₂, heart rate, blood pressure, and oxygen saturation were monitored continuously during the experiments and maintained within normal ranges. Intravenous catheters were placed in the forelimbs to deliver fluids and administer drugs. A laminectomy was performed to expose the L6 and L7 dorsal root ganglia on the left side. At the conclusion of the experiments, the animals were euthanized with KCL (120 mg/kg) injected IV.

3.2.2 The experiment

A custom frame was designed to support the cat's torso, spine, and pelvis while allowing the hind limb to move freely through its full range of motion (figure 10). A stereotaxic frame and

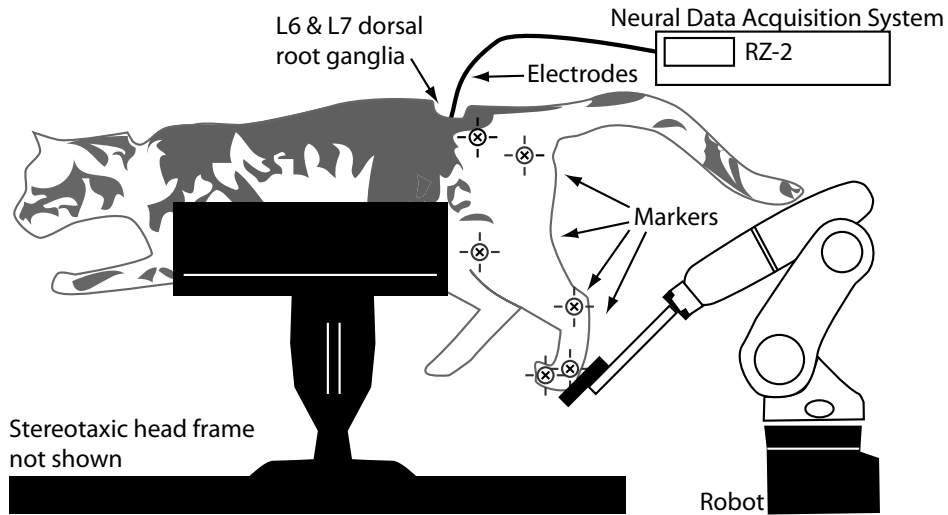


Figure 10: The animal was positioned in a custom designed frame to support the torso and pelvis, enabling unrestrained movement of the left hind limb. The foot was attached to a robotic arm and active markers were placed on the hind limb to track the hind limb kinematics. A 90 channel micro-electrode array was inserted in the L6/L7 DRG and the neural activity was recorded using a programmable real-time signal processing system (TDT RZ2).

vertebrae-clamp were used to support of the head and torso, and bone screws were placed bilaterally in the iliac crests to tether the pelvis with stainless steel wire (not shown in figure 10).

Hind limb kinematics were recorded with a high speed motion capture system (Impulse system, PhaseSpace Motion Capture, USA). Active LED markers were placed on the iliac crest (IC), hip, knee, ankle, and metatarsophalangeal (MTP) joints. During post-experiment analysis, the knee position was inferred from the femur and shank segment lengths and the hip and ankle markers because skin slip at the knee marker rendered position tracking based on the knee marker unreliable [106, 122]. Synchronization between neural and kinematic data was ensured by recording a time-stamp in the neural recording system for every captured kinematic frame.

A robotic arm (VS6556E, DENSO Robotics, USA) was used to move the left foot in the parasagittal plane. The foot was strapped in a custom holder attached to the robot via a pivoting joint that allowed free rotation of the foot in the parasagittal plane (figure 10). The robot was programmed to generate center-out and random movement patterns occupying most of the motion range for the foot. Center-out patterns were ramp and hold displacements of 4cm in eight directions from a center position. Random movements, defined by a uniform distribution of limb positions and velocities within the workspace, were approximated by manually manipulating the hind limb through the entire workspace over a period of 5 minutes. During this time, cameras recorded the trajectory and programmed the robotic manipulator to mimic this trajectory. The robot was then used to manipulate the hind limb during the remainder of the trials. This ensured that we could generate the same random movement in a reliable fashion and optimally use the entire workspace of the hind limb.

Penetrating microelectrode arrays (1.5mm length, Blackrock Microsystems LLC, USA) were inserted in the L7 (50 electrodes in 10x5 grid) and L6 (40 electrodes in 10x4 grid) dorsal root ganglia. The neural data was sampled at 25kHz using an RZ-2 real-time signal processing system from Tucker Davis Technologies, USA. The neural data was band-pass filtered between 300 and 3000 Hz. A threshold was manually determined for each channel and

spike events were defined as each instance the signal exceeded this threshold. Spike waveform snippets, 32 samples in length ($1.2ms$) were stored each time a spike event occurred, resulting in a time series of spikes and their corresponding waveforms per channel. Spike waveforms were sorted manually during the post-experiment analysis (Offline Sorter, TDT, Inc.).

3.2.3 Current decoding paradigm: reverse regression

Let $\mathbf{X} = (X_k, k = 1, \dots, K)$ be the vector of K kinematic variables we want to decode, based on the firing rates $\mathbf{FR} = (FR_i, i = 1, \dots, I)$ of I neurons. In this paper, \mathbf{X} is the limb state expressed in one of two different reference frames, a joint-based frame with state vector $(A_k, k = 1, 2, 3)$ that represents intersegmental angles for the hip, knee, and ankle joints, and an endpoint frame with state vector (R, θ) that represents the toe position relative to the hip in polar coordinates. We let $\dot{\mathbf{X}} = (\dot{X}_k, k = 1, \dots, K)$ denote the velocities of the kinematic variables, and $\mathbf{Z} = (\mathbf{X}, \dot{\mathbf{X}})$ the combined vector of limb kinematics and their velocities. A subscript t added to any variable means that we consider the value of that variable at time t . The methodologies described below can be applied to firing rates \mathbf{FR} that are either raw or smoothed spike counts. Here, we computed smoothed instantaneous firing rates by convolving the spike events with a one-sided Gaussian kernel ($\sigma = 50ms$) to ensure causality [106].

Reverse regression consists of modeling the mean of each kinematic variable X_k as a function of the spike-activity,

$$E(X_k) = f_k(\mathbf{FR}), \quad k = 1, \dots, K, \quad (3.1)$$

where f_k is some function deemed appropriate, for example a linear function as in (3.3). An estimate \hat{f}_k of f_k is obtained by least squares or maximum likelihood regression using a training set of simultaneously recorded values of \mathbf{X} and \mathbf{FR} . Then, given the observed neurons' firing rates \mathbf{FR}_t^{obs} at time t , the prediction of X_k at t is

$$X_{kt}^* = \hat{f}_k(\mathbf{FR}_t^{obs}), \quad k = 1, \dots, K. \quad (3.2)$$

The resulting decoded trajectories $\{X_{kt}^*, t = 1, 2, \dots\}$, $k = 1, \dots, K$, are typically much more variable than a natural movement, so they are often smoothed to fall within the expected response frequencies (typically < 20 Hz).

Reverse regression was used by [122] and [106] to predict joint and endpoint kinematics. They took f_k in (3.1) to be a linear function of spike activity, so that

$$X_k = \beta_{k0} + \sum_{i \in S_k} \beta_{ki} FR_i + \epsilon_k, \quad (3.3)$$

where S_k indexes the set of neurons whose firing rates correlate most strongly with X_k [106], and ϵ_k are uncorrelated random errors. We adopt the same approach with our data: we apply reverse regression with the linear model in (3.3) to decode joint angles (A_k , $k = 1, 2, 3$) and limb end point position (R, θ), and smooth the decoded trajectories by convolving the result with a gaussian kernel ($\sigma = 75ms$) to improve the decoding results.

One advantage of reverse regression is its simplicity: kinematic variables X_k are decoded separately and require just one equation each. However, the method does not allow physiologically meaningful modeling of the relationships between firing rates and kinematic variables. Indeed, not only do neurons often encode several kinematic variables simultaneously, the manner in which they encode these variables is not necessarily linear or additive. For example, many muscles in the hind limb span two joints, so that PA neurons code for multiple joint angles simultaneously. Such a neuron was shown in [119]: its firing rate depended both on ankle and knee angles, the relationship between firing rate and ankle angle was clearly non-linear, and the relationship changed for different values of knee angle, which suggested the existence of an interaction between the two joint angles. Such effects cannot be modeled in reverse regression. It is also possible for neurons to encode not only for kinematic variables but also for their derivatives; muscle spindle primary afferents (Ia) are such neurons. In that case it is possible to decode X_{kt} based on the relationship between its velocity $\dot{X}_{kt} \approx (X_{kt} - X_{k(t-\delta_t)})/\delta_t$ and the neurons' firing rates, by applying reverse regression with X_k replaced by \dot{X}_k in equations (3.1) and (3.2). Based on a linear function f_k , this prediction is

$$X_{kt}^* = X_{k(t-\delta_t)}^* + \delta_t \left(\hat{\alpha}_{k0} + \sum_{i \in S_k} \hat{\alpha}_{ki} FR_{it}^{obs} \right), \quad (3.4)$$

which is different than predicting X_{kt}^* from (3.3). Stein et al (2004) offered an ad-hoc method of combining these two predictions. However, because it is not motivated by a principle that guarantees superior results over either separate predictions, we did not consider this method for our data.

3.2.4 Firing rate models and likelihood decoding

Reverse regression is easy to apply, but it does not make efficient use of the information in the data since effects such as interactions or effects of derivatives cannot be accounted for. In contrast, a likelihood approach can account for such effects, and is further known to be efficient when the models involved are appropriate [56].

The likelihood approach is based on models that describe the physiological dependencies of firing rates on limb state, which restores the natural relationship between X_k and FR_i that are swapped in the reverse regression approach. That is, the mean firing rates FR_i of each neuron are now modeled as functions of the kinematic variables $\mathbf{Z} = (\mathbf{X}, \dot{\mathbf{X}})$,

$$E(FR_i) = g_i(\mathbf{Z}), \quad i = 1, \dots, I, \quad (3.5)$$

where the functions g_i are selected to accommodate any suspected effects between covariates, such as interactions. Sections 3.2.4.1 and 3.2.4.2 summarize the functions g_i we considered for our data. Although we could let g_i also depend on higher order derivatives of \mathbf{X} , such as acceleration, we did not consider that option because PA neurons are known to encode primarily for muscle lengths and their velocities [85, 64, 72], and previous work using reverse regression methods failed to generate accurate estimates of acceleration [123]. The maximum likelihood estimates \hat{g}_i of g_i , $i = 1, \dots, I$, are obtained based on a training set of simultaneously recorded values of \mathbf{Z} and \mathbf{FR} , and on an assumed distribution for FR_i . Here we used the Gaussian distribution since FR_i are smooth firing rates, but the Bernoulli or Poisson distributions could be used instead if FR_i were raw spike trains (i.e. unfiltered spike counts). Then, given the observed firing rates \mathbf{FR}_t^{obs} at time t , the prediction of \mathbf{Z} is obtained by solving the system of I equations

$$FR_{it}^{obs} = \hat{g}_i(\mathbf{Z}_t^*) + \epsilon_{it}, \quad i = 1, \dots, I \quad (3.6)$$

for \mathbf{Z}_t^* . Note that all components of \mathbf{Z} are decoded simultaneously, whereas they are decoded separately in reverse regression. When the firing rates are not modulated by the velocities, so that the g_i 's are functions only of \mathbf{X} , solving (3.6) amounts to performing standard least square estimation when the g_i 's are linear functions of their inputs; see section 3.2.8. Otherwise, it can be challenging. In particular, (3.6) should be solved subject to the constraint that the derivatives of the decoded positions match the decoded velocities.

We did not use likelihood decoding in this paper, partly because of the technical difficulties just mentioned, but mostly because state-space models (section 3.2.5) are superior. We nevertheless provided details because the likelihood is a component of the state-space model, and decoding under the two approaches are related.

3.2.4.1 Firing rate models in joint angle frame We considered hind limb biomechanics to guide our choice of physiologically plausible firing rate models in (3.5), as follows. We know that the firing rates of muscle spindle afferents depend primarily on the kinematic state of one or two adjacent joints since the host muscles are either mono or bi-articular. For example, a muscle spindle in the medial gastrocnemius muscle encodes movement of both ankle and knee, while a muscle spindle in the soleus muscle encodes only the movements of the ankle. Cutaneous afferent neurons are not so tightly linked to joint motion, but our previous work shows that even they exhibit responses that vary systematically with limb motion (see figure 3 in Stein, JPhysiol, 2004). Therefore we considered functions g_i in (3.5) that include the effect of a single joint, $s(A_j)$ with $j = 1, 2$ or 3 , or the additive effects of two adjacent joints, $s(A_j) + s(A_k)$ with $(j, k) = (1, 2)$ (ankle/knee) or $(j, k) = (2, 3)$ (knee/hip). The notation $s(A)$ signifies that a non-parametric smoother is applied to the covariate A , which models the potentially non-linear effect of A on the neuron's firing rate. Here, we took $s(\cdot)$ to be splines with 4 non-parametric degrees of freedom, but other smoothers could be used. Figure 3 in [119] also suggested that interactions between joints might be present, so we also considered the addition of interaction effects, which we denote by $s(A_j) : s(A_k)$, $(j, k) = (1, 2)$ or $(2, 3)$. We also know that muscle spindle primary afferents and possibly many rapidly adapting cutaneous afferents exhibit a velocity dependent response. Hence we allowed the ad-

dition of velocity terms $s(\dot{A}_j)$, $s(\dot{A}_j) + s(\dot{A}_k)$, or $s(\dot{A}_j) * s(\dot{A}_k) = s(\dot{A}_j) + s(\dot{A}_k) + s(\dot{A}_j) : s(\dot{A}_k)$ in the model for g_i in (3.5). Finally, we also included the interactions $s(A_j) : s(\dot{A}_j)$ between joints and their respective velocities, because we expect the velocity of a joint to get smaller when it is close to full extension or full flexion.

Table 1 contains the list of firing rate models we considered for our data. All models were fitted to all neurons by maximum likelihood using a standard statistical package (R, <http://www.R-project.org>), and the best model for each neuron was selected by the Bayesian information criterion (BIC) [97].

3.2.4.2 Firing rate models in limb end point frame We took a similar approach to select models for the relationship between firing rates and limb end point (MTP, or toe marker) defined by the polar coordinates (R, θ) , where R is the distance from the hip marker to the MTP marker and θ the angle between the horizontal and the vector spanned by the hip and MTP markers. For each neuron, we considered functions g_i in (3.5) that include either $s(R)$, $s(\theta)$, or both, and possibly their interaction. We also considered the addition of velocity terms $s(\dot{R})$, $s(\dot{\theta})$, $s(\dot{R}) + s(\dot{\theta})$, and their interaction, as well as $s(R) : s(\dot{R})$ and $s(\theta) : s(\dot{\theta})$, the interactions between effects and their respective velocities. For each neuron, the best model was determined by BIC.

3.2.5 State-space models

The firing rate models (3.5) describe the relationships between kinematic variables and spiking activity. Newer decoders provide significant improvements in decoding performance by supplementing the firing rate models with a probabilistic model that describes the intrinsic behavior of kinematic variables, such as constraints on velocity and trajectory smoothness.

For example, [19] suggest the *a priori* random walk model

$$\mathbf{z}_t = \begin{pmatrix} \mathbf{X}_t^T \\ \dot{\mathbf{X}}_t^T \end{pmatrix} = \begin{pmatrix} I_{K \times K} & \delta \times I_{K \times K} \\ 0 & I_{K \times K} \end{pmatrix} \begin{pmatrix} \mathbf{X}_{t-1}^T \\ \dot{\mathbf{X}}_{t-1}^T \end{pmatrix} + \begin{pmatrix} 0 \\ \epsilon_t \end{pmatrix}, \quad (3.7)$$

where ϵ_t , $t = 1, 2, \dots$, are independent vectors with mean 0 and $K \times K$ variance-covariance matrix Σ . For all $k = 1, \dots, K$, (3.7) specifies that $\dot{X}_{kt} = \dot{X}_{k(t-1)}$ plus some perturbation

Table 1: List of the 33 models considered to describe the effect of the three joint angles $A_k, k = 1, 2, 3$ on the firing rates of neurons. The notation $s(\cdot)$ is a spline basis with 4 non-parametric degrees of freedom. The notation $s(A_j) * s(A_k)$ means that the main effects $s(A_j), s(A_k)$, and their interaction $s(A_j) : s(A_k)$ are included in the model.

Index	Model description	Variations
1	$g_i = \beta_{0i}$	
2-4	$g_i = \beta_{0i} + s(A_j)$	$j = 1, 2, 3$
5-6	$g_i = \beta_{0i} + s(A_j) + s(A_k)$	$(j, k) = (1, 2), (2, 3)$
7-8	$g_i = \beta_{0i} + s(A_j) * s(A_k)$	$(j, k) = (1, 2), (2, 3)$
9-11	$g_i = \beta_{0i} + s(\dot{A}_j)$	$j = 1, 2, 3$
12-14	$g_i = \beta_{0i} + s(A_j) * s(\dot{A}_j)$	$j = 1, 2, 3$
15-18	$g_i = \beta_{0i} + s(A_j) * s(\dot{A}_j) + s(A_k)$	$(j, k) = (1, 2), (2, 1), (2, 3), (3, 2)$
19-22	$g_i = \beta_{0i} + s(A_j) * s(A_k) + s(\dot{A}_k)$	$(j, k) = (1, 2), (2, 1), (2, 3), (3, 2)$
23-25	$g_i = \beta_{0i} + s(A_j) + s(\dot{A}_j)$	$j = 1, 2, 3$
26-27	$g_i = \beta_{0i} + s(A_j) * s(\dot{A}_j) + s(A_k) * s(\dot{A}_k)$	$(j, k) = (1, 2), (2, 3)$
28-31	$g_i = \beta_{0i} + s(A_j) + s(\dot{A}_j) + s(A_k)$	$(j, k) = (1, 2), (2, 1), (2, 3), (3, 2)$
32-33	$g_i = \beta_{0i} + s(A_j) * s(A_k) + s(\dot{A}_j) + s(\dot{A}_k)$	$(j, k) = (1, 2), (2, 3)$

ϵ_{kt} , which forces the velocities to change smoothly over time if the perturbations are taken to be small enough. Equation (3.7) also specifies that $X_{kt} = X_{k(t-1)}$ plus the velocity $\dot{X}_{k(t-1)}$ multiplied by the size of the decoding window, δ msec. This not only forces the positions to be consistent with their respective velocities, but also induces the position paths to be smooth when the velocity paths are smooth. Alternatively, one can assume the more general random walk model

$$\begin{pmatrix} \mathbf{X}_t^T \\ \dot{\mathbf{X}}_t^T \end{pmatrix} = \mathbf{B} \begin{pmatrix} \mathbf{X}_{t-1}^T \\ \dot{\mathbf{X}}_{t-1}^T \end{pmatrix} + \epsilon_t, \quad (3.8)$$

where ϵ_t , $t = 1, 2, \dots$, are independent vectors with mean 0 and $2K \times 2K$ variance-covariance matrix Σ , and estimate \mathbf{B} and Σ by maximum likelihood according to

$$\mathbf{B} = \sum_{t=2}^n \mathbf{z}_t \mathbf{z}_{t-1}^T \left(\sum_{t=2}^n \mathbf{z}_{t-1} \mathbf{z}_{t-1}^T \right)^{-1}$$

$$\Sigma = \frac{1}{n-1} \left(\sum_{t=2}^n \mathbf{z}_t \mathbf{z}_t^T - \mathbf{B} \sum_{t=2}^n \mathbf{z}_{t-1} \mathbf{z}_t^T \right),$$

as in [130], where $\mathbf{z}_t, t = 1, \dots, n$, is a training set of kinematic data. We describe the specific kinematic models we used for our data in section 3.2.5.1, and until then use the generic notation

$$\mathbf{Z}_t = h(\mathbf{Z}_{t-1}) + \epsilon_t. \quad (3.9)$$

Once the firing rate and kinematic models are fitted to data, as described in this and the previous sections, decoding follows a recursive scheme. Let \mathbf{Z}_t^{post} be the prediction of \mathbf{Z} at time t ; \mathbf{Z}_t^{post} is a random variable since the kinematic prior model in (3.9) is stochastic, so the actual prediction \mathbf{Z}_t^* is usually taken to be the mean of \mathbf{Z}_t^{post} . Initially \mathbf{Z}_1^* is set to the initial hind limb state of the encoding dataset. At time $(t+1)$, we first use the current prediction \mathbf{Z}_t^{post} together with the kinematic model in (3.9) to obtain the *a priori* distribution of the next value of \mathbf{Z} ,

$$\mathbf{Z}_{(t+1)}^{prior} = h(\mathbf{Z}_t^{post}) + \epsilon_t.$$

Then we use the observed firing rate vector $\mathbf{FR}_{(t+1)}^{obs}$ at time $(t+1)$ with the firing rate models in (3.5) to update that prior into the posterior distribution of $\mathbf{Z}_{(t+1)}^{post}$, and finally take its mean to be the predicted kinematic state vector $\mathbf{Z}_{(t+1)}^*$. Depending on the forms of

the firing rate and kinematic models, the posterior calculation is carried out by Kalman or particle filtering; these methods are described in detail in [18, 129, 21]. Here we use particle filtering because the firing rate model in (3.5) involves splines. The resulting trajectories for \mathbf{X} are typically smooth enough and do not require additional smoothing.

3.2.5.1 Kinematic models For our data, we assumed the general random walk model (3.8) and used a training set of kinematic data to estimate \mathbf{B} . We obtained

$$\mathbf{B} \approx \begin{pmatrix} I_{3 \times 3} & 0.05 \times I_{3 \times 3} \\ 0 & I_{3 \times 3} \end{pmatrix}$$

for the three joint angles (A_1, A_2, A_3) , and

$$\mathbf{B} \approx \begin{pmatrix} I_{2 \times 2} & 0.05 \times I_{2 \times 2} \\ 0 & I_{2 \times 2} \end{pmatrix}$$

for the limb end-point kinematic variables (R, θ) , which are precisely the a priori kinematic models suggested by Brockwell, Kass and Schwartz (2007) in equation (3.7), with our decoding window of $\delta = 0.05$ msec.

The kinematic model for (A_1, A_2, A_3) can further be improved by taking into account the physical constraints between these angles. These constraints are seen in figure 11, which shows a 3D scatter plot of (A_1, A_2, A_3) in two movement patterns: a center out path (black) and a random path (gray). We see that hip and ankle angles are highly inter-dependent, as was already observed in [122, 12], since the data lie almost entirely on a 2D manifold. This explains why, when decoding via reverse regression, neurons that encode for hip could be used to decode the ankle angle as well, and vice versa. In all experiments, the limb was made to move by controlling only its foot position. Therefore, figure 11 displays the relative positions that the three angles assume *naturally* during imposed movement of the foot. Moreover, these natural positions appear consistent across experiments, since the data from the random and center-our experiments lie within the same sub-space. It is thus reasonable to assume that all passive movements share the constraints between joint angles displayed in figure 11. We could include this prior information in the kinematic model by forcing the

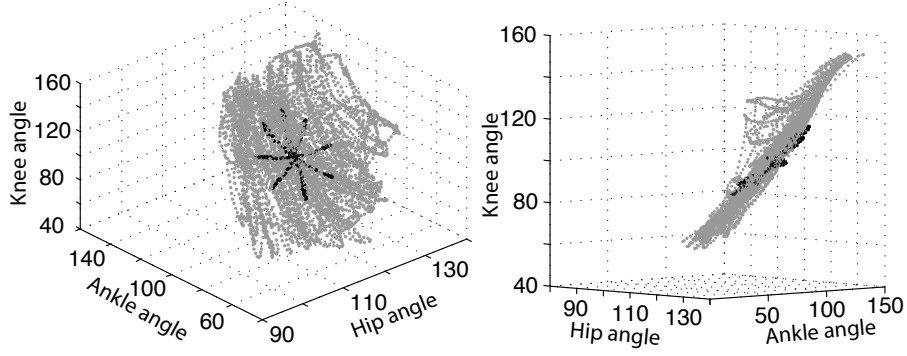


Figure 11: Observed trajectories of the three joint angles of the hind limb during random (gray) and a center-out (black) passive movements. The joint angles are clearly interdependent.

random walk in (3.8) to evolve within the envelope of the points in figure 11. However, this envelope is probably too tight since we did not observe all possible movements, so we will instead force the random walk to evolve near, rather than inside, the envelope, as follows.

Let $\mathbf{A}_t^* = (A_{1t}^*, A_{2t}^*, A_{3t}^*)$ be the predicted value of the joint angles at time t , depicted as \times in figure 12a; as mentioned earlier, \mathbf{A}_t^* is the mean of \mathbf{A}_t^{post} , whose distribution is depicted as the circular gray area in figure 12a. We identify the quarter of the points in figure 11 that are closest to \mathbf{A}_t^* , and obtain the 2D plane spanned by their first two principal components, depicted as the straight line in figure 12c; the most natural limb positions near \mathbf{A}_t^* should be close to that plane.

To obtain the prior distribution of \mathbf{A} at time $(t+1)$, we first use the kinematic model in (3.9) to transform the posterior distribution of \mathbf{A} at time t into an intermediate prior for \mathbf{A} at time $(t+1)$ (circular gray area in figure 12b), and we orthogonally project it half the distance towards the principal component plane (see figure 12c). This modified random walk loosely mimics or ‘accommodates’ the natural constraints on the joint angles. In particular, by using only a quarter of the training data to obtain the projection plane, we enable the prior model

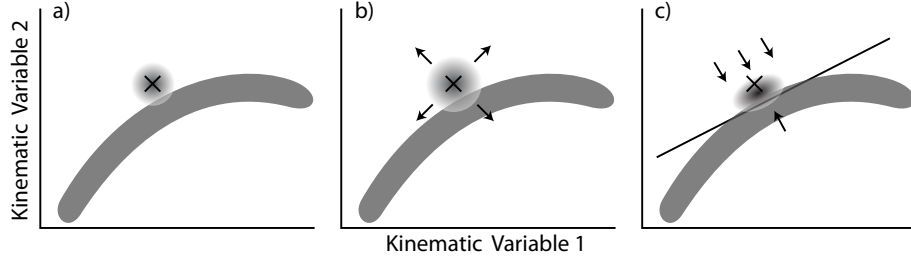


Figure 12: Depiction of the random walk prior model for the joint angles, in 2D rather than 3D to improve visibility. a) Location of the current predicted state (\times), posterior distribution of the state (small gray circular area, whose relative size represents the relative uncertainty of the current position), and kinematic data manifold (dark curved gray area). b) transformation of the posterior into the intermediate prior for the next state prediction, based on the kinematic model in (3.9). c) projection of the intermediate prior towards a locally defined plane representing the shape of the kinematic range of motion.

to follow the curvature of the cloud of points in figure 11. The polar coordinates appeared to be independent so we did not include any additional constraints in their kinematic model.

3.2.6 Decoding efficiency

We assessed the quality of decoded trajectories by the integrated squared error (ISE), defined as the squared difference between decoded and actual trajectories, integrated over all decoded time bins. The ISE is a combined measure of bias and variance, which typically decreases proportionally to the inverse of the number of neurons used to decode. Hence, when comparing two decoding methods, the ISE has the following interpretation: the accuracy of reverse regression, based on n_{RR} neurons, will be comparable to the accuracy of state-space decoding, based on n_{SS} neurons, if $n_{RR} = n_{SS} (ISE_{RR}/ISE_{SS})$. This means that if the ISE ratio ISE_{RR}/ISE_{SS} is one, the two methods are equally efficient; if the ratio is 1.5, reverse regression needs 50% more neurons to be as efficient as state-space decoding; etc. Therefore,

two decoding methods can be compared by computing the ratio of their respective ISEs. Because ISE ratios vary from dataset to dataset in repeated simulations, we summarized their distributions using violin plots.

Violin plots are close cousins of boxplots; both show the distributions of several variables side by side, and are therefore particularly well suited to compare these distributions. The better known boxplot does not display full distributions, but only side by side summaries in the form of boxes with edges marking the quartiles. Violin plots do not reduce the distributions to be compared to a small number of features, but instead plot the full distributions and their mirror images vertically. They also include a marker for the medians of the distributions.

3.2.7 State space algorithm for decoding limb state

The state space model applied in this work is an extension of the particle filter described in Brockwell et al. [18]. A thorough explanation of the particle filter can be found in the appendix of that work. In this appendix we summarize the procedure and indicate where our method diverges from the algorithm in Brockwell et al.

The objective of state space decoding is to estimate the state of the hind limb, $\mathbf{X} = (X_k, k = 1, \dots, K)$, based on the input firing rates of I neurons, $\mathbf{FR} = (FR_i, i = 1, \dots, I)$. It relies on an iterative algorithm which updates the posterior distribution of limb state (and therefore the mean of that posterior, which is used as the estimate of limb state) as new observations of spike counts/firing rates arrive. A Kalman filter calculates that posterior distribution analytically, a particle filter by simulation. In this paper, we used a particle filter with $m = 3000$ particles to approximate the posterior distribution, which means that a histogram of the m particles approximates that posterior. Below we explain how to update the particle cloud, and thus the limb state posterior distribution, at each time step.

1. Initial prior distribution for the limb state: we have no information about limb state when we start the algorithm, so we generate the m initial particles $\tilde{x}_0^{(j)}, j = 1, 2, \dots, m$ from a prior distribution that has mean at the center of the limb state space, and a large

variance to reflect the lack of information about limb state. This prior can be adjusted if there is prior information about the limb state.

Set $t = 1$.

2. Let $\tilde{x}_{t-1}^{(j)}, j = 1, 2, \dots, m$ denote the particle cloud at time $t - 1$, and \hat{z}_{t-1} the limb state prediction at $t - 1$. To obtain the limb state prediction at time t , we first collect the vector of observed firing rates \mathbf{FR}_t^{obs} .
3. We advance all particles $\tilde{x}_{t-1}^{(j)}$ by simulating the state model one step forward as per (9). The resulting particles, $x_t^{prior(j)}$ say, estimate the prior distribution of the kinematic state at time t . Equation (9) simply consists of adding Gaussian random noise to all the particles, with aim to increase the spread of the particle cloud so that it can envelop all possible limb states at t , given the current state \hat{z}_{t-1} . Adding too much noise results in particles being able to capture highly unlikely limb states, while adding too little prevents the algorithm from tracking fast movements. To avoid making an arbitrary decision, we estimated the variance-covariance matrix of the random noise from training data, as described section 2.5.
4. The next step is specific to the kinematic model used in this paper for the joint angles: project each particle $x_t^{prior(j)}$ towards the physiologically plausible kinematic space. To do that, we determine the quarter of the points in the training data set that are closest to the current state estimate \hat{z}_{t-1} , and express the coordinates of each particle as a linear combination of the 3 principle components spanning that quarter data. The first two PCs span a local approximation of the 2D plane of the physiologically plausible kinematic space, while the third PC is the orthogonal distance from that plane to the predicted state variable. Hence to project the particle $x_t^{prior(j)}$ towards the physiologically plausible space, we simply scale the third PC by $\zeta \in [0, 1]$. This operation reduces by a factor of ζ the orthogonal distance of each particle to the kinematic plane.
5. We compute a weight $w_t^{(j)}$ for each particle as

$$w_t^{(j)} = p\left(\mathbf{FR}_t^{obs} \mid x_t = x_t^{prior(j)}\right), \quad (3.10)$$

which is the probability of observing the firing rate vector \mathbf{FR}_t^{obs} if the kinematic variable takes value $x_t^{prior(j)}$. In this paper, we assumed that each firing rate FR_i has a Gaussian

distribution with mean $\hat{g}_i(\mathbf{Z})$ and variance s_i^2 , both estimated in the encoding stage (6), and we assumed that the neurons were independent, so that the weights reduce to

$$w_t^{(j)} = \prod_{i=1}^I \frac{1}{\sqrt{2\pi s_i^2}} \exp \left(-\frac{\left(FR_{it} - \hat{g}_i \left(x_t^{\text{prior}(j)}, \dot{x}_t^{\text{prior}(j)} \right) \right)^2}{2s_i^2} \right). \quad (3.11)$$

Then we normalize the weights $w_t^{(j)}$ so they sum to one.

6. We create the new particle cloud by sampling the current prior particles $x_t^{\text{prior}(j)}$ with weights $w_t^{(j)}$ and with replacement. Hence particles that have low weights are unlikely to be sampled, while particles that have high weights might be sampled several times. We call the new particles $\hat{x}_t^{(j)}, j = 1, 2, \dots, m$. This new particle cloud estimates the posterior distribution of the limb at time t . We take the estimate of the limb state at time t to be the sample mean of the particles,

$$\hat{z}_t = \frac{1}{m} \sum_{j=1}^m \hat{x}_t^{(j)} \quad (3.12)$$

7. Set t to $t + 1$ and go back to step (ii).

In summary, the estimate of the limb state evolves over time as new observations of the firing rates arrive. The estimate at t depends on the state estimate at the previous time point $t - 1$ and on the observed firing rates at time t . Since the limb state can only exist within a confined region of the space spanned by the kinematic inputs, we constrain the kinematic model to evolve close to that space.

3.2.8 Details for solving eq. 3.6

When the firing rates are not modulated by the velocities, so that the g_i 's are functions only of \mathbf{X} , solving 3.6 amounts to performing standard least square estimation when the g_i 's are linear functions of their inputs. Indeed in that case, 3.6 reduces to

$$FR_{it}^{obs} = \hat{\beta}_{0i} + \sum_{k=1}^K \hat{\beta}_{ki} X_{kt}^* + \epsilon_{it}, \quad i = 1, \dots, I,$$

where the ϵ_{it} are independent Gaussian random variables with mean 0, and the $\hat{\beta}_{ki}$ are known: they were estimated in the encoding stage. Therefore 3.6 is a linear regression model where the dependent variables are the FR_{it}^{obs} , the role of the dependent variables are played by the $\hat{\beta}_{ki}$, and the parameters to be estimated are the X_{kt}^* . This regression can be fitted using any statistical software. Eq. 3.6 can still be solved, although not quite as trivially, if the g_i functions are non-linear or involve derivatives of \mathbf{X} .

3.3 RESULTS

The data from two animals are included in the analysis of this paper. Spike sorting the neural data resulted in 158 and 116 classified neurons for each animal respectively. From these 274 neurons, 171 neurons (115 and 56 respectively) were included in the analysis based on the criteria described in section 3.3.1. Section 3.3.1 describes an analysis of the firing rate models to give insight into how well each of the various state variables and their interactions are represented in the PA ensemble. Analysis of decoded trajectories in joint angle space and endpoint space are presented in sections 3.3.2 and 3.3.3 respectively.

3.3.1 Encoding models

In the methods section, we argued that a decoding method that involves firing rate models would use the data more efficiently than reverse regression because it can account for effects of multiple joint angles and their derivatives. Here, we assess if such effects are present in our data.

Figure 13 shows the observed firing rate response of a primary muscle spindle during a center-out passive movement (thick gray curve). We fitted all the models in table 1 to that neuron and selected the best model by BIC. That model has an adjusted R^2 of 0.82; it includes terms for the hip and knee joint angles, terms for their respective velocities, and interactions terms between positions and velocities (models 26-27 in table 1). Figure 13B shows that the firing rate predicted by that model (solid curve) closely follows the observed firing rate, and provides a particularly good fit to the sharp firing rate increases that occur when the joint angles shift to different positions. Figure 13B also shows the fit of the best model with all the velocity terms omitted (dashed curve). The adjusted R^2 dropped to 0.49 and the accuracy of the fit during the rapid movements degraded markedly. This shows that the PA neuron used in figure 13 encodes not only for joint angles, but also for their velocities.

To evaluate the overall importance of the combined position and velocity models in the population of neurons for each neuron, we collected the adjusted R^2 value of three models; the best model involving only joint angles, the best model involving only joint angle velocities, and the overall best model. Figure 14-A shows the violin plots of the R^2 values of the three types of models. To clarify the plot, we dropped the neurons which achieved a maximum R^2 value less than 0.25, since they were deemed to encode little kinematic information. Velocity models outperform position models, which suggests that a large number of neurons encode information about joint angle velocity. Figure 14-A shows that the majority of the neurons are best modeled by a combination of joint angle positions and velocities (mean $R^2 = 0.68 \pm 0.12$), which agrees with a previous report on the encoding properties of PA neurons [106].

Next, we assessed which kinematic variables were represented in the neural population. We considered joint angle kinematic variables as well as polar coordinates of the MTP (i.e.

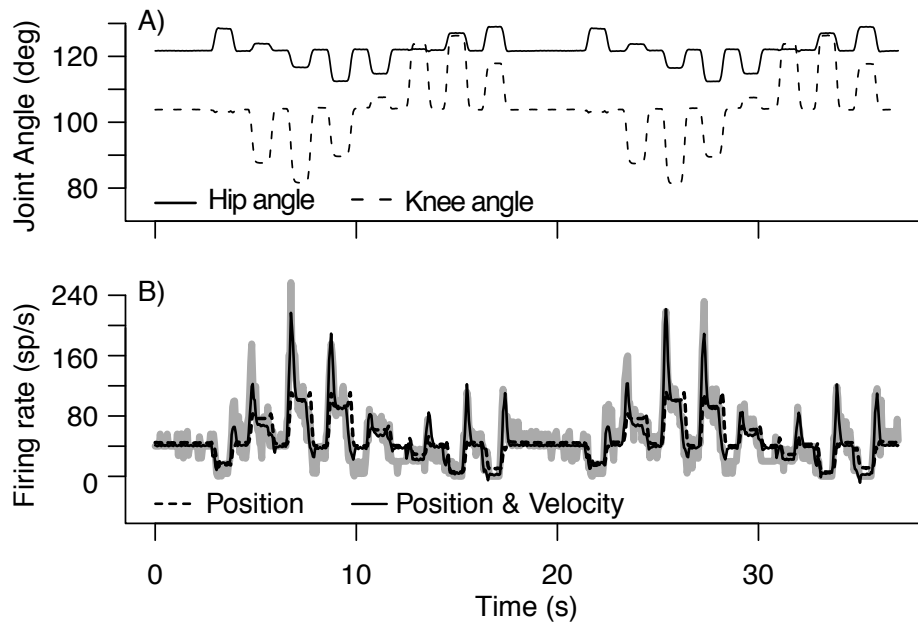


Figure 13: A) Kinematic trajectories of hip and knee angle during a center-out passive movement. B) Firing rate of a PA neuron during passive movement of the hind limb (thick gray curve). Overlaid are the predicted firing rates using models that include position of hip and knee angles(dashed curve) and position + velocity components (solid curve).

toe position relative to the hip). For each neuron, we collected the adjusted R^2 value of 5 firing rate models (hip, hip&knee, knee, knee&ankle and ankle) and 3 polar coordinate models (R , θ and R & θ). Figure 14B shows the violin plots of the R^2 distributions where we excluded neurons which achieved maximum R^2 values less than 0.25. Models that include two joint angles generally outperform models that include only one. Similarly, including both R and θ increases the R^2 value on average. Note that θ is represented poorly in the neural population. We can also see that the combination of R and θ results in R^2 values that are on par with the best joint angle models.

The results displayed in figure 14 suggests that most neurons encode for a combination of angles, and their velocities. In fact, after applying the firing rate model selection procedure outlined in section 3.2.4.1, we found that 90% of the neurons have firing rates that are best modeled by models 26-27 in table 1. This indicates that the firing rates of these neurons depend on multiple joint angles, on interactions between the joint angles, and on their velocities. The neurons were equally distributed between hip/knee and knee/ankle neurons. This makes sense since the neurons were recorded from the L6 and L7 DRG, which cover the proximal and distal portions of the hind limb [4]. Similarly, in endpoint space, over 90% of the best models include R , θ , \dot{R} , $\dot{\theta}$ and their interactions; $R : \dot{R}$ and $\theta : \dot{\theta}$.

3.3.2 Decoding joint angles

To compare the different decoding methods, we decoded limb kinematics using randomly selected groups of neurons. Performance results are in Figure 16. We first show in Figure 15 an example where the same 23 randomly selected units were used to decode the three joint angles using reverse regression and state-space modeling. In this case it is clear that state-space decoding is more accurate than reverse regression decoding.

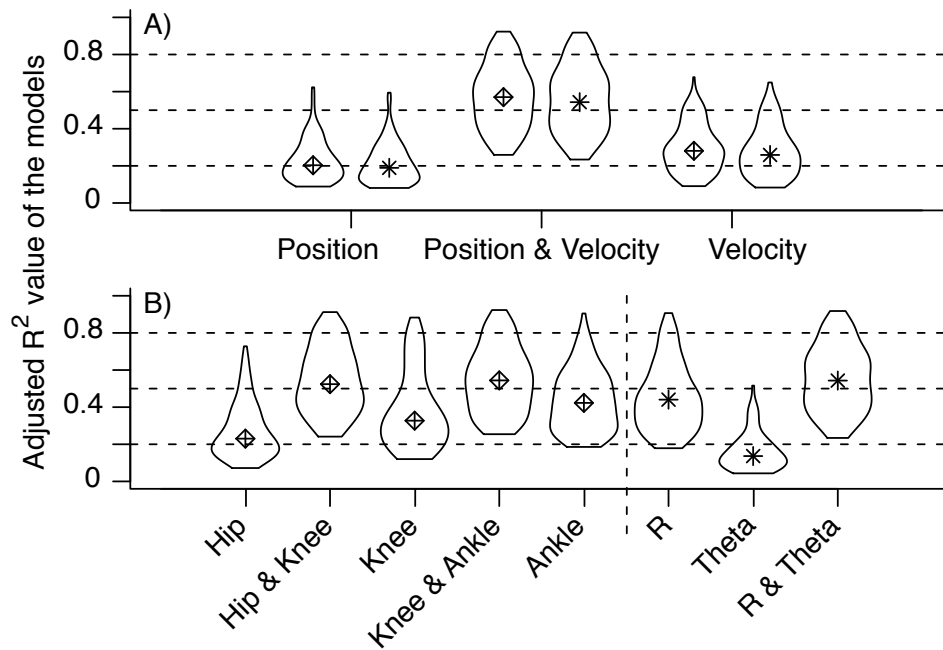


Figure 14: A) Summary of the accuracy of firing rate models comparing position, velocity and the combination of position and velocity. Models were trained and tested on random-pattern datasets. B) Summary of the accuracy of firing models comparing various kinematic explanatory variables in joint angle space and endpoint space. Each distribution contains the R^2 value of the fitted trajectories of 162 firing rate models.

The ISE ratios for the three joint angles are 3.5, 4.3 and 5.4 respectively, which means that to obtain the same accuracy as the state space approach, reverse regression needs approximately 4 to 5 times more neurons. The reverse regression estimates have large errors particularly during periods of rapid displacement, which is presumably due to the lack of velocity integration. State-space decoding integrates the velocity components of the firing rates and thus tracks more closely the kinematics trajectories.

We repeated the analysis of joint angle decoding based on 50 sets of 3, 8, 13, 18, 23 and 28 randomly selected neurons, for each of two animals. The two passive movement patterns described in section 3.2.2 were decoded separately using each set. The ISE values of the decoded trajectories for the two animals were combined, resulting in 200 ISE ratios per decoding method and per data set size. Figure 16 summarizes these results as a function of the size of the neural population used for decoding. It shows that our state-space model is clearly superior to reverse regression, especially in decoding the knee angle. When using 28 randomly selected neurons, the median ISE ratio is 1.6, 2.5 and 2.1 for the hip, knee and ankle angles respectively. This means that reverse regression needs approximately twice as many neurons to produce results as accurate as the state-space approach on average. The proportionally large increase in accuracy for the knee angle estimates is probably due to the fact that 96% of the firing rate models include the knee joint and/or its derivative as one of the explanatory variables. During decoding, this translated into a large number of neurons contributing to the prediction of the knee angle.

Our motivation for using small groups of neurons in Figure 16 is two-fold. First, we are interested in comparing the two decoding methods when only a limited number of neurons are available for decoding, since it may not always be possible in practice to collect a large population of neurons from which a set of good decoding neurons can be extracted. Second, we need to use groups that are significantly smaller than the population available, so that the variability observed across the repeat simulations is comparable to the variability one would observe in practice; we have only 56 good neurons from the second animal, so we capped at $56/2 = 28$ the decoding population size. Note however that when we used more than 28 neurons for decoding (not shown), the variability of the decoding efficiency decreased across

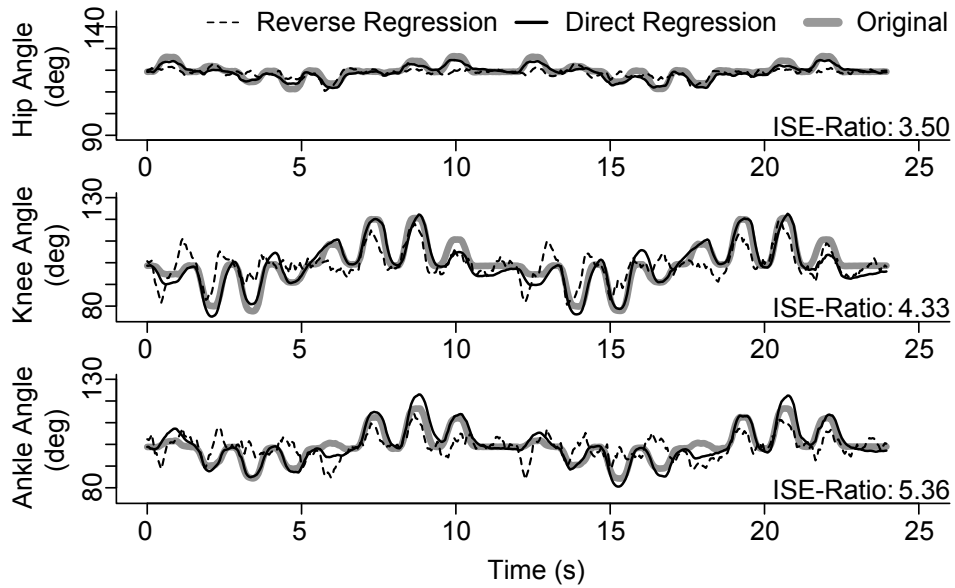


Figure 15: Example of hip, knee, and ankle joint angle trajectories decoded with the state-space and reverse regression models. This result was generated as one of the simulations with 23 randomly selected neurons. We filtered the decoded trajectory of the reverse regression post-decoding to smooth the resultant estimates. The ISE ratio's are displayed for each of the kinematic variables.

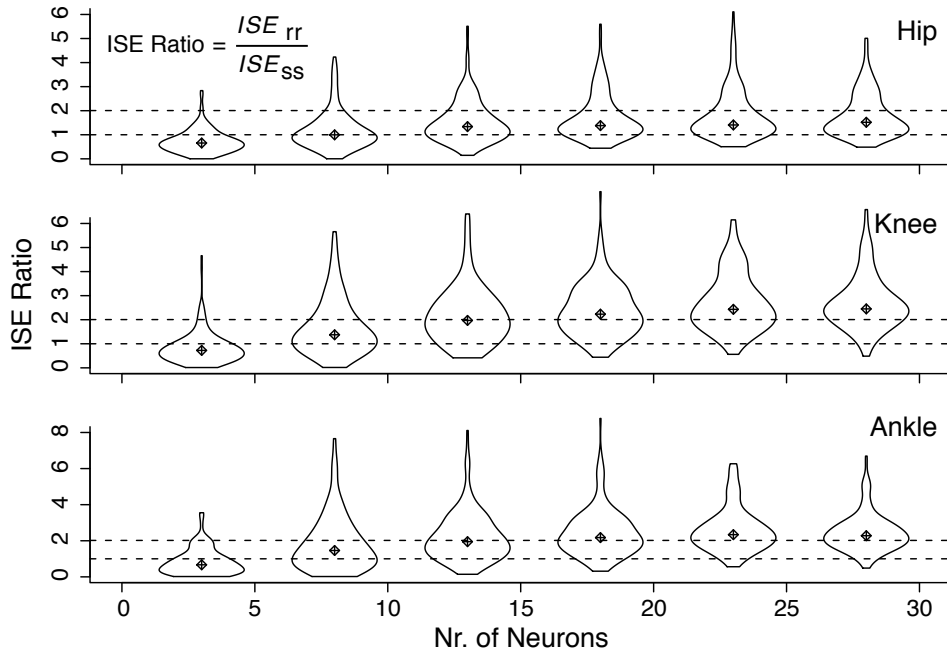


Figure 16: The ISE ratios plotted as a function of the number of neurons that are used for decoding. The distribution of the ratio is plotted for groups of 3, 8, 13, 18, 23, and 28 neurons. The included data is comprised of decoded trajectories from 50 center-out and 50 random trials per animal per distribution. Therefore, each violin plot is based on 200 simulations. Firing rate models were fit to data comprised of a combination of center-out and random trials. The median of the distribution is indicated with a dot. A ratio greater than 1 favors the state-space decoding method. A ratio of 2 means that twice the amount of neurons are needed with reverse regression to attain the same accuracy as the state-space method.

datasets, so that the violin plots became very short, which is to be expected since neurons are drawn from a comparatively small population; however the mean decoding improvement of the particle filter remained constant and similar to using 28 neurons, with median ISE ratios approximately 1.6, 2.5 and 2.1 for the hip, knee and ankle angles respectively.

Finally, it is interesting to note that reverse regression does a little better on average when very few neurons are available for decoding ($n = 3$). However, the actual ISE values are very high, meaning that neither method performs well. The relatively better performance achieved by reverse regression can be explained by the direct relation between the decoded trajectory and the constant coefficient in (3.3): in the absence of any kinematic information in the neural response, the decoded trajectory is predicted to be the constant coefficient of the regression. In contrast, the state-space method is unable to produce meaningful predictions since there is insufficient information in the neural data.

3.3.3 Decoding endpoint coordinates

The decoding efficiency of polar coordinates of the endpoint were analyzed in a similar manner. The firing rates were modeled as functions of R and θ as described in section 3.2.4.2. We found that over 90% of the models included both kinematic variables, their derivatives and the interaction between the variable and their derivatives. Figure 17 shows the efficiency results of decoding in polar coordinates, based on the same sets of neurons and trajectories used to produce figure 16. We see that state-space decoding significantly outperforms reverse regression for R , but does not show similar improvements for θ . The problem with θ is that it is poorly encoded by the neurons, as was shown in figure 14B. The consequence is that both methods decode θ poorly. Reverse regression tends to predict a constant for θ , so the estimate is biased with low variability, while the state-space model produced a highly variable estimate due to lack of information about θ .

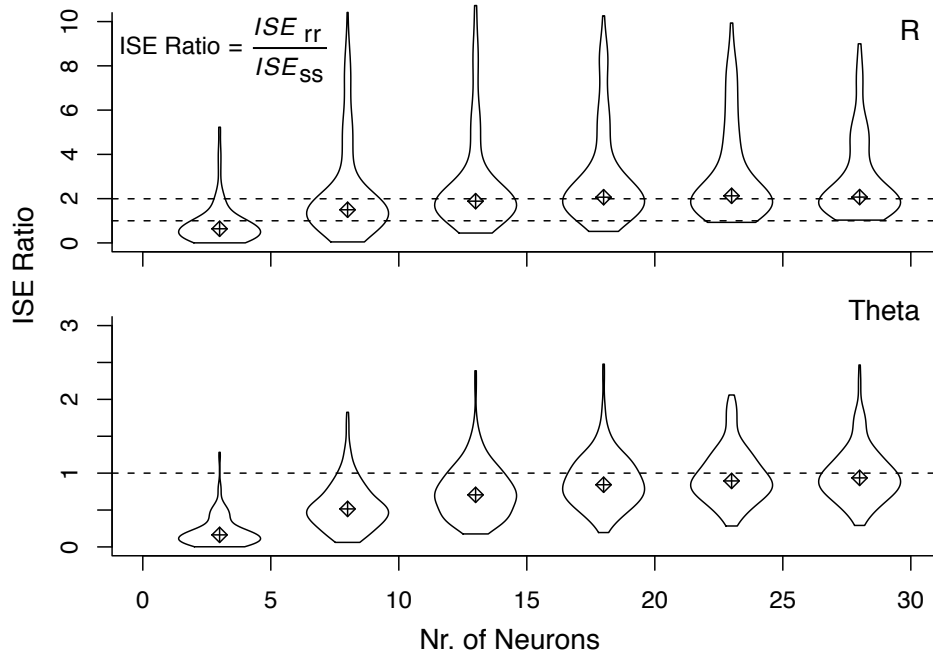


Figure 17: The ISE ratios plotted as a function of the number of neurons that are used for decoding. The distribution of the ratio is plotted for groups of 3, 8, 13, 18, 23, and 28 neurons. The included data is comprised of decoded trajectories from 50 center-out and 50 random trials per animal per distribution.

As a final remark, note that the trajectories for R and θ could also be inferred from the trajectories of ankle, knee, and hip angles when the segment lengths between the hip, knee, ankle and MTP marker are known. We found that the reverse regression trajectories were particularly poor compared to state-space decoding, presumably because the three angles are decoded separately so that their prediction errors accumulate.

3.4 DISCUSSION

This paper addresses the problem of estimating limb state from the firing rates of an ensemble of PA neurons recorded simultaneously in the DRG. It is an extension of previous studies that used linear decoding models to estimate each of several kinematic variables as a weighted sum of firing rates in the PA ensemble. In those studies, a reverse regression approach was taken to build decoding models, which provided estimates of hind limb motion during both passive [106] and active [122, 123] movements. However, reverse regression has some apparent limitations in decoding the activity of PA neurons, motivating a change to maximum likelihood estimation methods such as state-space decoding. A comparison between reverse regression and state-space decoding is provided below. We also discuss implications of this and related work for developing a neural interface to provide limb-state feedback for control of FES systems.

3.4.1 State-space decoding methods of primary afferent activity

We showed that state-space decoding performs significantly better than reverse regression. The main limitation of reverse regression is that it is based on modeling the variations of each state variable as functions of neural activity, i.e. $\text{state} = f(\text{rate})$, when in reality PA neurons are the true dependent variables modulated by one or usually multiple state variables and their time derivatives (i.e. velocities). The representations $\text{state} = f(\text{rate})$ do not allow such multivariate dependencies to be modeled, with the consequence that the information in the firing rates cannot be used efficiently. Previously published results show that reverse

regression is capable of producing decent estimates of limb kinematics with, as few as, 5 of the ‘best tuned’ neurons [123, 106]. One of the key characteristics of reverse regression that enables this accuracy is that, despite the use of linear regression, the firing rates of individual neurons do not necessarily need to be linearly related to the kinematics. By reversing the actual dependencies, reverse regression merely assumes that each kinematic variable is a linear combination of the included PA neuron firing rates.

On the other hand, the state-space framework relies on modeling the actual dependencies on the state variables that drive the neuron’s firing rate, i.e. $\text{rate} = f(\text{state})$. It accommodates effects such as multivariate dependencies and interactions and thus makes the most efficient use of information embedded in the firing rate. In this paper, we modeled the physiological encoding properties of PA neurons by fitting their firing rates to non-linear functions of one or more state variables, and applied model selection to ensure that the natural encoding properties of each PA neuron were represented accurately. Previously, [106] showed that non-linear functions could improve the accuracy of encoding models; a cubic polynomial was used there to account for regions where the firing rates saturated (i.e. at firing rates = 0 and the maximum discharge rate). In this paper, we used non-parametric functions consisting of moving lines with 4 non-parametric degrees of freedom to produce a more general non-linear fit to the firing rate models.

The state-space approach also involves a probabilistic model that describes the intrinsic behavior of the state variables. Standard models typically account for the fact that realistic state trajectories, eg. trajectory of the limb, should be smooth. In this paper, we not only accounted for trajectories smoothness, but also for the apparent inter-dependencies between the state variables in the joint angle frame (see figure 11).

Specifically, we designed a kinematic model that forces the decoded trajectories to comply with the observed kinematic constraints. Note that with reverse regression, the effect of kinematic dependencies is that some neurons are included in multiple state decoding models. For example, the ankle and hip movements tend to be highly correlated, and thus, neurons

that encode primarily for hip joint angle can also be used to estimate motion of the ankle joint. In contrast, the state-space approach maintains the physiological relationships between the state variables and the resulting PA firing rates.

We found that including velocity in the firing rate models improved the overall efficiency of the decoder, and simultaneous decoding of all kinematic variables results in lower prediction errors than decoding the joint angles individually. State-space decoding minimized the prediction error over the complete limb state, whereas reverse regression minimized it for each variable; i.e. state-space decoding provides the most likely limb posture given the firing rates and associated encoding models for a population of PA neurons. Similarly, Wu et al. found that simultaneous decoding of the full behavioral state vector (i.e. 2D position, velocity, and acceleration for the hand expressed in Cartesian coordinates) yielded the best performance in decoding neural activity in primary motor cortex.[\[129\]](#)

Loeb and also Prochazka [\[84\]](#) pioneered the development of techniques that enabled the first recordings of muscle spindle activity in awake, behaving animals. Both groups used microwires implanted chronically in the DRG to record simultaneously from PA neurons in locomoting cats. Data from these experiments was useful for developing computational models for estimating the firing rate of muscle spindle afferents as a function of muscle length, stretch rate, and fusimotor drive to the spindles [\[82, 72\]](#). However, these mechanistic models of spindle function have not yet been used to decode limb kinematics from muscle spindle recordings, likely because the models are nonlinear and difficult to invert. State-space decoding could be combined with these more physiologically accurate models to generate estimates of muscle length and stretch rate. One more step would be required to convert the muscle-state estimates into joint angular positions and velocities, but this would be rather straightforward given knowledge of musculoskeletal biomechanics, such as described for the cat hind limb in [\[40\]](#).

Our last comment concerns the aggregation of information across neurons. Stein et al. [\[106\]](#) noted that, with reverse regression, optimal decoding performance could be achieved with approximately five ‘best-tuned’ neurons having the highest correlations with a kinematic variable, and that including additional neurons that correlate well with kinematic variables

did not necessarily improve decoding performance. This means that the performance of reverse regression is highly dependent on particular neurons, and that the method fails to incorporate the information provided by other neurons. This is likely to be an issue in realistic applications, when a limited set of recorded neurons might not yield a large enough crop of ‘best-tuned’ neurons. In contrast, the state-space approach appropriately aggregates the information contained in all firing rate models via the likelihood function, and thus makes it possible to obtain accurate decoding from a non-select set of recorded neurons.

3.4.2 Natural feedback for FES control

Microelectrode recordings of PA activity can be used to provide feedback for controlling FES-enabled movements. Yoshida and Horch [131] recorded muscle spindle activity in the tibialis anterior and lateral gastrocnemius muscles in response to ankle extensions generated by stimulating the medial gastrocnemius muscle with a longitudinal intrafascicular electrode (LIFE) in the tibial nerve. Ankle joint angle estimates from the decoded LIFE recordings were used as feedback for a FES controller programmed to reach and maintain a range of fixed and time-varying joint position targets [131]. Another study used the Utah Slant Electrode Array (USEA) to establish a peripheral nerve interface for both stimulating and recording activity in motor and sensory fibers in the sciatic nerve of anesthetized cats [17]. This technology was advanced recently by incorporating a telemetry chip into the array assembly to create a fully implantable, wireless neural interface capable of recording and transmitting 100 channels of unit activity (i.e. spike-threshold crossings) from peripheral nerve or cerebral cortex [43]. Thus, the technology for establishing high-bandwidth neural interfaces with motor and sensory nerves is advancing rapidly and holds great promise for FES applications, as well as basic research.

To be suitable in a medical device application, the neural interface must remain viable and stable for several years, longevity that has yet to be demonstrated with any microelectrode interface in peripheral nerve. To date, long-term recording stability with penetrating microelectrode arrays in either peripheral nerve or DRG has not been demonstrated, and more work is needed to establish reliable, long-lasting neural interfaces [122, 91]. An al-

ternative to penetrating microelectrodes is to use nerve cuff electrodes, which measure the combined activity of many nerve fibers passing through the cuff. However, attempts at providing graded measurements of limb-state (e.g. ground reaction force or joint position) with nerve cuff recordings have had limited success [52]. In general, research towards the use of nerve cuff recordings for continuous joint-angle estimation has been limited to a single isolated joint, typically the ankle, and tested only in anesthetized animals [23, 52, 53, 71]. Cavallaro et al. [23] sought to improve continuous state estimation from nerve cuff recordings and tested several advanced signal processing methods, but reported difficulty in achieving generalization, especially for movements with large joint angular excursions. However, newer nerve cuff electrode designs such as the flat intra-fascicular nerve electrode (FINE) contain a higher density of electrodes and are designed to reshape the nerve to improve alignment and access to central fascicles [62]. Finite element modeling studies have shown that FINE electrodes may be capable of resolving compound nerve activity within individual fascicles using beam-forming techniques, an approach that may greatly increase the quality of information that can be extracted from nerve cuff recordings. [32].

As further improvements towards chronically stable neural interfaces proceed, focus will shift towards interpreting the recorded signals. Advanced decoding methods, such as the state-space decoder discussed here, will enable us to extract meaningful information from PA firing rates and take us a step closer to incorporating afferent feedback in closed loop neuroprostheses.

3.5 CONCLUSIONS

The results of the present study and those reviewed above demonstrate the potential for using PA neuronal activity to generate estimates of limb-state, which would be useful feedback for controlling FES systems. State space decoding is a principled and accurate method for decoding kinematics based on population recordings of PA neurons in the DRG. Because of its ability to efficiently use all neural responses to predict limb state, fewer neurons are

needed to attain a similar accuracy as reverse regression, and multi-joint dependencies are correctly incorporated in the neural models. The ensembles of PA neurons provide significant information about limb state and is well-suited for incorporation in a neural interface. However, the stability and reliability of the neural interface needs to be addressed before these decoding efforts can successfully be used to provide limb state feedback for controlling neural prostheses.

4.0 ALTERNATIVE DECODING TECHNIQUES FOR PREDICTING LIMB STATE

The previously described decoding methods resulted in accurate predictions of limb kinematics and overall described a more principled method to decode the firing rates of primary afferents. However, processing power requirements of these algorithms are currently too demanding to be implemented in a ‘real-time’ application such as a neural prosthesis. This chapter discusses alternative methods that can be used to improve the currently used decoding techniques.

4.1 DYNAMIC FUZZY NEURAL NETWORKS

In 1985, fuzzy modeling was developed as a fast and cost-efficient way to model multi-dimensional non-linear systems [110, 108]. Although fuzzy reasoning had been applied as an engineering tool before 1985, Takagi and Sugeno’s approach limited the requirement of operator-based learning and dynamically partitioned the input variable space in fuzzy sets, greatly reducing the complexity seen in previous methods [110].

The fuzzy model Takagi and Sugeno proposed has been the seed of various efforts to generalize and formalize fuzzy logic in a neural network package. Below, I summarize the idea of the fuzzy model; refer to the original paper for a detailed walkthrough [110]. A fuzzy set A is denoted by a membership function $A(x), x \in X$, which has a range between $[0, 1]$; see figure 18-B. Each of the fuzzy sets is associated with a linear model that predicts the

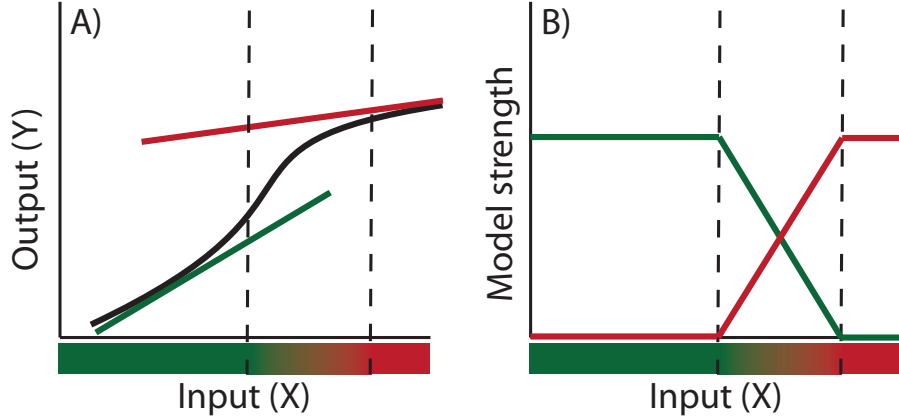


Figure 18: A) A non-linear function can be described by multiple linear functions provided that B) additional functions are provided that model the strength of each linear function over the span of the input variable.

models the desired variable as a linear function of the inputs. At time i , given input variables \mathbf{x}^i and output variable y^i , then an implication L^i is defined as:

$$L^i : \text{If } x_1 \text{ is } A_1, x_2 \text{ is } A_2, \dots, x_p \text{ is } A_p, \quad (4.1)$$

$$\text{then } y^i = c_0^i + c_1^i x_1 + c_2^i x_2 + \dots + c_p^i x_p$$

where A_j is a fuzzy set indicating a particular range of $x_1 \dots x_p$. In other words, this states that if the input variables are exactly in the range of the i -th fuzzy set, then the variable y can be fully described by the i -th implication. When the inputs are not fully determined by a single implication, the output y^* is inferred by taking the weighted average of the y^i 's from multiple implications:

$$y^* = \frac{\sum_{i=1}^q w^i y^i}{\sum_{i=1}^q w^i} \quad (4.2)$$

where w^i indicates the weight of the i -th implication. The estimate y^* in equation 4.2 is calculated by finding the weights $w^1 \dots w^q$ which represent the ‘closeness’ of the current observation to each of the implications. By taking the weighted average of all $y^i \dots y^q$, y^* describes a non-linear model comprised of a set of linear equations y^i .

Figure 18 visualizes fuzzy reasoning in a simplified matter. In A), we see the non-linear relation we are trying to model in black. In red, and green are two local linear approximates of the relation. We can approximate the non-linear relation by combining the two linear models with varying degrees depending on the value of input X. In B), we show the relative strength of each of the linear models as a function of the value of X. We see that for small X, the green model is used and for large X, the red. In the ‘fuzzy’ part, we can approximate the non-linear function by taking a weighted average of the two models with relative strengths as indicated in B). Although this example operates in a single dimension, this approach can be extended to a multidimensional input space and/or a multivariate output [127].

Various derivatives of the TSK-model calculate the weights in different ways as functions of the input variables. Takagi et al. used unit step-functions with linear falloffs (see figure 18-B), but more recent implementations use gaussian shaped kernels to infer the weight of an implication [127, 128, 86, 71, 118]. We can regard the identification of the model during the training session as a search to partition the input space into the fewest fuzzy subspaces that satisfy predetermined encoding accuracy requirements [108]. The method by which the underlying structure is identified has been the main differentiating factor between solutions proposed by various groups.

In the early 1990’s, fuzzy neural networks were introduced as a framework for implementing the TSK-algorithm [63], which was followed by the D-FNN [127] and GD-FNN algorithms [128]. The latter algorithm is particularly interesting as it is capable of dynamically partitioning the input space with limited user interaction. The GD-FNN framework utilizes a neural network with 4 layers indicating the inputs, membership function, rules and output variables. Training the neural network is described as an iterative process where the rules are added and removed dynamically as the data is observed [128].

In 2001, Micera et al. demonstrated that fuzzy neural networks could be used for decoding angular information from muscle afferents using two nerve cuffs implanted around the tibial and peroneal nerve [71].

A slight variation of the GD-FNN method was developed by Rigosa et al. in an effort to decode limb state information from ensembles of simultaneously recorded dorsal root neurons [89]. As part of a collaboration with this group, we implemented a similar algorithm as a tool for decoding primary afferent firing rates in ‘real-time’. The next subsection will describe the overall methodology used and indicate some differences between the implemented method and the GD-FNN algorithm.

4.1.1 Alternative implementation of the GD-FNN

In order to investigate the use of the GD-FNN algorithm for real-time feedback for FES control, I worked closely with Rigosa et al. [89] in developing a fuzzy neural network algorithm in MATLAB. The method presented in this thesis differs slightly from the method described in [89] as I continued to develop the algorithm following the analysis presented in the published paper. Both developed algorithms are adapted versions of the GD-FNN algorithm as presented by Wu et al. [128]. A thorough explanation of the training algorithm can be found in that work. This section summarizes the GD-FNN algorithm and will indicate where we diverge from the GD-FNN algorithm. The main differences are listed below:

- During encoding, in order to determine whether the existing set of membership functions envelope the observed data sufficiently, a distance measure is used to find the ‘distance’ of the observed data to each of the existing membership functions. The GD-FNN method uses the euclidean distance to the center of the membership function which was copied from the D-FNN method. However, although the euclidean distance measure was justified in the D-FNN method, this should not have been used in the GD-FNN method. The reason that the euclidean distance was valid in the D-FNN method was that the width of each of the membership functions was equal and could be eliminated from the measure. As this is not the case in the GD-FNN method, the euclidean distance is no longer a

valid measure to find the ‘distance’ to the membership functions. Therefore, instead of the euclidean distance, the evaluated value for each membership function was used to determine the ‘closeness’ to a membership function.

- Second, the original TSK model normalizes the weights of the fuzzy parameters (see equation 4.2) which is not implemented in the GD-FNN algorithm. This seems to introduce some problems which, for example, could result in a highly sectioned input space whereas the underlying correlations could actually be represented by a single linear model. In the revised method, the weights of the rules were normalized for each evaluation of the model which solves this situation and is more true to the original fuzzy neural theory.
- Finally, the suggested approach for assigning a new rule as described in equation 20-22 of [128] cannot be implemented as such due to the boundary conditions the authors applied. We simplified this step in order to accommodate all situations.

The object of training the fuzzy neural network is to partition the input variable space $\mathbf{F} = (F_k, k = 1, \dots, K)$, and locally define linear regression models

$$\mathbf{A}_r = a_0^r + \sum_{k=1}^K a_k^r F_k, r = 1, \dots, R, \quad (4.3)$$

with R equals the number of partitions defined during the training. The general structure of the GD-FNN is presented in figure 1 of [128]. Each input variable has p membership functions $A_{kj}(j = 1, 2, \dots, p)$ which take on the form of Gaussian functions with mean:

$$u_{kj} = \exp \left[-\frac{(f_i - c_{kj})^2}{\sigma_{kj}^2} \right] \quad (4.4)$$

The partitions in the input space are referred to as rules (R) in fuzzy neural networks. The strength of the j -th rule $R_j, j = 1, \dots, p$ can be described as a function of the regularized mahalanobis distance (M-distance)

$$\theta_j = \exp [-md^2(j)] \quad (4.5)$$

with

$$md(j) = \sqrt{(\mathbf{F} - \mathbf{C}_j)^T \Sigma_j^{-1} (\mathbf{F} - \mathbf{C}_j)} \quad (4.6)$$

and \mathbf{C}_j the centers of the membership functions belonging to the j -th rule and Σ_j^{-1} the an array with the widths (σ_j) of the accompanying membership functions on the diagonal.

The training algorithm relies on an iterative algorithm that creates, removes rules and updates the consequent parameters a_k^r based on the training data. Below, a summary of the iterative process during encoding is given below. Details for each of these steps can be found in [128].

1. Generate first rule based on initial observed firing rate values \mathbf{F}_0 . The mean c_{k1} is set to the observed values and σ_{k1} is set to a predefined value. This value could be based on the range of the input space. Set $t = 2$.
2. Collect the observed firing rates \mathbf{F}_t^{obs} at t and compute the mahalanobis distance \mathbf{md} to each of the existing rules A .
3. Compute the output error e_t^k as the difference between the estimated value at time t and the training data set using the currently defined rules .
4. if $e_t^k > e_{th}$, with e_{th} the threshold for the decoding error, proceed to 5, else proceed to 7.
5. If $\min(\mathbf{md}) > md_{th}$, with md_{th} the threshold mahalanobis distance, then proceed to 5.a, otherwise goto 5.b
 - a. The observed value is not represented using the previously defined rules. Increase the number of rules $j = j + 1$ Add a rule with the center $\mathbf{c}_j = \mathbf{F}_t$. The width of the membership functions are chosen according to function 19 in [128]. Goto item 6

- b. Although the mahalanobis distance does not cross the threshold, the actual prediction error exceeds the limits. Reduce the widths of the closest existing rule such that it spans a reduced partition of the input space. Goto item 7
6. Analyze the existing rules by finding the subset of significant rules and delete any rules that are no longer significant in the regression model.
7. Update $t = t + 1$ and go to item 2.

Figure 19 shows a simulation which illustrates the capabilities of the implemented algorithm. In A) we defined a ‘kinematic’ variable and defined two thresholds that were later used to create non-linear responses in the simulated neurons. We simulated the firing rate of 10 neurons as linear functions of the kinematic variable (B) and introduced noise on each channel. An offset was introduced when the ‘kinematic’ variable crossed the predefined thresholds. The fitted models of the fuzzy neural network and reverse regression are shown in panel C). It can be seen clearly that reverse regression fails to capture the non-linear components whereas the FNN does so correctly. The final panel shows the 3 rules that were dynamically generated during the encoding process. The algorithm correctly identified the three sections characterized by the thresholds in A).

Subsequently, the GD-FNN algorithm was used to decode the limb kinematics during a center-out passive movement trial. The model was trained on two consecutive center-out patterns and decoded on a different data-set. Figure 20-A shows the resulting predicted hip angle as well as the predicted hip angle using ordinary reverse regression. Both reverse regression and GD-FNN estimates were smoothed following the prediction using a 150ms moving average.

The GD-FNN estimate clearly outperforms the ordinary method. Similar results were attained looking at the knee and ankle angle (not displayed). The figure also shows a graphic representation of the strength of the active rules during the prediction. As the strengths are normalized, the sum equals 1 at all times. It can be seen that the dynamic encoding process assigned three rules which are active in different partitions of the multidimensional input space.

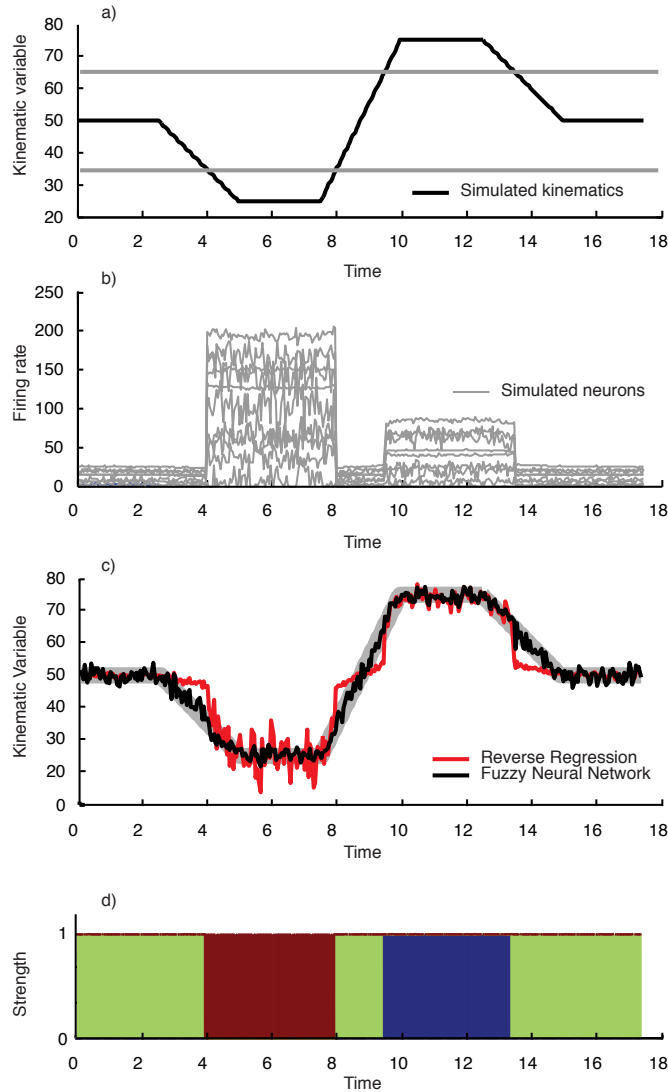


Figure 19: Demonstration of non-linear decoding using fuzzy neural networks. In this example, highly non-linear neurons are simulated and used to decode a single kinematic variable. a) The kinematic variable that will be predicted using linear regression and a fuzzy logic NN. The dotted lines indicate threshold values used to introduce the non-linearities in the firing rates. b) The firing rate response of 10 simulated neurons. c) The actual trajectory with the predicted values from both decoding methods. d) The strength of the dynamically generated rules; the fuzzy logic NN correctly identifies the three partitions in the input space.

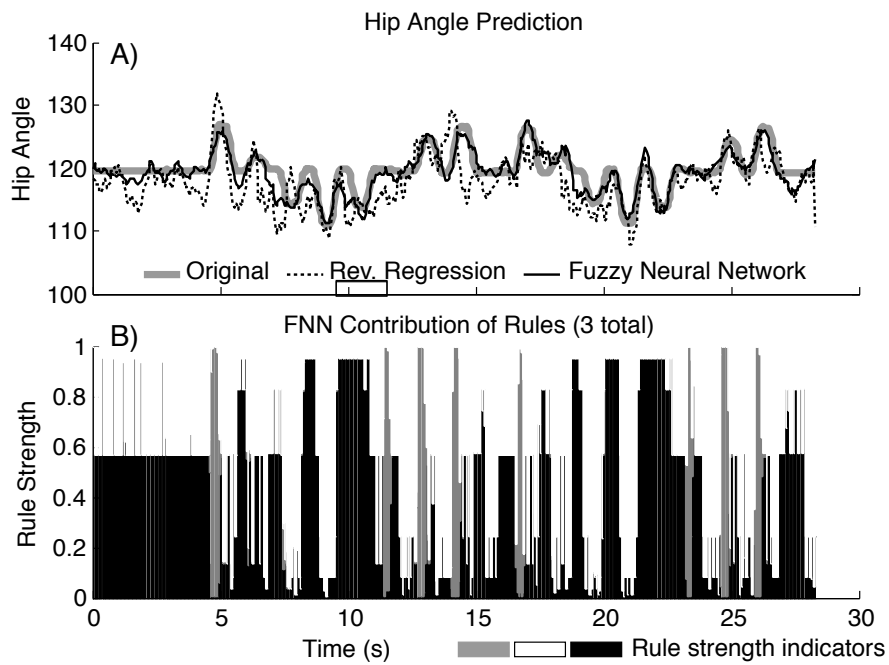


Figure 20: Example of a decoded hip angle during a center-out passive movement trial. A) The hip angle plotted versus time and the estimates of the hip angle using reverse regression decoding and fuzzy neural network decoding. B) The strength of the rules over time during decoding using the fuzzy neural network. The sum of the strength of the rules equals 1 at all times. It is clear that different rules are utilized for various states of the limb kinematics.

Although fuzzy neural networks are widely utilized by the engineering community to implement non-linear controllers, alternative algorithms modeling non-linear behavior have been proposed which are rooted in a more statistical reference frame. Spline regression models provide a similar methodology to partition the input space and apply local linear models for decoding. The next section will present decoding results using splines in an extension of the reverse regression method.

4.2 SPLINE REVERSE REGRESSION

Instead of using fuzzy neural networks, one can extend the reverse regression models to allow for non-linear effects of the firing rates on the kinematic variable. As described in section 2.2.2, we modeled each kinematic variable A_k as a function of the primary afferent firing rates \mathbf{FR} ,

$$A_k = \beta_{k0} + \sum_{i \in S_k} s_i(FR_i) \quad (4.7)$$

where $s(\cdot)$ indicates a spline and S_k the set of neurons used in the analysis.

Using the same data-set as the previous example, we plotted the estimates of hip-angle using reverse regression and spline based reverse regression in figure 21. For this example we used splines with 4 non-parametric degrees of freedom for all regression variables. As expected, the spline based regression outperforms the reverse regression significantly.

Using splines, the input variable space is also sectioned and locally fitted. For each regression variable, a linear or quadratic function is fitted for each of the sections marked by the knots. Therefore, the number and location of the knots influence the variability of the fitted model. As with fuzzy neural networks, model selection is the main difficulty when using spline bases for the reverse regression method. Especially with the large number of regression variables (the firing rates), there are an infinite number of feasible models. In order to simplify the model selection, we can try to estimate the number and locations of the knots for each regression variable separately and use the resulting knots for the kinematic

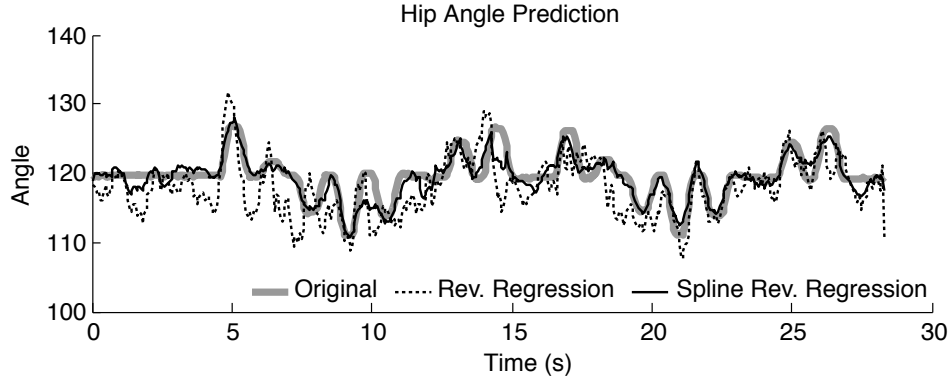


Figure 21: Decoding center-out movement using spline reverse regression. Limb kinematic predictions are shown for reverse regression and reverse regression using smoothing splines with 4 degrees of freedom.

model described in equation 4.7. We can then proceed to eliminate knots from the new model to minimize the degrees of freedom if necessary. Thus, in order to find an accurate model for kinematic variable A_k , we first try to model this variable directly using each of the recorded afferent firing rates individually.

We define the set of models $A_k = \beta_{k0} + s_i(FR_i)$, where we vary the number of knots and/or their location. For example, we can start by performing a model selection on the models with 1, 2 or 3 knots at equidistance. Model selection is used to determine the most appropriate knot locations for that particular spline. Once this is done for all neurons, we use the resulting knot locations as an initial guess for the splines in equation 4.7. We can continue our model selection by randomly removing knots to minimize the degrees of freedom in our kinematic model.

In summary, fuzzy logic neural networks are capable of describing a non-linear transfer function in terms of a weighted average of linear functions. The methodology is relatively easy to interpret which might be one of the reasons that the technique still is popular amongst engineers for non-linear modeling. However, using non-parametric splines for non-

linear multivariate modeling can result in similar or better estimates and is well regarded with the statistical community. Although the primary focus of this chapter has been on the fuzzy neural networks as a result of the collaboration with Dr. Silvestro Micera, at the ARTS laboratory of the Scuola Superiore Sant'Anna in Italy, it seems that regression splines should be considered as the more viable option for improving the accuracy of decoded trajectories in a 'real-time' neuroprostheses. Implementation of such methods in Labview and or Matlab are currently being pursuit in the lab and will be used during subsequent experiments.

5.0 CLOSED LOOP CONTROL OF FUNCTIONAL ELECTRICAL STIMULATION

A functioning demonstration of closed loop control of limb state using primary afferent firing rates as the feedback loop for the controller is presented in this chapter. It will address and discuss the hypothesis described in the 4th specific aim of this thesis. It combines the techniques described in the previous chapters and provides a stepping stone for further development towards continuous, stable and reliable feedback control of FES.

5.1 INTRODUCTION

Functional electrical stimulation (FES) has long been recognized as a viable way to restore function in the extremities of paraplegic patients. Recognizing that the muscle is an efficient actuator for limb movement, it is not surprising that many studies have focussed on the implementation of FES for limb kinetic restoration. To date, multiple devices have been developed and are commercially used such as, the bionic glove [81], the WalkAid [28, 107] and the NESS Handmaster [42].

The Walk-aid is the only application within these examples that can be regarded as a closed loop FES-system because stimulation is based on the angle of the shank of the affected leg. When the subject reaches the end of the stance phase, the stimulator turns on, lifting the foot which enables the swing phase to be executed appropriately. Despite this success story, feedback sensors have proven difficult to implement in prosthesis due to their unreliability, fragility and practical difficulties.

Despite these difficulties, it is widely recognized that a FES system would benefit tremendously from sensory feedback in terms of adaptability and functionality as long as the feedback system would be reliable [79, 67]. With closed loop control of FES, it is possible to change the stimulation parameters dynamically and make them dependent on the feedback from the sensors. If accurate predictions of limb state are available to the FES controller, it will be able to compensate for muscle fatigue and possibly be able to adjust for unexpected perturbations of the extremity, e.g. stumbling.

Although the single external sensor works well in the case of the WalkAid, this approach might not work as well when detailed multivariate information is required as the feedback for the neuroprosthesis [67, 53]. Implantable sensors have been suggested as a viable alternative to external sensors. In 2004, Tan et al. described a method to use the antenna coils of implantable stimulation units (BIONs) to infer limb state variables. They conclude that using such sensors can potentially be combined with other sensing techniques to ultimately provide sufficient accuracy for closed loop control of FES for patients with paralysis [112, 111].

Alternatively, one can record from the natural sensors of the nervous system and decode the limb state based on their neural response. Muscle spindles as well as golgi tendon organs and cutaneous afferents are known to be contributors to proprioception although it is generally accepted that the muscle spindles are the main contributors to proprioception [35]. The firing rate response of these afferents can be correlated to global kinematic variables such as endpoint position of the extremity of joint angles (see section 1.1.3).

With current technology, it is possible to record simultaneously from many of those afferents and previous research has showed that by recording from these afferent neurons in the Dorsal Root Ganglia (DRG), it is possible to predict the limb state accurately throughout a movement [106, 122, 119, 120]. In these experiments, the hind limb of a cat was passively manipulated throughout various movement patterns while kinematics and primary afferents were recorded. After the experiment, the data was analyzed and limb kinematics were predicted using the recorded firing rates of the primary afferents. For neural prosthesis, a realtime version has to be implemented that is capable of estimating the limb state in real time.

There are various ways to implement the interface for electrical stimulation. Surface stimulation and intra-muscular stimulation are the most direct method of activating the muscles. Alternative methods have been proposed over the years such as selective stimulation using a multi-site nerve cuff [62] and intra-spinal micro-stimulation [5, 41]. These methods have the advantage that they require lower stimulation currents and have lower stimulation artifacts as a result. In addition, these methods target multiple muscles using a single interface which makes it attractive for clinical use. ISMS also claims to potentially activate synergies of muscles which may be beneficial to the correct recruitment of muscle tissue [60]. In this work however, we used intramuscular stimulation as it is the easiest to implement and the most reliable way to stimulate different muscles in an experimental setup.

The following sections investigate the feasibility of using primary afferent signals in a ‘real-time’ closed loop controller for FES. The work described in this chapter leading towards the complete closed loop controller includes discussions about various aspects of this engineering problem; 1) The real-time decoding algorithm will be discussed, 2) a method for removing the stimulation artifacts and its implications on the decoded signal will be discussed and 3) a state-machine based stimulation controller is proposed as an initial approach towards a closed loop FES controller.

5.2 METHODS

5.2.1 Surgical procedures

All procedures were approved by the Institutional Animal Care and Use Committee of the University of Pittsburgh. Four animals were used in these procedures. Anesthesia was initiated using Isoflurane (1-2%) and switched to Alpha Chloralose for the duration of the trials. Temperature, end tidal CO₂, heart rate, blood pressure and oxygen saturation were monitored continuously during the experiments and maintained within normal ranges. Intravenous catheters were placed in the forelimbs to deliver fluids and administer drugs. A laminectomy was performed on the left side and penetrating micro-electrode arrays (1.5mm

length, Blackrock Microsystems LLC, USA) were inserted in the L7 (50 electrodes in 10x5 grid) and L6 (40 electrodes in 10x4 grid) dorsal root ganglia. A combination of patch and intramuscular stimulating electrodes were placed in various muscles spanning hip, knee and ankle joints. Suitable locations for electrode placement were found by stimulating the site with a mono-polar probe. At the conclusion of the experiments, the animals were euthanized with KCL (120 mg kg⁻¹).

5.2.2 Experiment setup

A custom frame was designed to support the cats torso, spine and pelvis while allowing the hind limb to move freely through its full range of motion. A stereotaxic frame and vertebrae clamp were used to support the head and torso, and bone screws were placed bilaterally in the iliac crests to tether the pelvis with stainless steel wire (see figure 22).

Neural data was sampled at $25kHz$ using an RZ-2 real time signal processing system (Tucker Davis Technologies, USA). The neural data was filtered using a bandpass filter with cutoff frequencies of 300 and 3000 Hz. Neural activity was defined as an event where the raw recorded signal crossed a manually set threshold. This threshold was set manually for each channel depending on the signal to noise ratio of the particular electrode. A snippet of 1ms was recorded each time the signal crossed the threshold and the neural sources on a single channel were discriminated using a k-means clustering algorithm which was implemented to function on the recording hardware (RZ-2). Events (spikes) were binned for each independent source in 50ms windows within the RZ-2 device and subsequently streamed over the ethernet using the UDP protocol to the ‘real-time’ stimulation controller.

Kinematic data was captured using a high speed motion capture system (Impulse system, PhaseSpace Motion Capture, USA). Joint angles for hip, knee and ankle were computed in realtime using custom developed software and were streamed over the ethernet to the ‘real-time’ stimulation controller using the UDP protocol. A haptic device (Phantom Premium 1.5HF, Sensable Technologies Inc, USA) was used to create an artificial floor and estimate ground reaction forces during the FES trials. In addition, a slight viscous force field was simulated to dampen the effect of stimulation and reduce unwanted oscillations.

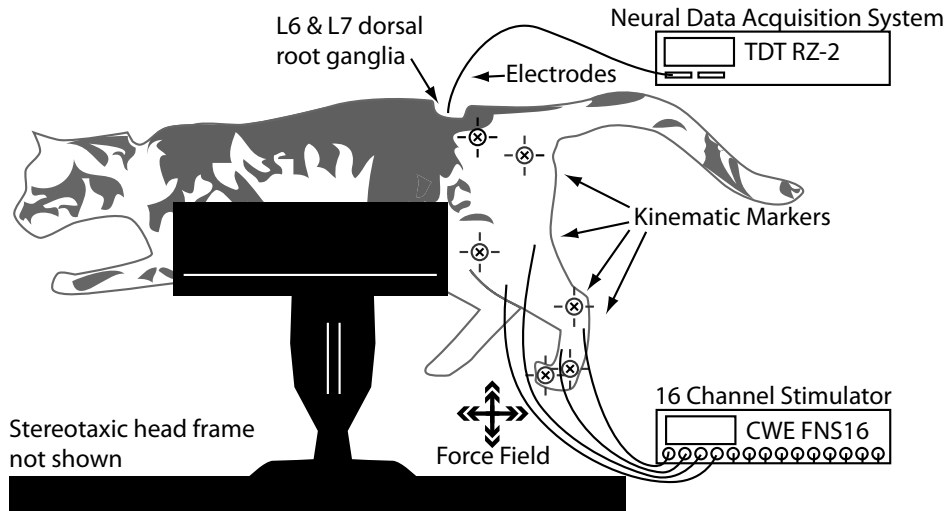


Figure 22: The animal was positioned in a custom designed frame to support the torso and pelvis, enabling unrestrained movement of the left hind limb. Active markers were placed to track the hind limb kinematics and a 90-channel micro electrode array was inserted in the L6/L7 DRG to record neural activity. Intra-muscular electrodes were placed in various hind limb muscles to evoke movement and a phantom robot was attached to the foot to generate an artificial floor by means of a force field (not shown).

Binned spike counts and joint angles were retrieved by the stimulation controller PC running custom analysis software developed in Labview (National Instruments, Austin, USA). Binned spike counts were smoothed by convolving a triangular window (150ms) were paired with the recorded kinematics. The joint data-structure was used to train and decode the kinematic models. Both neural and kinematic data were processed in 50ms windows to facilitate the software to compute the kinematic predictions. This conforms with low-pass filtering methods used in previous experiments using reverse regression methods [122, 106].

5.2.3 Realtime encoding of firing rate models

Offline decoding limb kinematics from a population of primary afferents in the DRG has been demonstrated previously using various decoding techniques such as reverse regression and state-space modeling [106, 119, 120]. Although the state-space modeling algorithms were found to be clearly superior to the previously used reverse regression techniques, we implemented the latter because of implementation considerations (see chapter 4 for additional information). For these experiments, we did not use any non-parametric splines as the development package did not natively support this type of regression algorithm.

For this work, let $\mathbf{X} = (X_k, k = 1, \dots, K)$ be the vector of K kinematic variables we want to decode, based on the firing rates $\mathbf{FR} = (FR_i, i = 1, \dots, I)$ of I neurons. In this work we considered two reference frames to express limb state (\mathbf{X}); a joint-based frame with state vector $(A_k, k = 1, 2, 3)$ that represents intersegmental angles for the hip, knee, and ankle joints, and a endpoint force frame with state vector (X, Z) that represents the vertical and forward force generated at the endpoint of the extremity. A subscript t added to any variable means that we consider the value of that variable at time t . The firing rates \mathbf{FR} were obtained by smoothing the incoming binned spike counts using a triangular window spanning $150ms$. Using reverse regression we can predict the joint angles and endpoint forces by modeling these variables as a linear function of the observed firing rates, such that

$$X_k = \beta_{k0} + \sum_{i \in S_k} \beta_{ki} FR_i + \epsilon_k, \quad (5.1)$$

where S_k indexes the set of neurons which were classified in realtime by the clustering algorithm, and ϵ_k are uncorrelated random errors. The predictions are obtained by evaluating the model at the observed firing rates.

5.2.4 Removing stimulation artifact

Stimulation of the muscles results in significant artifacts in the recorded neural data and can potentially give rise to erroneous estimates of neural firing rates. Previous studies have used input blanking to remove stimulation artifacts during recording, shielded the stimulation sites to minimize artifacts [131] or used the fact that a stimulus artifact appears on all channels simultaneously to eliminate these events in an offline analysis [123].

In order to estimate the effect of stimulation artifact on the recorded neural data and the ability to record meaningful afferent responses, we simulated the amount of time stimulation artifacts would mask the input channels as a function of the average stimulation frequency and the number of independent channels of stimulation. Figure 23 shows the percentage of time available for uncontaminated recording as a function of these variables. We can see that the number of independent channels of stimulation significantly degrades the possibility to record afferents. To circumvent this problem, we programmed the stimulation controller such that all channels were synchronized during stimulation. The stimulation frequency was set to 30Hz and the intensity of the stimulation was solely determined by the amplitude of the stimulation pulses. At 30 Hz stimulation, muscles in general display tonic contractions. By using synchronous stimulation of the electrodes, we can eliminate the effects of multiple electrodes and, given a blanking window of 1ms, still have approximately 95% of the time for neural decoding.

One problem with blanking the input channels during stimulation is that this introduced discontinuities of the values on the input channels. As neural data are usually smoothed before processing, this introduces unwanted oscillations following blanking. In the worst case scenario, this could result in an unwanted spike event when the oscillations exceed the channel threshold. In addition, blanking the inputs removes all data during that period and makes offline analysis and verification of the method impossible.

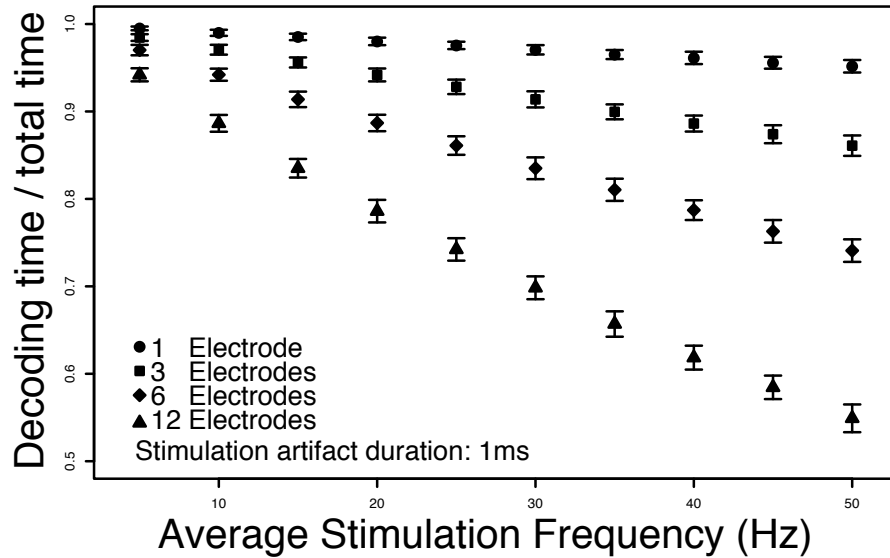


Figure 23: Effects of blanking stimulus artifacts on the available time to record neural data. As the average stimulation frequency increases or multiple electrodes are active in a non-synchronous way, the remaining time for decoding the firing rates decreases. This plot was generated using multiple simulations of multichannel stimulation. The decoding time was defined as the time where no stimulation was occurring.

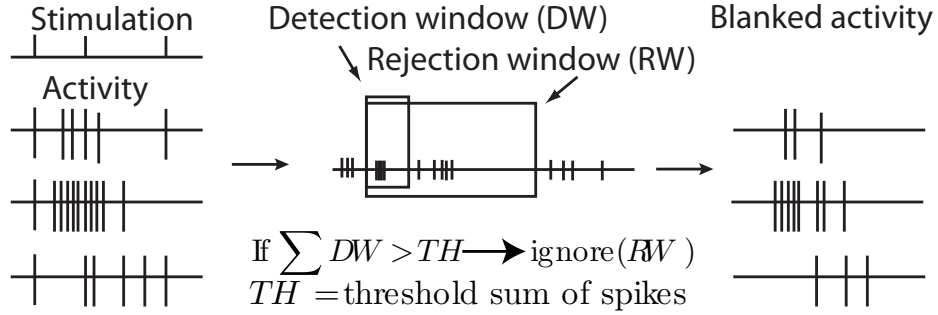


Figure 24: This simulated schematic describes the stimulation artifact removal algorithm as implemented on the RZ2 DSPs. Spike activity from all channels is represented on a single time-axis. The number of spikes recorded during the detection window (DW) are summed and if this number exceeds a threshold ($TH = 0.9 \cdot \text{number of channels}$), all recorded spikes in the rejection window (RW) are ignored. The size of RW can be equal or bigger than the size of the DW.

Using a state of the art neural data acquisition system, we were able to implement a hardware based version of the synchronous event detection algorithm. Figure 24 shows the implemented method. We defined a small time window ($DW = 1\text{ms}$) and summed all recorded events within at each time-point. In case more than 90% of the channels recorded a spike during that interval, all spikes in the rejection window RW were excluded from the calculation of the instantaneous firing rates of the units. The RW could be set to an arbitrary length and could be used to exclude afferent responses generated by direct stimulation of the afferent fibers. The instantaneous firing rate was subsequently calculated per unit on the neural data acquisition system and streamed over the ethernet using the UDP protocol. Using this artifact rejection method, all signals including stimulation artifacts will be recorded for offline analysis while they will be omitted during the realtime control of FES.

5.3 RESULTS

Data from multiple closed loop FES experiments are presented in this section. As previous chapters discussed the ability to decode limb kinematics from primary afferent firing rates in detail, no example will be given in this chapter. Analysis of realtime encoding and decoding of limb kinematics will be presented in section 5.3.1. Section 5.3.2 will present data on the ability to decode during functional electrical stimulation and finally, section 5.3.3 will present an example of closed loop FES.

5.3.1 Realtime decoding of primary afferents

An example of real-time decoding using reverse regression is presented in figure 25. Here, the hindlimb was passively manipulated through a series of center-out movement tasks. At $t = 0s$, the kinematics and observed instantaneous firing rates were used to update models for the kinematic parameters (joint angles). At $t = 60s$, the estimated models were used in combination with the observed firing rates to predict the kinematics. The results in figure 25 were produced during the trial and not manipulated afterwards. The typical noisy characteristic of reverse regression and the incorrect predictions during high velocity movement (overshoot) can easily be seen although the overall predicted values for hip, knee and ankle angle seem accurate.

Figure 26 shows the progression of the coefficients during the ‘realtime’ encoding process during a random walk passive movement test. The bottom panel shows the joint angles for hip, knee and ankle during the encoding process and the top panel shows a heat-map representing the influence of each neuron in the model of the accompanying kinematic variable. The influence was calculated by multiplying the value of the coefficient by the the maximum firing rate of that neuron over the course of the encoding process. Subsequently all resulting values were normalized to fall within a range of $[-1,1]$. The encoding algorithm was implemented in Labview and developed such that the models were updated as fast as possible during the trial which resulted in an update rate from 200ms to 3 seconds as the encoding trial progressed.

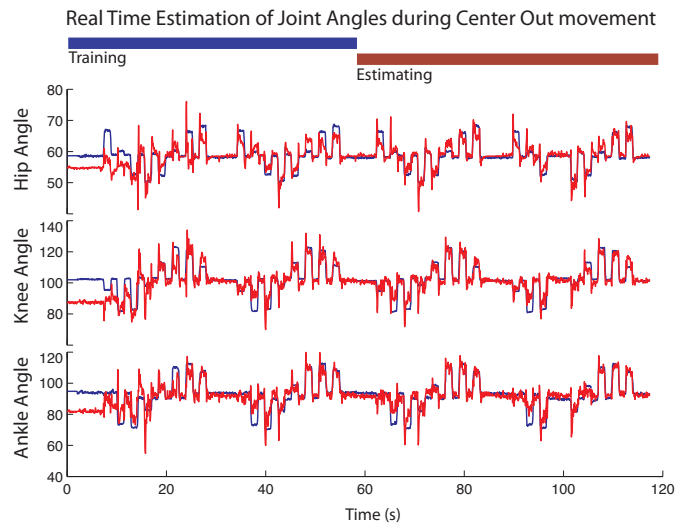


Figure 25: Realtime encoding and decoding of the firing rates of primary afferents during a passive center-out movement trial. During the first minute, the kinematic and the observed firing rates are used to encode the kinematic models, during the second minute the observed firing rates are used to predict limb kinematics.

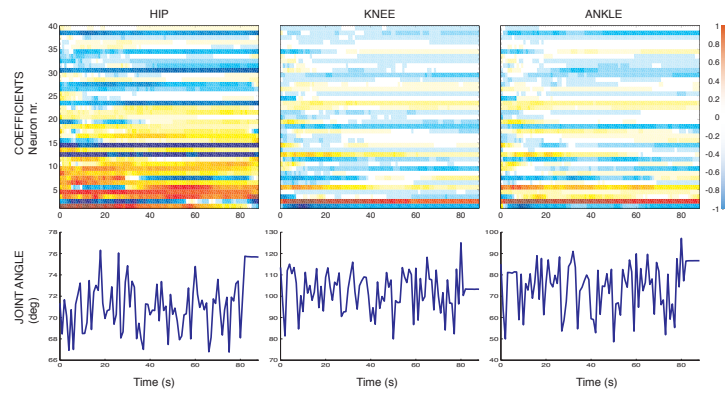


Figure 26: Progression of regression coefficients during model encoding. Three kinematic models for hip, knee and ankle joint angles were continuously updated during a random passive movement trial. Each row in the upper plots represents the firing rate of a single neuron. The influence was calculated by multiplying the value of the coefficient by the the maximum firing rate of that neuron over the course of the encoding process. Subsequently all resulting values were normalized to fall within a range of $[-1,1]$.

The neurons corresponding to each row are matched across the different models. This implies that some of the same neurons heavily influence the predictions of multiple models. In addition, we can see that a relatively large group of neurons have equal contributions for the hip model whereas for knee and ankle, a limited set of neurons convey all information about the kinematic variable.

5.3.2 Decoding during stimulation

Decoding during FES requires the controller to dismiss stimulation artifact. Figure 27 shows that the observed firing rates of primary afferents continue to provide information about limb state during stimulation. Here, the hind limb was manipulated through a series of flexion and extension movements using a robotic manipulator. During the second set of movements, electrical stimulation was applied to generate stimulation artifact at a rate of 30 Hz. The location and amplitude of the stimulation was chosen such that no significant muscle force was generated during these trials. It can be seen that the example neurons carry information about ankle position under both scenarios. This demonstrates that information can be extracted from the primary afferent population in the presence of FES.

To demonstrate that the primary afferent neurons continue to generate graded responses to the desired variables, we used FES to generate ground reaction forces in a semi-isometric preparation. Here, the foot was strapped to a stationary force transducer. Limb extensors were stimulated at 30 Hz over a prolonged period of time to induce fatigue. The stimulation was alternated on/off manually to generate an alternating pattern of ground reaction forces. Figure 28 shows the neural response as well as the stimulation times. Overlaid is a prediction of the ground reaction forces based on the primary firing rates recorded in the DRG. The ability to track the forces during fatigue demonstrates that the decoded forces are not merely tracking the periods of stimulation.

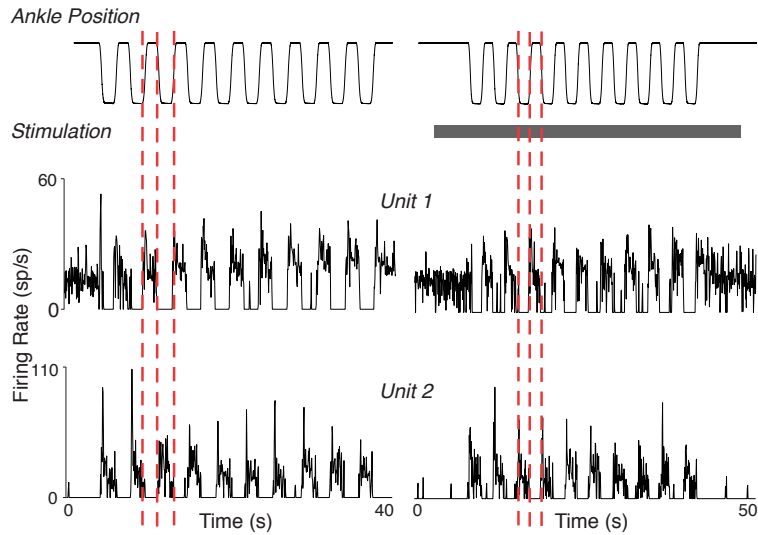


Figure 27: Primary afferent firing rates recorded during passive flexion and extension of the hind-limb with and without stimulation. It can be seen that the firing rate response of both units is maintained during stimulation of the leg. In this scenario the amplitude of the stimulation created significant artifacts during recording but did not produce any significant activation of a muscle.

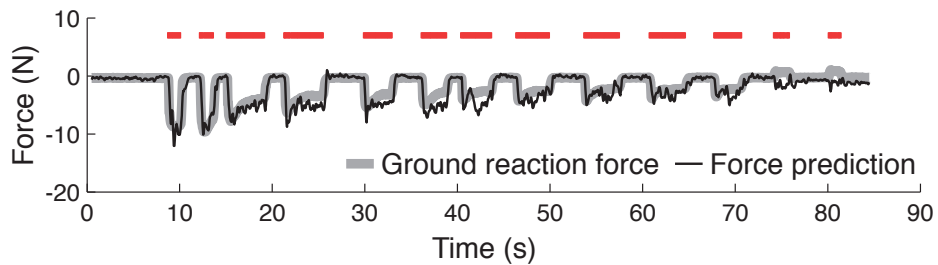


Figure 28: Decoding ground reaction forces during functional electrical stimulation. The stimulation was manually triggered and forces were recorded with the foot fixed to a stationary load cell. Fatigue of the muscle is accurately predicted using primary afferent firing rates during stimulation.

5.3.3 Closed loop control of FES

Labview was used to implement a ‘real-time’ closed loop FES controller which was capable of switching stimulations parameters using a state machine triggered by the endpoint kinematics of the hindlimb (actual or predicted). Figure 30 shows the front-end of this state machine as well as some of the trajectories obtained using FES on multiple channels. This display is similar to the display used to define the state-machine during the actual experiments.

The hindlimb is represented by a stick-figure with segments between the Iliac Crest and the Hip, Hip-Knee, Knee-Ankle and Ankle-Foot. The state machine can be configured by ‘drawing’ boxes in the workspace to indicate the regions in which the controller should increment the state of the stimulation paradigm and accompanying stimulation parameters. In this case, we defined 4 states. The transition between the states was initiated when the endpoint of the hind limb entered a switch point section and remained there for a predetermined amount of time. Transitions between states could be set to instantaneously or could be changed gradually by fading in/out of the stimulation amplitudes. All channels were set to stimulate at 30 Hz in synchrony to minimize the stimulation artifacts.

Prior to the trial, we selected a subset of stimulation channels per state such that the resulting limb movement was directed towards the next stimulation switch location. We could do so by selecting individual channels and amplitudes per state. Minimum and maximum stimulation period were enforced such that the trial was aborted when the next box was not reached.

Figure 30 also shows some recorded trajectories during a closed loop trial. In this particular case, we switched the stimulation states based on the kinematics recorded with the camera setup. Other trials using the predicted kinematics from the neural data showed similar results, albeit a little less accurately.

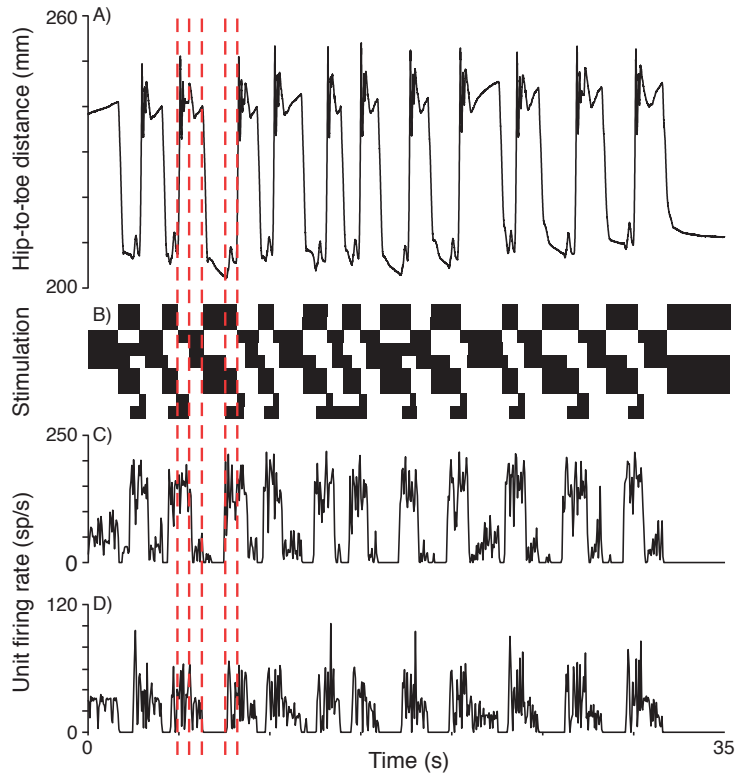


Figure 29: Limb movement and afferent responses during a closed loop stepping trial in which movement was created by FES using 9 channels and 4 different states in the state-machine. A) The kinematic variable indicating the distance between the hip and toe marker. B) The stimulation pulses on 9 channels; the red lines indicate the 4 different stimulation patterns. C) and D) show the response of two primary afferent neurons, both neurons correlate with the kinematics independently of the stimulation.

Subsequently, we imposed perturbations to the leg by obstructing its movement during stimulation (not shown). This resulted in prolonged period of stimulation of the same pattern as the leg was not able to reach the following state switch point. Although the estimates of limb state were sufficient to drive the state-machine during these closed loop trials, the accuracy of the decoded trajectories has room for improvement. New decoding methods, such as those proposed in the previous chapters, should provide the required improvements and will be implemented in future experiments.

Figure 29 shows the response of two primary afferent neurons during the closed loop stimulation. In A), we plotted the distance between the hip marker and the toe marker for a series of FES evoked steps. As the foot is placed forward (First red dotted line), we can see some oscillations resulting from the simulated floor created by the haptic device. Subsequently, the foot is pushed back, lifted up and moved forward before repeating the sequence.

The second panel (B) shows the stimulation sequence on the 9 implanted stimulation sites. We can see the four distinct patterns responsible for the different stages in the step-cycle. Panels C) and D) show the response of two units which are correlated to the kinematic variables. During these trials, all recorded unit activity was used to decode the kinematics; that is, there was no selection of neurons used for decoding.

5.4 DISCUSSION

A closed loop neural prosthesis should be regarded as a complex system integrating different challenges such as afferent recording, kinematic state decoding, actuating the muscles and the accompanying control algorithms. The results presented in this chapter should be regarded as an initial attempt to combine these challenges in order to understand the complexity of the task. We showed that with the current technology, it is possible to develop a rudimentary closed loop FES controller which is able to generate walking-like behavior in a closed loop fashion.

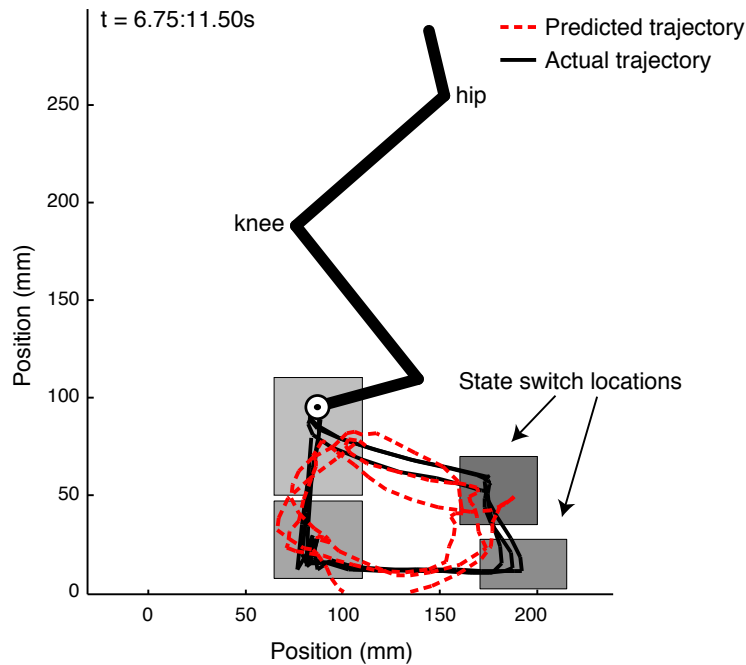


Figure 30: Example trajectories produced by closed loop FES. The solid thick black stick figure represents the hind limb of the animal and the endpoint is used to trigger the state-machine. The state switch location boxes can be positioned by the experimenter and indicate the areas where the state-machine should switch stimulation parameters. The displayed boxes are an approximate location in this particular trial. The black thin line represents the actual limb endpoint kinematics over 4 cycles and the red dotted line represents the limb endpoint prediction using the firing rates of the recorded primary afferent neurons.

Although reverse regression has been proven to provide good estimates of limb kinematics, recent work has shown that other decoding techniques can improve the estimates significantly. State-space decoding improves the resulting estimates by a factor of two. However, this decoding technique is not fast enough to be implemented in real time. An alternative is to use a fuzzy logic decoding algorithm. Rigosa et al. showed that this type of decoder can also improve the estimates significantly in an offline situation [89]. Fuzzy logic decoding sections the input variable space and defines a linear model for each subspace. Limb kinematics are inferred by a weighted average of the models where the weights are determined by a measure of proximity of the inputs to each section. The previous chapter also introduced spline regression as a viable extension to reverse regression. Challenges will include the implementation of such decoders in a ‘real-time’ environment as currently developed in Labview.

Alternatively, as the stimulation parameters are driven by a state-machine, it can be suggested to use a classifier decoding method rather than a continuous representation of limb angles. Such a method could predict the likelihood of the leg being in one of the switching states. Such a method might result in more robust state switching but will lose the ability to track the limb-state variables.

Artifact rejection is an integral part of a closed loop controller using functional electrical stimulation as the muscle activator. We showed that when the stimulation paradigm is tuned to minimize the stimulation artifact by aligning stimulation on different channels, it is possible to remove the stimulation artifacts without losing the ability to decode limb state variables from the primary afferent population. Although direct stimulation artifacts are relatively easy to identify and reject based on amplitude and wave-shape, this is not the case for artifact arising from direct stimulation of the afferent neurons as the recorded signal will be indistinguishable from a neural response related to a change in limb state. However, synchrony detection across a large number of channels might be able to separate the different scenarios. This type of artifact could potentially be greatly reduced by changing the stimulation paradigm.

A vast body of research has been published on the application of functional electrical stimulation as a means of reanimating paralyzed extremities. Intra-spinal micro stimulation (ISMS) has been suggested as an alternative to intra-muscular and surface stimulation during the recent years [5, 41]. ISMS has the advantage that it uses very small stimulation artifacts as compared to surface stimulation and can potentially activate synergies of muscles which may be beneficial to the correct recruitment of muscle tissue [60]. Using the DRG or the ventral roots as the location for stimulation has also been suggested as an alternative location [5]. Our lab is currently investigating the feasibility of using these alternative locations for stimulation.

The relationship between muscle length and joint or limb position is typically complex and in many cases indeterminate [9], suggesting that other sources of feedback are required to resolve ambiguities in spindle feedback related to joint position [26]. In addition, sensory receptors as the muscle spindle are innervated by modulated motor neurons (γ) that change the behavior of the sensors constantly. Spinal cord injuries change this descending neural track and therefore alter the afferent coding scheme. The impact of this change on the ability to decode accurately from the afferent population is unknown but highly relevant for applications of FES while spinal cord patients are part of the target population.

In summary, a closed loop neural prosthesis comprises a complex system integrating different challenges such as afferent recording, kinematic state decoding, actuating the muscles and the accompanying control algorithms. The results presented in this chapter should be regarded as an initial attempt to combine these challenges in order to understand the complexity of the task. They showed that with the current technology, it is possible to develop a rudimentary closed loop FES controller which is able to generate walking like behavior in a closed loop fashion.

Advancements in the neural engineering field are largely reliant of improvements of the stability and reliability of the neural interfaces used in these applications. Continuing efforts to improve FES control, afferent decoding and interface technology should be pursued to enable the use of closed loop FES neuroprostheses in the future.

6.0 GENERAL DISCUSSION

In this final chapter of my thesis, I will elaborate on the results presented in this work as well as provide my view on the necessary research to be conducted extending the presented work. Section 6.1 will summarize and discuss the findings in this work and section 6.2 will discuss its significance in the bioengineering field and suggest directions for future work.

6.1 SUMMARY

It is believed that the nervous system represents the kinematic state of extremities in various ways throughout the nervous system [38, 11, 12]. An interface with the nervous system to extract this sensory information would significantly aid the development of advanced neuroprostheses using FES to animate paralyzed extremities. By means of sensory integration, the CNS is thought to be able to reduce the highly redundant input space into a representation of limb state that is more useful to process. The location of the interface can therefore influence the types of signals we are able to extract. The work presented in this document has focussed solely on the sensory nervous system at the level of the DRG; the firing rates of the individual sensory neurons.

The foundation for the work presented in this thesis originates with the work of Stein and Weber who presented methods for decoding limb kinematics from the firing rates of populations of primary afferent neurons in [105, 122]. In chapter 2, we provided a more generalized and principled method for decoding limb kinematics from the firing rates of primary afferent neurons. We showed that by modeling the firing rate of the primary afferents

instead of modeling the kinematic variables, the decoder could take into account that the firing rate of an afferent neurons could be non-linearly related to multiple kinematic variable.

Subsequently, in chapter 3, we extended these methods to be able to incorporate velocity components of the firing rate. In addition, we showed how state-space modeling can be used to predict multiple correlated kinematic variables in a principled way. The resulting estimates of limb state were on average twice as accurate as previously suggested methods (reverse regression). Although the results of state-space modeling were promising, it required significant computing power to execute and was therefore not ready for implementation in a ‘real-time’ environment at this time.

Chapter 4 discussed some alternative methods for decoding limb kinematics that would be fast enough to implement in ‘real-time’. Fuzzy neural networks have been proposed to find a set of input-output relations describing a non-linear process [108]. We showed that an adapted version of the TSK fuzzy logic decoder can be used to decode limb kinematics and improve decoding accuracy over reverse regression. Alternatively we found that spline regression shows equal improvements over reverse regression and is more principled and easier to implement than fuzzy neural networks. Although both methods improve upon reverse regression, they are not as principled as state-space modeling because velocity components and the coupling between kinematic variables are not taken into account.

Finally, in chapter 5, various aspects and challenges of a closed loop FES neuroprosthesis are presented. A ‘real-time’ controller was implemented and it was shown that the firing rates of primary afferents could be recorded, sorted and used for decoding limb kinematics in such a setup. Stimulation artifacts were removed in hardware using a sliding window and a synchronous detection algorithm. The FES controller was updated using a state-machine based on the predicted limb kinematics.

In summary, the work in this thesis provides methods for decoding primary afferent neurons and sets a foundation for further development of closed loop FES control of paralyzed extremities. Although a complete closed loop neuroprosthesis for natural behavior seems far away, the premise of this work argues that an interface at the dorsal root ganglia should be considered as a viable option.

6.2 SIGNIFICANCE AND FUTURE WORK

Functional electrical stimulation has been regarded as highly potential for restoring functionality in hemi/paraplegic patients. It has been proven to facilitate improved hand functionality [81], standing capability [29, 30], improved walking capability [107] and is used in many other applications. Using muscles to generate movement might be the most power efficient way to displace extremities which facilitates assisted movement of extremities with a relatively small power source. In addition, FES helps the body to maintain muscle mass, rigidity, and in general be in a more healthy state.

However, FES applications suffer from multiple drawbacks that require additional attention before FES can be used reliably as a means to restore the functionality of an affected extremity. One of the most important issues that need to be addressed is how to measure the actual kinematic state of the limb while using the prosthesis to facilitate closed-loop control of FES [44]. Exteriorly placed sensors such as gyroscopes and goniometers, force sensors and stretch sensors have been proposed and tested in closed loop FES applications [78, 28, 103]. Although these options are viable when limited information is needed, the use of exterior placed sensors rapidly becomes difficult due to practicality issues when multiple degrees of freedom are necessary. Therefore, the use of the body's own sensory signals has seen an increasing amount of attention and has been the focus of this dissertation.

Fundamental knowledge of the mechanisms and nature of proprioception is necessary to understand the neural processes responsible for motor planning, control, and adaptation. Despite a large body of literature that describes many details of primary afferent response characteristics, and their projections to intra-spinal networks and ascending pathways to the brain, relatively little is known about the actual neural coding and decoding processes that support representations of limb state at any level of the sensory system. Thus, there are several fundamental, yet unanswered questions about the nature of somatosensory feedback. Which state variables are represented and which classes of afferent neurons contribute to the neural representation of each state variable? Although this thesis has mostly focussed on the practicality of using primary afferents for neuroprostheses, more knowledge about the

physiology, interactions and changes of primary afferent firing rates as a result of spinal cord injury will likely be beneficial to the development of viable neuroprostheses.

This work has argued that afferent feedback is required to be able to compensate for fatigue and account for unexpected perturbations as represented schematically in figure 5. However, in the particular scenario where the person has impaired motor control but intact sensory perception, one could argue against the need to decode the afferent signals for closed loop control of FES. Although not represented in figure 5, direct connections exist between sensory and motor areas in the higher regions of the CNS which might provide an adequate feedback loop in this scenario. Therefore, when afferent pathways remain intact and the patient only suffers from diminished motor control, it is possible that feedback loops in higher regions of the CNS are sufficient to compensate the motor intent signal to the FES controller.

It has been shown that a monkey can control a robot arm using cortical signals with increasing accuracy and degrees of freedom [38, 117]. However, state feedback of the robotic arm is purely visually in these experiments. An interesting extension of this work would be to investigate whether proprioception will provide alternative/additive information which could potentially result in better control of the neural prosthesis. This untested hypothesis would be interesting to explore in an animal model as this could give us direct insight in the flexibility of higher regions in the CNS to afferent information.

In order to address these questions, one could surgically sever the ventral roots innervating one of the upper extremities in a monkey while leaving the dorsal roots intact. Alternatively, one could use botulinum toxin (BOTOX®) to temporarily paralyze the muscles while leaving the afferent response intact. Although both methods would also affect the gamma motor drive to muscle spindles, it would provide a good model for the investigated scenario. The affected extremity could then either be fitted with a custom exoskeletal robotic manipulator or with surgically implanted FES electrodes (BOTOX®inhibits Acetylcholine release and it should therefore still be possible to use direct stimulation of the muscles using FES). Results of reaching/drawing tasks could be compared to results obtained using only visual feedback.

In the neural engineering community, there has been a steady search for the coordinate frame in which the CNS encodes proprioception. In 2000, Bosco and Poppele presented studies in which they claimed that secondary afferent neurons in the dorsal spinocerebellar tract (DSCT) can signal foot position independently from the specific joint angles [12]. This could suggest that an abstraction of the primary afferent sensory space is performed at relative low levels of the CNS. However, a closer look at their observations raises the question whether the conclusions they present really reflect the observed behavior of the DSCT neurons. For example, figure 8 in [12] is supposed to show that a neuron is invariant to endpoint position while having different behavior in joint angle space when its response is compared in a restraint and passive movement task. They argue that the data during the passive trial can best be described by a linear function whereas the data in the constraint trial is best described by a quadratic. However, this is most likely caused by the fact that the range of motion of the hip angle is drastically smaller in the passive trial than in the constraint trial. In my opinion, it is very likely that if the researchers would have ‘forced’ to record data over the same movement range, it would look exactly similar. As it might be hypothesized that the neuron used for in the paper is a better than average example, it seems that there is insufficient evidence from either statistical point or visually to infer any underlying mechanisms in my opinion. They correctly conclude that an alternative explanation is that the DSCT cells respond to additional unmeasured input variables such as forces acting on the joint as a result of their setup [12].

In general, we should be very careful about statements explaining how the CNS interprets the afferent firing rates and kinematic variables. Statements about the CNS representing limb state only in endpoint coordinates can easily be rejected as this kinematic representation is our ability to sense and we obviously experience more than pure endpoint positions of our extremities. This does not mean that a reduced kinematic representation cannot be found somewhere in our CNS but does prove that the CNS does not directly integrate all afferent inputs to form a very reduced variable space before processing it in higher regions of the CNS.

Over the last couple of years, we advanced from offline reverse regression methods to state space modeling and ‘real-time’ FES applications. Specifically looking at the ‘real-time’ application, I think that we could have focussed more directly on a decoding method based on state classification rather than continuous decoding. The advantage of classifiers is that it directly address the events you are interested in. Especially in gait, this might be a more solid and robust solution to switch between the different stimulation states. However, a continuous prediction of limb kinematics might be advantageous when more detailed information is required. For example, if we want to detect perturbations and unexpected events. The reason we decided to start with the continuous predictions is that it relates to previous published work for decoding primary afferent firing rates in an offline setup.

An unmentioned, but interesting, topic concerning FES neuroprosthesis is the location of the stimulation. We used intra-muscular electrodes for stimulation during the closed loop experiments because of their practicality and easy of implementation. However, the large currents necessary for muscle animation produced significant stimulation artifacts. In addition, this type of stimulation is prone to activating the sensory receptors directly, resulting in a distorted representation of limb kinematics directly following a stimulation pulse. Intra-spinal microstimulation has been suggested as an alternative strategy which lacks the drawback previously mentioned but has shown mixed results as well [109, 60]. Using the DRG or the ventral roots as the location for stimulation has previously been suggested as an alternative location [5]. Unpublished experiments in our lab show that micro-stimulation in these areas show potential as they can selectively activate different muscle groups. Additional research will have to investigate the feasibility in more detail.

Finally, as mentioned in previous chapters, the physical interface with the nervous system is a crucial point of interest for neuroprostheses and its stability and reliability needs to be addressed before any decoding efforts can successfully be used to provide limb state feedback for controlling neural prostheses.

6.3 FINAL THOUGHTS

In pursuit of functional applications for neuroprostheses, one should realize that state of the art hardware and software will continue to be one of the drivers behind their success or failure. The experimental setup required for experiments towards these goals tend to grow increasingly complex and the quantity of processed data require serious investments towards analysis strategies. As this trend continues, it will be important to develop standardized protocols for data interaction, manipulation and storage in order to maintain an efficient research facility.

In addition, as the technology advances and the reality of bi-directional brain computer interfaces inches closer, collaborations between the fields of Bioengineering, Robotics, Neuroscience, Computer science and Statistics will be more important with every step. One of the biggest challenges will be to combine the knowledge in these fields and to rely on each-others expertise.

BIBLIOGRAPHY

- [1] E D Adrian. The impulses produced by sensory nerve endings: Part i. *J Physiol*, 61(1):49–72, Mar 1926.
- [2] E D Adrian and Y Zotterman. The impulses produced by sensory nerve-endings: Part ii. the response of a single end-organ. *J Physiol*, 61(2):151–71, Apr 1926.
- [3] E Alnaes, J K Jansen, and T Rudjord. Fusimotor activity in the spinal cat. *Acta Physiol Scand*, 63:197–212, 1965 Mar.
- [4] Y Aoyagi, R B Stein, A Branner, K G Pearson, and R A Normann. Capabilities of a penetrating microelectrode array for recording single units in dorsal root ganglia of the cat. *J Neurosci Methods*, 128(1-2):9–20, Sep 2003.
- [5] Yoichiro Aoyagi, Vivian K Mushahwar, Richard B Stein, and Arthur Prochazka. Movements elicited by electrical stimulation of muscles, nerves, intermediate spinal cord, and spinal roots in anesthetized and decerebrate cats. *IEEE Trans Neural Syst Rehabil Eng*, 12(1):1–11, 2004.
- [6] R S Arutiunian. Changes in the sensitivity of the muscle spindles of fast and slow-contracting muscle fibers following chronic de-efferentation. *Neirofiziologija*, 13(2):204–209, 1981.
- [7] D J Bennett, S J De Serres, and R B Stein. Regulation of soleus muscle spindle sensitivity in decerebrate and spinal cats during postural and locomotor activities. *J Physiol*, 495 (Pt 3):835–850, 1996 Sep 15.
- [8] Rajmohan Bhandari, Sandeep Negi, and Florian Solzbacher. Wafer-scale fabrication of penetrating neural microelectrode arrays. *Biomed Microdevices*, 12(5):797–807, Oct 2010.
- [9] J Biggs and K Horch. Biomechanical model predicts directional tuning of spindles in finger muscles facilitates precision pinch and power grasp. *Somatosens Mot Res*, 16(3):251–262, 1999.

- [10] Jaimie F Borisoff, Lowell T McPhail, James T W Saunders, Gary E Birch, and Matt S Ramer. Detection and classification of sensory information from acute spinal cord recordings. *IEEE Trans Biomed Eng*, 53(8):1715–1719, 2006.
- [11] G Bosco and R E Poppele. Reference frames for spinal proprioception: kinematics based or kinetics based? *J Neurophysiol*, 83(5):2946–2955, 2000.
- [12] G Bosco, R E Poppele, and J Eian. Reference frames for spinal proprioception: limb endpoint based or joint-level based? *J Neurophysiol*, 83(5):2931–2945, 2000.
- [13] G Bosco, A Rankin, and R Poppele. Representation of passive hindlimb postures in cat spinocerebellar activity. *J Neurophysiol*, 76(2):715–26, 1996.
- [14] L J G Bouyer and S Rossignol. Contribution of cutaneous inputs from the hindpaw to the control of locomotion. i. intact cats. *J Neurophysiol*, 90(6):3625–3639, 2003.
- [15] L J G Bouyer and S Rossignol. Contribution of cutaneous inputs from the hindpaw to the control of locomotion. ii. spinal cats. *J Neurophysiol*, 90(6):3640–3653, 2003.
- [16] A Branner and R A Normann. A multielectrode array for intrafascicular recording and stimulation in sciatic nerve of cats. *Brain Res Bull*, 51(4):293–306, Mar 2000.
- [17] A Branner, R B Stein, E Fernandez, Y Aoyagi, and R A Normann. Long-term stimulation and recording with a penetrating microelectrode array in cat sciatic nerve. *IEEE Trans Biomed Eng*, 51(1):146–157, Jan 2004.
- [18] A E Brockwell, A L Rojas, and R E Kass. Recursive bayesian decoding of motor cortical signals by particle filtering. *J Neurophysiol*, 91(4):1899–907, 2004.
- [19] AE Brockwell, RE Kass, and AB Schwartz. Statistical signal processing and the motor cortex. In *Proceedings of the IEEE*, volume 95, pages 881–898, 2007.
- [20] E N Brown, L M Frank, D Tang, M C Quirk, and M A Wilson. A statistical paradigm for neural spike train decoding applied to position prediction from ensemble firing patterns of rat hippocampal place cells. *J Neurosci*, 18(18):7411–7425, Sep 1998.
- [21] E N Brown, L M Frank, D Tang, M C Quirk, and M A Wilson. A statistical paradigm for neural spike train decoding applied to position prediction from ensemble firing patterns of rat hippocampal place cells. *J Neurosci*, 18(18):7411–25, Sep 1998.
- [22] Jane H Burridge, Morten Haugland, Birgit Larsen, Ruth M Pickering, Niels Svaneborg, Helle K Iversen, P Brøgger Christensen, Jens Haase, Jannick Brennum, and Thomas Sinkjaer. Phase ii trial to evaluate the actigait implanted drop-foot stimulator in established hemiplegia. *J Rehabil Med*, 39(3):212–8, Apr 2007.
- [23] Ettore Cavallaro, Silvestro Micera, Paolo Dario, Winnie Jensen, and Thomas Sinkjaer. On the intersubject generalization ability in extracting kinematic information from

- afferent nervous signals. *IEEE transactions on bio-medical engineering*, 50(9):1063–73, Sep 2003.
- [24] Cynthia A Chestek, Vikash Gilja, Paul Nuyujukian, Ryan J Kier, Florian Solzbacher, Stephen I Ryu, Reid R Harrison, and Krishna V Shenoy. Hermesc: low-power wireless neural recording system for freely moving primates. *IEEE Trans Neural Syst Rehabil Eng*, 17(4):330–8, Aug 2009.
- [25] D F Collins and A Prochazka. Movement illusions evoked by ensemble cutaneous input from the dorsum of the human hand. *J Physiol*, 496 (Pt 3):857–71, Nov 1996.
- [26] D F Collins, K M Refshauge, and S C Gandevia. Sensory integration in the perception of movements at the human metacarpophalangeal joint. *J Physiol*, 529 Pt 2:505–515, 2000.
- [27] X Cui, V A Lee, Y Raphael, J A Wiler, J F Hetke, D J Anderson, and D C Martin. Surface modification of neural recording electrodes with conducting polymer/biomolecule blends. *J Biomed Mater Res*, 56(2):261–72, Aug 2001.
- [28] R Dai, R B Stein, B J Andrews, K B James, and M Wieler. Application of tilt sensors in functional electrical stimulation. *IEEE Trans Rehabil Eng*, 4(2):63–72, 1996.
- [29] R Davis, T Houdayer, B Andrews, and A Barriskill. Paraplegia: prolonged standing using closed-loop functional electrical stimulation and andrews ankle-foot orthosis. *Artif Organs*, 23(5):418–420, 1999.
- [30] M J Dolan, B J Andrews, and P H Veltink. Switching curve controller for fes-assisted standing up and sitting down. *IEEE Trans Rehabil Eng*, 6(2):167–171, 1998.
- [31] John P. Donoghue. Bridging the brain to the world: A perspective on neural interface systems. *Neuron*, 60(3):511 – 521, 2008.
- [32] D Durand, H Park, and B Wodlinger. Localization and control of activity in peripheral nerves. *Engineering in Medicine and Biology Society*, Jan 2008.
- [33] B Edin. Cutaneous afferents provide information about knee joint movements in humans. *J Physiol*, 531(Pt 1):289–297, 2001.
- [34] James B Fallon and Vaughan G Macefield. Vibration sensitivity of human muscle spindles and golgi tendon organs. *Muscle Nerve*, 36(1):21–9, Jul 2007.
- [35] S C Gandevia, D I McCloskey, and D Burke. Kinaesthetic signals and muscle contraction. *Trends Neurosci*, 15(2):62–5, Feb 1992.
- [36] S. C. Gandevia, J. L. Smith, M. Crawford, U. Proske, and J. L. Taylor. Motor commands contribute to human position sense. *Journal of Physiology*, 571(3):703–710, 2006.

- [37] Simon C Gandevia, Kathryn M Refshauge, and David F Collins. Proprioception: peripheral inputs and perceptual interactions. *Adv Exp Med Biol*, 508:61–68, 2002.
- [38] A P Georgopoulos, A B Schwartz, and R E Kettner. Neuronal population coding of movement direction. *Science*, 233(4771):1416–9, 1986.
- [39] E V Goodall, T M Lefurge, and K W Horch. Information contained in sensory nerve recordings made with intrafascicular electrodes. *IEEE Trans Biomed Eng*, 38(9):846–50, Sep 1991.
- [40] G E Jr Goslow, R M Reinking, and D G Stuart. The cat step cycle: hind limb joint angles and muscle lengths during unrestrained locomotion. *J Morphol*, 141(1):1–41, 1973.
- [41] Lisa Guevremont, Jonathan A Norton, and Vivian K Mushahwar. Physiologically based controller for generating overground locomotion using functional electrical stimulation. *J Neurophysiol*, 97(3):2499–2510, 2007.
- [42] H. T. Handricks, M. J. LJzerman, J. R. deKroon, and G. Zilvold. Functional electrical stimulation by means of the 'ness handmaster orthosis' in chronic stroke patients: An exploratory study. *Clinical Rehabilitation*, 15(2):217–220, 2001.
- [43] R.R Harrison, R.J Kier, C.A Chestek, V Gilja, P Nuyujukian, S Kim, L Rieth, D.J Warren, N.M Ledbetter, S.I Ryu, K.V Shenoy, G.A Clark, and F Solzbacher. A wireless neural interface for chronic recording. *Proceedings of the 2008 IEEE Biomedical Circuits and Systems Conference*, 2008.
- [44] M Haugland and T Sinkjaer. Interfacing the body's own sensing receptors into neural prosthesis devices. *Technol Health Care*, 7(6):393–399, 1999.
- [45] M.K. Haugland and T. Sinkjaer. Cutaneous whole nerve recordings used for correction of footdrop in hemiplegic man. *Rehabilitation Engineering, IEEE Transactions on*, 3(4):307 –317, December 1995.
- [46] J F Hetke, J L Lund, K Najafi, K D Wise, and D J Anderson. Silicon ribbon cables for chronically implantable microelectrode arrays. *IEEE Trans Biomed Eng*, 41(4):314–21, Apr 1994.
- [47] Leigh R Hochberg, Mijail D Serruya, Gerhard M Friehs, Jon A Mukand, Maryam Saleh, Abraham H Caplan, Almut Branner, David Chen, Richard D Penn, and John P Donoghue. Neuronal ensemble control of prosthetic devices by a human with tetraplegia. *Nature*, 442(7099):164–71, Jul 2006.
- [48] A. L. Hodgkin and A. F. Huxley. Action Potentials record from inside a nerve fiber. *Nature (Lond)*, 144:710–711, October 1939.

- [49] A L Hodgkin and A F Huxley. A quantitative description of membrane current and its application to conduction and excitation in nerve. *J Physiol*, 117(4):500–44, Aug 1952.
- [50] Valérie Hospod, Jean-Marc Aimonetti, Jean-Pierre Roll, and Edith Ribot-Ciscar. Changes in human muscle spindle sensitivity during a proprioceptive attention task. *J Neurosci*, 27(19):5172–8, May 2007.
- [51] J C Houk, R W Cornew, and L Stark. A model of adaptation in amphibian spindle receptors. *J Theor Biol*, 12(2):196–215, 1966.
- [52] W Jensen, S M Lawrence, R R Riso, and T Sinkjaer. Effect of initial joint position on nerve-cuff recordings of muscle afferents in rabbits. *IEEE transactions on neural systems and rehabilitation engineering : a publication of the IEEE Engineering in Medicine and Biology Society*, 9(3):265–73, Sep 2001.
- [53] Winnie Jensen, Thomas Sinkjaer, and Francisco Sepulveda. Improving signal reliability for on-line joint angle estimation from nerve cuff recordings of muscle afferents. *IEEE transactions on neural systems and rehabilitation engineering : a publication of the IEEE Engineering in Medicine and Biology Society*, 10(3):133–9, Sep 2002.
- [54] S Jezernik, W M Grill, and T Sinkjaer. Neural network classification of nerve activity recorded in a mixed nerve. *Neurol Res*, 23(5):429–34, Jul 2001.
- [55] Kelly Jones, Patrick Campbell, and Richard Normann. A glass/silicon composite intracortical electrode array. *Annals of Biomedical Engineering*, 20:423–437, 1992. 10.1007/BF02368134.
- [56] Robert E Kass, Valerie Ventura, and Emery N Brown. Statistical issues in the analysis of neuronal data. *J Neurophysiol*, 94(1):8–25, Jul 2005.
- [57] Bernard Katz. *Nerve, muscle, and synapse*. McGraw-Hill Books, New York, 1966.
- [58] Sung-Phil Kim, John D Simeral, Leigh R Hochberg, John P Donoghue, and Michael J Black. Neural control of computer cursor velocity by decoding motor cortical spiking activity in humans with tetraplegia. *J Neural Eng*, 5(4):455–76, Dec 2008.
- [59] Daryl R Kipke, Rio J Vetter, Justin C Williams, and Jamille F Hetke. Silicon-substrate intracortical microelectrode arrays for long-term recording of neuronal spike activity in cerebral cortex. *IEEE Trans Neural Syst Rehabil Eng*, 11(2):151–5, Jun 2003.
- [60] Bernice Lau, Lisa Guevremont, and Vivian K Mushahwar. Strategies for generating prolonged functional standing using intramuscular stimulation or intraspinal microstimulation. *IEEE Trans Neural Syst Rehabil Eng*, 15(2):273–285, 2007 Jun.

- [61] S M Lawrence, G S Dhillon, W Jensen, K Yoshida, and K W Horch. Acute peripheral nerve recording characteristics of polymer-based longitudinal intrafascicular electrodes. *IEEE Trans Neural Syst Rehabil Eng*, 12(3):345–348, Sep 2004.
- [62] Daniel K Leventhal and Dominique M Durand. Subfascicle stimulation selectivity with the flat interface nerve electrode. *Annals of biomedical engineering*, 31(6):643–52, Jun 2003.
- [63] Faa-Jeng Lin, Chih-Hong Lin, and Po-Hung Shen. Self-constructing fuzzy neural network speed controller for permanent-magnet synchronous motor drive. *Fuzzy Systems, IEEE Transactions on*, 9(5):751–759, October 2001.
- [64] G E Loeb, M J Bak, and J Duysens. Long-term unit recording from somatosensory neurons in the spinal ganglia of the freely walking cat. *Science*, 197(4309):1192–4, Sep 1977.
- [65] Gerard M Lyons, Thomas Sinkjaer, Jane H Burridge, and David J Wilcox. A review of portable fes-based neural orthoses for the correction of drop foot. *IEEE Trans Neural Syst Rehabil Eng*, 10(4):260–79, Dec 2002.
- [66] Mitchell G Maltenfort and R E Burke. Spindle model responsive to mixed fusimotor inputs and testable predictions of beta feedback effects. *J Neurophysiol*, 89(5):2797–2809, 2003 May.
- [67] Z Matjacic, K Hunt, H Gollee, and T Sinkjaer. Control of posture with fes systems. *Med Eng Phys*, 25(1):51–62, 2003.
- [68] P B Matthews. Muscle spindles and their motor control. *Physiol Rev*, 44:219–288, 1964.
- [69] P B Matthews and R B Stein. The sensitivity of muscle spindle afferents to small sinusoidal changes of length. *J Physiol*, 200(3):723–743, 1969.
- [70] T G McNaughton and K W Horch. Action potential classification with dual channel intrafascicular electrodes. *IEEE Trans Biomed Eng*, 41(7):609–16, Jul 1994.
- [71] S Micera, W Jensen, F Sepulveda, R R Riso, and T Sinkjaer. Neuro-fuzzy extraction of angular information from muscle afferents for ankle control during standing in paraplegic subjects: an animal model. *IEEE transactions on bio-medical engineering*, 48(7):787–94, Jul 2001.
- [72] Milana P Mileusnic, Ian E Brown, Ning Lan, and Gerald E Loeb. Mathematical models of proprioceptors. i. control and transduction in the muscle spindle. *J Neurophysiol*, 96(4):1772–1788, 2006.

- [73] Milana P Mileusnic and Gerald E Loeb. Mathematical models of proprioceptors. ii. structure and function of the golgi tendon organ. *J Neurophysiol*, 96(4):1789–1802, 2006.
- [74] Mark E Nelson. Electrophysiological models of neural processing. *Wiley Interdiscip Rev Syst Biol Med*, 3(1):74–92, 2011.
- [75] M A Nicolelis. Actions from thoughts. *Nature*, 409(6818):403–7, Jan 2001.
- [76] J B Nielsen, C Crone, and H Hultborn. The spinal pathophysiology of spasticity—from a basic science point of view. *Acta Physiol (Oxf)*, 189(2):171–180, 2007.
- [77] Craig T. Nordhausen, Edwin M. Maynard, and Richard A. Normann. Single unit recording capabilities of a 100 microelectrode array. *Brain Research*, 726(1-2):129 – 140, 1996.
- [78] I P Pappas, M R Popovic, T Keller, V Dietz, and M Morari. A reliable gait phase detection system. *IEEE Trans Neural Syst Rehabil Eng*, 9(2):113–125, 2001.
- [79] M R Popovic, A Curt, T Keller, and V Dietz. Functional electrical stimulation for grasping and walking: indications and limitations. *Spinal Cord*, 39(8):403–412, 2001.
- [80] R E Poppele and R J Bowman. Quantitative description of linear behavior of mammalian muscle spindles. *J Neurophysiol*, 33(1):59–72, 1970.
- [81] A Prochazka, M Gauthier, M Wieler, and Z Kenwell. The bionic glove: an electrical stimulator garment that provides controlled grasp and hand opening in quadriplegia. *Arch Phys Med Rehabil*, 78(6):608–614, 1997.
- [82] A Prochazka and M Gorassini. Models of ensemble firing of muscle spindle afferents recorded during normal locomotion in cats. *J Physiol*, 507 (Pt 1):277–291, 1998.
- [83] A Prochazka, M Hulliger, P Zangger, and K Appenteng. ‘fusimotor set’: new evidence for alpha-independent control of gamma-motoneurons during movement in the awake cat. *Brain Res*, 339(1):136–140, 1985.
- [84] A Prochazka, R A Westerman, and S P Ziccone. Discharges of single hindlimb afferents in the freely moving cat. *J Neurophysiol*, 39(5):1090–1104, Sep 1976.
- [85] A Prochazka, R A Westerman, and S P Ziccone. Ia afferent activity during a variety of voluntary movements in the cat. *J Physiol*, 268(2):423–448, Jun 1977.
- [86] Kian Hong Quah and Chai Quek. Ftsk: online local learning with generic fuzzy input takagi-sugeno-kang fuzzy framework for nonlinear system estimation. *Systems, Man, and Cybernetics, Part B: Cybernetics, IEEE Transactions on*, 36(1):166 –178, 2006.

- [87] P M Rack and D R Westbury. The effects of suxamethonium and acetylcholine on the behaviour of cat muscle spindles during dynamics stretching, and during fusimotor stimulation. *J Physiol*, 186(3):698–713, 1966.
- [88] Edith Ribot-Ciscar, Valérie Hospod, Jean-Pierre Roll, and Jean-Marc Aimonetti. Fusimotor drive may adjust muscle spindle feedback to task requirements in humans. *J Neurophysiol*, 101(2):633–40, Feb 2009.
- [89] J Rigosa, D J Weber, A Prochazka, R B Stein, and S Micera. Neuro-fuzzy decoding of sensory information from ensembles of simultaneously recorded dorsal root ganglion neurons for fes applications. *J Neural Eng*, In press, 2011.
- [90] Serge Rossignol, Réjean Dubuc, and Jean-Pierre Gossard. Dynamic sensorimotor interactions in locomotion. *Physiol Rev*, 86(1):89–154, Jan 2006.
- [91] P J Rousche and R A Normann. Chronic recording capability of the utah intracortical electrode array in cat sensory cortex. *J Neurosci Methods*, 82(1):1–15, Jul 1998.
- [92] E Salinas and L F Abbott. Vector reconstruction from firing rates. *J Comput Neurosci*, 1(1-2):89–107, Jun 1994.
- [93] T D Sanger. Probability density estimation for the interpretation of neural population codes. *J Neurophysiol*, 76(4):2790–2793, Oct 1996.
- [94] A B Schwartz. Direct cortical representation of drawing. *Science*, 265(5171):540–2, Jul 1994.
- [95] Andrew B Schwartz. Cortical neural prosthetics. *Annu Rev Neurosci*, 27:487–507, 2004.
- [96] Andrew B. Schwartz, X. Tracy Cui, Douglas J. Weber, and Daniel W. Moran. Brain-controlled interfaces: Movement restoration with neural prosthetics. *Neuron*, 52(1):205 – 220, 2006.
- [97] Gideon Schwarz. Estimating the dimension of a model. *The Annals of Statistics*, 6(2):461–464, Mar 1978.
- [98] S H Scott and G E Loeb. The computation of position sense from spindles in mono- and multiarticular muscles. *J Neurosci*, 14(12):7529–40, 1994.
- [99] K Seidl, S Spieth, S Herwik, J Steigert, R Zengerle, O Paul, and P Ruther. In-plane silicon probes for simultaneous neural recording and drug delivery. *Journal of Micromechanics and Microengineering*, 20(10):105006, 2010.
- [100] John P Seymour and Daryl R Kipke. Neural probe design for reduced tissue encapsulation in cns. *Biomaterials*, 28(25):3594–607, Sep 2007.

- [101] C. S. Sherrington. On the anatomical constitution of nerves of skeletal muscles; with remarks on recurrent fibres in the ventral spinal nerve-root. *J Physiol*, 3-4(17), 1894.
- [102] C.S. Sherrington. *The Integrative Action of the Nervous System*. New York: C Scribner's sons, 1906.
- [103] Y Shimada, K Sato, T Matsunaga, Y Tsutsumi, A Misawa, S Ando, T Minato, M Sato, S Chida, and K Hatakeyama. Closed-loop control using a stretch sensor for restoration of standing with functional electrical stimulation in complete paraplegia. *Tohoku J Exp Med*, 193(3):221–227, 2001.
- [104] F B Simmons, J M EPLEY, R C Lummis, N Guttman, L S Frishkopf, L D Harmon, and E Zwicker. Auditory nerve: Electrical stimulation in man. *Science*, 148:104–6, Apr 1965.
- [105] R B Stein, Y Aoyagi, D J Weber, S Shoham, and R A Normann. Encoding mechanisms for sensory neurons studied with a multielectrode array in the cat dorsal root ganglion. *Can J Physiol Pharmacol*, 82(8-9):757–68, 2004.
- [106] R B Stein, D J Weber, Y Aoyagi, A Prochazka, J B Wagenaar, and R A Normann. Coding of position by simultaneously recorded sensory neurones in the cat dorsal root ganglion. *J Physiol*, 560(Pt 3):883–896, 2004.
- [107] Richard B Stein, Suling Chong, Dirk G Everaert, Robert Rolf, Aiko K Thompson, Maura Whittaker, Jenny Robertson, Joyce Fung, Richard Preuss, Kimito Momose, and Kouji Ihashi. A multicenter trial of a footdrop stimulator controlled by a tilt sensor. *Neurorehabil Neural Repair*, 20(3):371–379, 2006.
- [108] M. Sugeno and G. T. Kang. Structure identification of fuzzy model. *Fuzzy Sets and Systems*, 28(1):15 – 33, 1988.
- [109] C. Tai, A. M. Booth, C. J. Robinson, W. C. De Groat, and J. R. Roppolo. Multi-joint movement of the cat hindlimb evoked by microstimulation of the lumbosacral spinal cord. *Experimental Neurology*, 183(2):620–627, 2003.
- [110] Tomohiro Takagi and Michio Sugeno. Fuzzy identification of systems and its applications to modeling and control. *IEEE Transactions on Systems, Man, and Cybernetics*, 15(1):116–132, February 1985.
- [111] Wei Tan and Gerald E Loeb. Feasibility of prosthetic posture sensing via injectable electronic modules. *IEEE Trans Neural Syst Rehabil Eng*, 15(2):295–309, 2007.
- [112] Wei Tan, Qiang Zou, E S Kim, and Gerald E Loeb. Sensing human arm posture with implantable sensors. *Conf Proc IEEE Eng Med Biol Soc*, 6:4290–4293, 2004.

- [113] A Taylor, P H Ellaway, R Durbaba, and S Rawlinson. Distinctive patterns of static and dynamic gamma motor activity during locomotion in the decerebrate cat. *J Physiol*, 529 Pt 3:825–836, 2000.
- [114] A Taylor, J F Rodgers, A J Fowle, and R Durbaba. The effect of succinylcholine on cat gastrocnemius muscle spindle afferents of different types. *J Physiol*, 456:629–44, Oct 1992.
- [115] Dawn M Taylor, Stephen I Helms Tillery, and Andrew B Schwartz. Direct cortical control of 3d neuroprosthetic devices. *Science*, 296(5574):1829–32, 2002.
- [116] Artur S P Varejao and Vitor M Filipe. Contribution of cutaneous inputs from the hindpaw to the control of locomotion in rats. *Behav Brain Res*, 176(2):193–201, 2007.
- [117] Meel Velliste, Sagi Perel, M Chance Spalding, Andrew S Whitford, and Andrew B Schwartz. Cortical control of a prosthetic arm for self-feeding. *Nature*, 453(7198):1098–101, Jun 2008.
- [118] R Vinjamuri, D J Weber, A D Degenhart, J L Collinger, G P Sudre, P D Adelson, D L Holder, M L Boninger, A B Schwartz, D J Crammond, E C Tyler-Kabara, and W Wang. A fuzzy logic model for hand posture control using human cortical activity recorded by micro-ecog electrodes. *Conf Proc IEEE Eng Med Biol Soc*, 2009:4339–4342, 2009.
- [119] J B Wagenaar, V Ventura, and D J Weber. Improved decoding of limb-state feedback from natural sensors. *Conf Proc IEEE Eng Med Biol Soc*, 1:4206–9, 2009.
- [120] J B Wagenaar, V Ventura, and D J Weber. State-space decoding of primary afferent neuron firing rates. *J Neural Eng*, 8(1):016002, Jan 2011.
- [121] Matthew P Ward, Pooja Rajdev, Casey Ellison, and Pedro P Irazoqui. Toward a comparison of microelectrodes for acute and chronic recordings. *Brain Res*, 1282:183–200, Jul 2009.
- [122] D. J. Weber, R. B. Stein, D. G. Everaert, and A. Prochazka. Decoding sensory feedback from firing rates of afferent ensembles recorded in cat dorsal root ganglia in normal locomotion. *IEEE Transactions on Neural Systems and Rehabilitation Engineering*, 14(2):240–243, 2006.
- [123] D J Weber, R B Stein, D G Everaert, and A Prochazka. Limb-state feedback from ensembles of simultaneously recorded dorsal root ganglion neurons. *J Neural Eng*, 4(3):S168–80, 2007.
- [124] J C Williams, R L Rennaker, and D R Kipke. Long-term neural recording characteristics of wire microelectrode arrays implanted in cerebral cortex. *Brain Res Brain Res Protoc*, 4(3):303–13, Dec 1999.

- [125] L R Wilson, S C Gandevia, J T Inglis, J Gracies, and D Burke. Muscle spindle activity in the affected upper limb after a unilateral stroke. *Brain*, 122 (Pt 11):2079–2088, 1999 Nov.
- [126] Jeffrey Winslow, Patrick L Jacobs, and Dejan Tepavac. Fatigue compensation during fes using surface emg. *J Electromyogr Kinesiol*, 13(6):555–68, Dec 2003.
- [127] Shiqian Wu and Meng Joo Er. Dynamic fuzzy neural networks-a novel approach to function approximation. *Systems, Man, and Cybernetics, Part B: Cybernetics, IEEE Transactions on*, 30(2):358 –364, April 2000.
- [128] Shiqian Wu, Meng Joo Er, and Yang Gao. A fast approach for automatic generation of fuzzy rules by generalized dynamic fuzzy neural networks. *Fuzzy Systems, IEEE Transactions on*, 9(4):578 –594, August 2001.
- [129] W Wu, Y Gao, E Bienenstock, J P Donoghue, and M J Black. Bayesian population decoding of motor cortical activity using a kalman filter. *Neural Comput*, 18(1):80–118, Jan 2006.
- [130] Wei Wu, Michael J Black, David Mumford, Yun Gao, Elie Bienenstock, and John P Donoghue. Modeling and decoding motor cortical activity using a switching kalman filter. *IEEE Trans Biomed Eng*, 51(6):933–42, Jun 2004.
- [131] K Yoshida and K Horch. Closed-loop control of ankle position using muscle afferent feedback with functional neuromuscular stimulation. *IEEE Trans Biomed Eng*, 43(2):167–176, 1996.
- [132] K Yoshida and R B Stein. Characterization of signals and noise rejection with bipolar longitudinal intrafascicular electrodes. *IEEE Trans Biomed Eng*, 46(2):226–34, Feb 1999.
- [133] K Zhang, I Ginzburg, B L McNaughton, and T J Sejnowski. Interpreting neuronal population activity by reconstruction: unified framework with application to hippocampal place cells. *J Neurophysiol*, 79(2):1017–1044, Feb 1998.